THEORETICAL MODELLING OF GLOBAL OSCILLATIONS IN SOLAR PROMINENCES

Parthasarathi Joarder

A Thesis Submitted for the Degree of PhD
at the
University of St Andrews

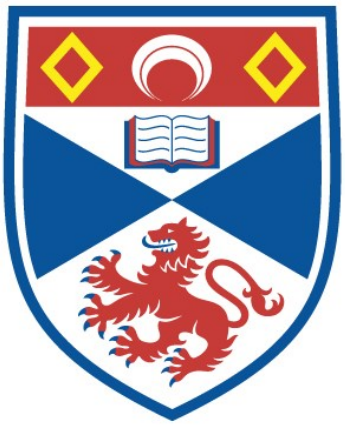

1994

Full metadata for this item is available in
St Andrews Research Repository
at:
http://research-repository.st-andrews.ac.uk/

Please use this identifier to cite or link to this item:
http://hdl.handle.net/10023/14169

This item is protected by original copyright

Theoretical Modelling Of Global Oscillations In Solar Prominences

Parthasarathi Joarder

A thesis submitted for the degree of Doctor of Philosophy at the University of St. Andrews

ProQuest Number: 10167113

All rights reserved

INFORMATION TO ALL USERS
The quality of this reproduction is dependent upon the quality of the copy submitted.

In the unlikely event that the author did not send a complete manuscript
and there are missing pages, these will be noted. Also, if material had to be removed,
a note will indicate the deletion.

ProQuest 10167113

Published by ProQuest LLC (2017). Copyright of the Dissertation is held by the Author.

All rights reserved.
This work is protected against unauthorized copying under Title 17, United States Code
Microform Edition © ProQuest LLC.

ProQuest LLC.
789 East Eisenhower Parkway
P.O. Box 1346
Ann Arbor, MI 48106 – 1346

TL

B 416

Declarations

I, Parthasarathi Joarder, hereby certify that this thesis has been composed by myself, that it is the record of my own work, and that it has not been accepted in partial or complete fulfilment of any other degree or professional qualification.

Signed..... Date.....

I was admitted to the Faculty of Science of the University of St. Andrews under Ordinance General No 12 on October 1989 and as a candidate for the degree of Ph. D. on October 1990.

Signed..... Date.....

I hereby certify that the candidate has fulfilled the conditions of the Resolution and Regulations appropriate to the degree of Ph. D.

Signature of Supervisor.. Date 8 June '93

BIBLIOTHECA UNIVERSITATIS

Copyright

In submitting this thesis to the University of St. Andrews I understand that I am giving the permission for it to be made available for use in accordance with the regulations of the University Library for the time being in force, subject to any copyright vested in the work not being affected thereby. I also understand that the title and abstract will be published and that a copy of the work may be made and supplied to any **bona fide** library or research worker.

Acknowledgement

I take this opportunity to thank my thesis supervisor, Dr. Bernard Roberts, for his constant guidance and inspiration during the course of this work. Being introduced to his elegant methodology of solar research is perhaps the most valuable experience that I gained during my stay in St. Andrews.

I would like to thank all the staffs, and particularly the members of the Solar Physics Group, of the University of St. Andrews for the research facilities that I enjoyed for three years. Particularly helpful were the discussions with Dr. Alan Hood, whose suggestions proved much useful in several stages of the work, and also improved my general background knowledge of solar physics. I also thank the Head of the Solar Physics Group, Prof. E. R. Priest, whose personal initiative made it possible for me to join the group for my Ph.D research.

My postgraudate studies in St Andrews were supported by a University Research Scholarship and an Overseas Research Studentship (ORS) award. I thank the University authority and the Commitee of Vice-Chancellors and Principals (CVCP) for those grants.

Special thanks are due for Richard Ireland and Alan Johnston (and Karen too), whose friendliness and encouragement were pivotal at a crucial stage of my social interactions with the collegues in the department. I also express my gratefulness to Drs. Richard Rijnbeek, Ruhul Amin and Ian Hardie in this context.

Finally and most importantly, I express my deep sense of gratitude to my parents and to my sister whose care, love and company has always been so inspiring even in some of the most difficult times of despair in my life. To them I dedicate this thesis.

Table of Contents

Abstract

This thesis aims to provide a basic theoretical explanation for the oscillatory motions observed in solar quiescent prominences.

The prominence is treated as a simple plasma slab embedded in a hotter and rarer uniform coronal plasma. Both the slab and its environment are permeated by a uniform magnetic field. The field lines are anchored at rigid walls placed on either side of the plasma slab and representing the photospheric line-tying effect. The magnetohydrodynamic modes of oscillation of the plasma slab are then examined for different orientations of the magnetic field with respect to the long axis of the slab.

Particularly interesting in this study is the appearance of the 'string MHD' modes that are analogous to the fundamental vibrations of a mass-loaded stretched elastic string. Such modes appear whenever the magnetic field vector is inclined to the long axis of the slab, thus producing a magnetic field component in the direction transverse to the axis of the slab. Observationally, this inclination of the field is generally small.

For realistic values of the angle of inclination of the magnetic field lines, the 'string Alfven' mode and an 'internal slow' mode yield periods in the range 1/2-2 hr. These modes may correspond to the observed long period (40-90 minutes) oscillations in quiescent prominences. Intermediate periodicities, in the range 8-20 min, may be associated with an 'internal Alfven' mode and a 'fast string' mode of the prominence slab. The observed short periodicities, in the range 2-5 min, may correspond to an 'internal fast' mode in prominences.

Having thus established a foundation for the theoretical modelling of prominence oscillations in terms of the magnetohydrodynamic modes of oscillation of a non-gravitating plasma slab, we discuss several factors, such as the effects of gravitational stratification, the curvature of the magnetic field lines, and the fine-structures in a prominence, that may complicate a description of its oscillatory modes. Some preliminary investigations of simple magnetohydrostatic equilibrium models suggest that gravity and the curvature of the magnetic field lines play only a secondary role in determining the periods of the oscillatory modes in prominences, the basic structure of the modes being similar to that present in simple slab models.

Chapter I

Introduction

This introductory chapter aims to provide a general background knowledge of (i) solar prominences, and (ii) the waves and oscillations in a magnetohydrodynamic medium. We also present a brief summary of the observations of oscillatory motions in quiescent prominences, discuss the importance of the study of these oscillatory motions, and give an account of some of the earlier attempts to develop theoretical descriptions of these oscillations.

1.1 Solar Prominences

1.1.1. General description and classification: 'Solar prominences are of great interest in their own right and are of wider importance both for solar physics and for many areas of astrophysics. Their basic properties are not well understood at all, but they may be crucial for the mass and magnetic flux balance of the solar corona. Also they mark out large scale magnetic polarity inversion lines in the photosphere, as well as the cores of large scale magnetic arcades in the corona. The eruption of a prominence often produces a coronal mass ejection and sometimes a large two-ribbon flare. As far as astrophysics as a whole is concerned, prominences represent regions where magnetic fields are interacting with plasma in subtle ways, where dense plasma is being supported against gravity and where thermal instability is producing a cool condensation, and so by studying prominences in detail we can learn how these fundamental processes are likely to operate elsewhere in the Universe.' (Priest, 1989).

For decades solar physicists have thus pondered over the beauty and the puzzles of solar prominences. Considerable progress has been made in collecting observational data and providing theoretical interpretations on the nature of prominences. Here we outline some of the important observed properties and theoretical models of solar prominences. More detailed descriptions can be found in the references given throughout the text, and in several excellent books and reviews on prominences (eg. Tandberg-Hanssen, 1974; Priest, 1989, 1990; Hirayama, 1985, 1990; Ballester and Priest, 1988; Zirker, 1989; Ruzdjak and Tandberg-Hanssen, 1990; Rompolt, 1990; Demoulin, 1991).

Prominences are most simply described as cool and dense plasma material that is in suspension against the gravitational forces in the solar corona. They possess a temperature of about a hundred times lower than coronal values and densities are about a hundred times greater than coronal values. Seen against the solar disk they look like dark filaments, while projected onto the sky they appear as bright objects on the solar limb. They have been classified morphologically in several different ways (eg. Secchi, 1875; Young, 1896; Pettit, 1925, 1932, 1936, 1943, 1950; Newton, 1934, 1935; Menzel and Evans, 1953; Severny, 1954, 1959; Severny and Khokhlova, 1953; De Jager, 1959; Zirin, 1966), but there appear to be two basic types, namely, *active* and *quiescent prominences* ; cf. Secchi (1875), Newton (1934, 1935), Zirin (1966), Tandberg-Hanssen, (1974), Priest (1982), Hirayama (1985).

Active prominences are located in active regions (ie. regions of the chromosphere and corona that have strong re-entrant magnetic fields) and are usually associated with solar flares. They are dynamic structures with violent motions and have life-times of only minutes or hours. The highly dynamic nature of active prominences makes them difficult to observe with high resolution and even more difficult to model theoretically.

Quiescent prominences are long-lived; they can exist for months (several solar rotations). They always form gradually over a neutral line separating regions of opposite line-of-sight magnetic polarity in the photosphere. In the course of a prominence's life-time, its global structure remains virtually unaltered, though the small-scale structures may change in tens of minutes (eg. Engvold, 1976, 1978). As time proceeds, the quiescent prominence is mostly observed to start rising slowly to higher altitudes, and finally ending its life in a violent upward eruption. This eruption may create a solar flare, or the erupting prominence may suddenly disappear (commonly referred to as 'dispartition brusque') creating a large coronal mass ejection.

In this thesis, we consider quiescent prominences only. We first look at some of the observational results concerning important physical properties, such as density, temperature, size, structure, and magnetic field strength in quiescent prominences.

1.1.2 Characteristic properties of quiescent prominences: A quiescent prominence is a thin, vertical slab of dense material often linked to the solar surface by several feet. The prominence slab is typically of

length 2 10^5 km, height 5 10^4 km and width of about 5000-10,000 km (eg. Tandberg-Hanssen, 1974; Priest, 1982). The observed properties of the plasma and the magnetic field in quiescent prominences are well summarized in the reviews by Tandberg-Hanssen (1974), Hirayama (1985, 1990), Leroy (1989), Priest (1989, 1990), Schmieder (1989), Zirker (1989), Kim (1990), Rompolt (1990), Demoulin (1991). The most convenient reference for a prominence-theorist is, perhaps, the summary presented by Jensen and Wiik (1990). Following a brief tabular summary of the observed parameters by Engvold et al. (1990, Hvar Reference Atmosphere of Quiescent Prominences), Jensen and Wiik tabulate the upper and lower bounds of most of the important physical parameters in quiescent prominences. These bounds are determined either observationally or theoretically. In Table 1.1, we reproduce their results for physical quantities that prove necessary for theoretical modelling in the subsequent chapters.

Table 1.1. *Upper and lower limits of quiescent prominence parameters (after Jensen and Wiik, 1990).*

Parameter (units)	Prominence centre	Prominence edge
Temperature (K)	4300-8500	8000-12000
Density (gcm^{-3})	2 10^{-14}-2 10^{-12}	7 10^{-14}
Magnetic field (G)	4-20	4-20
Mean molecular weight	0.6-0.9	0.9
Gas pressure (cgs)	0.1-2	2 10^{-2}
Plasma-beta	6 10^{-3} - 3	(1-30) 10^{-3}

The summary provided by Jensen and Wiik (1990), presenting the range of measured magnetic field strength in prominences, does not however include information regarding the orientation of the field. Such information can be found in the observations of Harvey (1969), Tandberg-Hanssen and Anzer (1970), Leroy (1979, 1989), Leroy et al. (1983, 1984), Athay et al. (1983a, b), Querfeld et al. (1985), Bommier et al. (1985a,b), Kim (1990) and Kim et al. (1988). These works have confirmed that the magnetic field vector in a quiescent prominence is inclined to the horizontal plane by a small angle, of the order of 10^o or smaller; also, the angle between the magnetic field and the long axis of the prominence also appears to be small, lying somewhere around 20^o.

We end this subsection with a few comments on the fine-scale structures observed in prominences. Such fine structures of various densities and temperatures have been detected in quiescent prominences by Dunn (1959, 1960), Engvold (1976, 1978), Engvold et al. (1989); Hirayama (1986), Zirker and Koutchmy (1990) and Chiuderi-Drago et al. (1992); see recent review by Heinzel and Vial (1992). Both vertical and (field-aligned) horizontal thread-like structures are observed. Diameters of these threads are generally estimated to be a few hundred kilometers (< 200 km, according to Zirker and Koutchmy, 1990), but such estimates are uncertain due to the limitations imposed by instrumental resolution and 'atmospheric seeing'. In fact, a thread diameter as small as ten kilometers can not be ruled out (Hirayama, 1986). Recently, Yi Zhang and Engvold (1991) and Yi Zhang et al. (1991) have also resolved the field-aligned fine structures in the velocity and intensity oscillations in quiescent prominences (see a review of prominence oscillations given below).

Poland and Mariska (1986), Demoulin et al. (1987); Priest et al. (1991) have discussed a number of mechanisms for the formation of prominence fine structure. Recently, Van der Linden (1993, see also Demoulin et al. 1987) has shown that the formation of the field aligned structures can be explained in terms of radiative instability (Field, 1965), if the thermal conductivity perpendicular to the magnetic field is included. Similar length scales of condensation can also be obtained by including electrical resistivity in the calculations (Ireland et al. 1992).

1.1.3. Prominence models: The observed flows ($\lesssim 3$ kms^{-1}) in quiescent prominences are much smaller than their free-fall speed $(gh)^{1/2}$ of about 100 kms^{-1}(Engvold, 1976; Mein, 1977; Martres et al. 1981). With a few exceptions (eg. Pikelner, 1971; Kuijpers, 1989), most of the prominence models are therefore magnetohydrostatic equilibrium models, where gravity is exactly balanced by the magnetic pressure and curvature force associated with the field lines surrounding and threading the prominence.

Most of the prominence models proposed so far can be classified into two groups, namely, *normal* and *inverse* polarity models (eg. Anzer, 1979, 1989; Hirayama, 1985; Leroy, 1989) . In the first group, the magnetic polarity in the prominence is the same as the polarity of the underlying photosphere, whereas the opposite is true for the second group. The former group generally represents the low latitude prominences near active regions. On the other hand, the second group mostly represents the

high latitude polar crown prominences, cf. Athay et al. (1983b), Leroy et al. (1983, 1984), Bommier et al. (1985a, b). The Kippenhahn-Schluter (1957) model is a typical normal polarity type, whereas, the Kuperus-Raadu (1974) model is a typical example of an inverse polarity prominence.

The first mathematical model of a prominence-type equilibrium was given by Menzel (1951). This simple model has several serious drawbacks, notably that it is isothermal, it does not include a magnetic field component along the prominence axis (as in the case of many other models), magnetic field lines are periodic around the prominence, and also, in its original form, it predicts a height for the prominence that is much shorter than its observed height. This model has recently been generalized by Hood and Anzer (1990), who have included both the internal and the external structure of the prominence as well as a magnetic field component along the prominence axis. The resulting normal polarity prominence model yields reasonable agreement with prominence conditions. Menzel's model is, however, interesting due to its mathematical simplicity. We examine this model more closely in a later chapter.

The best known normal polarity prominence model is the Kippenhahn-Schluter (1957) model. Here the prominence is modelled by an infinitely thin current sheet, residing in a coronal magnetic arcade that has a dip at its top, where the prominence plasma is supported against gravity by magnetic curvature forces. Both the internal prominence structure and an external potential magnetic field were calculated. In the original model, the current sheet representing the prominence was assumed infinite, but in a later extension Malherbe and Priest (1983) introduced the effect of finite height. The resulting equlibrium then looks similar to Fig.1.1(a). Modifications to the basic Kippenhahn-Schluter model have also been done by Poland and Anzer (1971), Anzer (1972), Low (1975a,b; 1981), Aly and Amari (1988) and Demoulin, Malherbe and Priest (1989). Attempts to include thermal equilibrium condition into the the basic model have also been carried out, see Poland and Anzer (1971), Heasley and Mihalas (1976), Lerche and Low (1977) and Milne et al. (1979).

The basic inverse polarity model is due to Kuperus and Raadu (1974). They suggested that the prominence forms in a current-sheet of an open field line configuration (an essentially vertical field, changing direction through the current sheet). The prominence is represented by a line current I at a height h above the photosphere, and is supported

against gravity by repulsion between I and an induced mirror current -I at depth h in the photosphere. This leads to a geometry as in figure 1.1(b). Genaralizations and modifications of this basic model have been done by Malherbe and Priest (1983), Anzer (1984), and Amari and Aly (1989, 1990).

Among the various other models of quiescent prominences, particularly interesting is a twisted flux tube model (an inverse-polarity prominence model), that has been recently proposed by Priest, Hood and Anzer (1989). In this model, the prominence sheet is considered to reside in a nearly force-free flux-tube with its mass being supported by the twisted field lines, that are concave upward below the prominence, see Fig. 1.1(c). Only the solution for the external field structure has been given so far. Attempts to incorporate the field structure inside the prominence sheet is in progress.

Only a very brief overview of the prominence models are given in this subsection. More detailed discussion on this subject can be found in the recent reviews by Anzer (1989) and Priest (1990).

1.2 Observations of prominence oscillations

1.2.1. Importance of the study of prominence oscillations: In the previous section, we described various equilibrium models that are proposed for the structure of solar quiescent prominences. The mathematical elegance of these models is unquestionable, although they have not so far been proved entirely sufficient for our understanding of the structure of solar prominences. A wide range of such mathematical models are now available, but only a very few of them incorporate the magnetic field along the prominence axis and describe both the internal magnetic field and its coupling to the bipolar coronal field in a satisfactory way. Moreover, the stability properties of only a fraction of these equilibrium models have been critically studied (eg. Brown, 1958; Anzer, 1969; Zweibel, 1982; Migliuolo, 1982; Galindo-Trejo, 1987, 1989a,b; Galindo-Trejo and Schindler, 1984; De Bruyne, 1990) and whenever such a study is undertaken, it is found that even an apparently satisfactory model is either unstable against small perturbations, or is stable only for a very restricted choice of parameter values (see, for example, De Bruyne (1990) for an examination of Low (1981) and Hood and Anzer (1990) prominences).

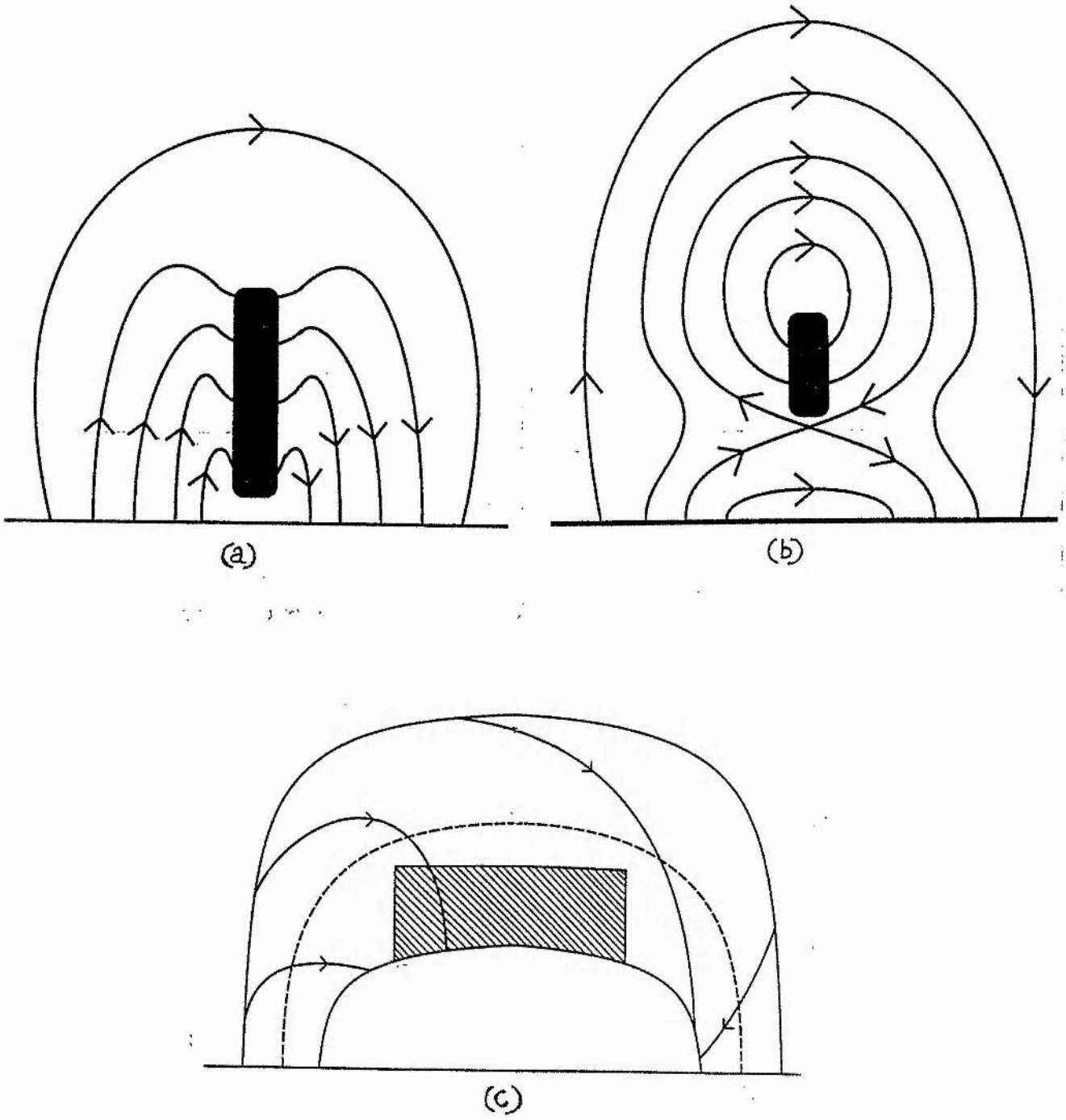

Fig. 1.1. Schematic diagrams of (a) Kippenhahn-Schlüter (b) Kuperus-Raadu and (c) Priest, Hood and Anzer (1989) prominence models.

It may, in any case, be admitted that the mathematical modelling of prominence equilibria is rather indirect a way to obtain information about the conditions that prevail in solar quiescent prominences. Fortunately, with the discovery and detailed study of prominence oscillations, there arises a hope that we may, in future, have a more direct means of obtaining diagnostic information about the physical conditions and magnetic structure in prominences and their coronal environment, much as helioseismology is giving us information about the internal structure of the Sun (see reviews on helioseismology in Deubner and Gough, 1984; Leibacher et al. 1985; Christensen-Dalsgaard, 1989). The observation of prominence oscillations is, of course, still in its infancy. Only the approximate orders of magnitude of the periods are confirmed and at this stage of development the duty of a prominence-theorist must therefore be to find out the basic physical ingredients in prominences, that go together to determine such periods. We will mainly be concerned with such a theoretical goal in this thesis.

1.2.2. Oscillations related to solar activity: Oscillations of prominences, that are excited by the disturbances generated by solar flares had previously been identified in the so-called 'winking filaments' (eg. Newton, 1935; Dodson, 1949; Dodson and Hedeman, 1964; Bruzek, 1951, 1958; Moreton, 1960, 1965; Hyder, 1966; Ramsey and Smith, 1966; Kleczek and Kuperus, 1969). Observations of such flare-induced oscillations in quiescent prominences have been summarized by Tandberg-Hanssen (1974). The observed winking filaments generally show an initial receeding motion followed by one to four damped oscillations. Oscillations in both vertical or horizontal directions were observed. The frequency of such oscillations varies from one filament to another, and does not appear to relate to the importance of the flare. Ramsey and Smith (1966) observed a filament which was disturbed four times in a three day period, and each time it oscillated with essentially the same frequency. There is further a preferential direction, or rather a cone, in which the disturbance propagates from the flare site. Filaments lying inside this cone as seen from the flare may be activated, those outside are not.

Aside from such winking phenomena in quiescent prominences, Malville and Schindler (1981) detected a period of 75 s, and Vrsnak (1984) detected a period of 8 min in their observations of loop prominences. Recently, Vrsnak (1990a,b) and Vrsnak et al. (1988, 1990,

1991) carried out a detailed study of the structural and dynamical properties of some of the active loop prominences in their pre-eruptive to post-eruptive phases of evolution. Intermittent oscillations of a complex nature were detected during the post-eruptive phase of one prominence with their periodicities ranging from 4 to 9 minutes (Vrsnak et al. 1990). Such oscillations in loop prominences are essentially related to the process of activation of the prominence.

1.2.3. Oscillations in steady quiescent prominences: In this thesis, we are primarily concerned with the oscillations in quiescent prominences that are unrelated, at least directly, to flare events or the activation of prominences. Observations have been made to detect such oscillations in all of the line-intensity, line-width and the line-of-sight Doppler shift of certain emission or absorption lines in prominences. The periods of oscillation found in these observations, can broadly be classified into three groups (Joarder and Roberts, 1992a):

(a) long period oscillations with periods in the range 1/2-2 hr;

(b) intermediate periodicities in the range 8-20 min;

(c) short period oscillations with periods in the range 2-5 min.

Tables 1.2(a) -(c) summarize all the important observations pertinent to these three classes of oscillations in quiescent prominences; reviews of observational results can also be found in Tsubaki (1988) and Schmieder (1989, 1990).

We may also note some of the special features that characterize some of the observations mentioned in Tables 1.2(a)-(c). For example, Bashkirtsev and Mashnich (1984) reported that the observed long period velocity oscillations in prominences seem to arise due to a helical motion along the axis of a magnetic flux-loop. In their recent observations, these authors obtained a complicated, highly time-dependent, and quasi-periodic variation for oscillation frequencies below 1 mHz (Mashnich and Bashkirtsev, 1990). In some power spectra of velocity oscillations in quiescent prominences, Balthasar et al. (1986) obtained broad power humps around 5 min and 3 min that resemble the power spectra of the well-known photospheric and chromospheric oscillations (eg. Leibacher

Table 1.2(a). *Observations made to detect long period oscillations in prominences.*

Authors	Year of publication	Spectral line chosen	Intensity	Line-width	Velocity
Landman et al.	1977	HeI D_3	22, 31 min	22 min	No
Bashkirtsev et al.	1983	Hβ	No	_	77, 82 min
Bashkirtsev and Mashnich	1984	Hβ	No	_	42-82 min (±.2 -6 kms^{-1})
Wiehr et al.	1984	Hα	No	_	50-64 min (±1-2 kms^{-1})
Balthasar et al.	1986	Hα	No	_	48 min
Balthasar et al.	1988a,b	Hα, $Ca^{+}H$, Hε	_	_	40-80 min
Gheonjian et al.	1990	Hα	_	_	40 min
Mashnich and Bashkirtsev	1990	Hβ	_	_	23-114 min (.2-.3 kms^{-1})

and Stein, 1981) around these frequencies. In their magnetographic observations, Gheonjian et al. (1990) found periodic oscillations in all of the line-intensity, line-width and the Doppler shifted line-centre fluctuations, and also in the variations of the line-of sight magnetic field component in prominences. They suggested, however, that only the fluctuations of the Doppler velocity may be of solar origin, while the periodic variations produced in other quantities may be caused by some wave phenomena in the terrestrial atmosphere. Tsubaki and Takeuchi (1986) and Tsubaki et al. (1987) conjectured that the intermediate to short period oscillations may be associated with particular structural parts of the prominence. Similar conclusions have also been drawn in the recent observations by Balthasar et al. (1988a, b), Thompson and Schmieder (1991), Yi Zhang and Engvold (1991), and Yi Zhang et al. (1991). Yi Zhang and his collaborators could

even resolve the fibril structures in prominences in both the HeI $\lambda 10830\text{Å}$ line-intensity and Doppler shift fluctuations. These authors further suggest that the intensity fluctuation lags behind the velocity fluctuation by a time that is approximately 1/3 of the oscillatory period.

Table 1.2(b). *Observations made to detect intermediate periodicities in prominences.*

Authors	Year of Publication	Spectral line chosen	Intensity	Line-width	Velocity
Malherbe et al.	1981	Hα	No	_	No
Malherbe et al.	1987	Hα, $\lambda 1548\text{Å}$ CIV	No	_	No
Tsubaki et al.	1987	CaII K	No	No	10 min (± 2-3 kms^{-1})
Balthasar et al.	1988a,b	Hα, $Ca^{+}H$, Hε	_	_	7-20 min
Yi Zhang et al.	1991	HeI $\lambda 10830\text{Å}$	12 min	_	9-16 min (± 0.5 kms^{-1})
Yi Zhang and Engvold	1991	HeI $\lambda 10830\text{Å}$	quasi-periodic variation	_	9, 14, 22 min

These special features of the observations of prominence oscillations are here mentioned only to keep a faithful recording of the observational results that may prove useful for future reference. These features are not well confirmed yet and it would therefore be unwise to attempt to incorporate all these detailed aspects in our theoretical modelling. Only the orders of magnitude of the periods of these oscillatory motions in prominences seem to be well confirmed, as can be seen from the observational results displayed in Tables 1.2(a)-(c).

In this thesis, we therefore propose to explain the basic timescales observed in prominence oscillations, considering the periods of the global magnetohydrodynamic modes of oscillation of prominence-like

Table 1.2(c). *Observations made to detect short period oscillations in prominences.*

Authors	Year of Publication	Spectral line chosen	Intensity	Line-width	Velocity
Engvold	1981	CaII K	No	_	No
Malherbe et al.	1981	Hα	No	_	No
Wiehr et al.	1984	Hα	No	_	3,5 min (± .2 kms^{-1})
Tsubaki and Takeuchi	1986	CaII K	No	No	210-240s (± 2 kms^{-1})
Balthasar et al.	1986	Hα	No	_	210-400s (± 2 kms-1)
Malherbe et al.	1987	Hα, λ1548Å CIV	No	_	No
Tsubaki et al.	1987	CaII K	240s (weak)	No	160s (±.8-1.4 kms^{-1})
Balthasar et al.	1988a,b	Hα, $Ca^{+}H$, Hε	_	_	3, 5 min, 110s
Gheonjian et al.	1990	Hα	_	_	5-6 min
Mashnich and Bashkirtsev	1990	Hβ	_	_	No
Thompson and Schmieder	1991	Hα	_	_	150, 200, 250s (±1 kms^{-1})
Yi Zhang et al.	1991	HeI λ10830Å	5 min	_	5 min

structures.The equilibrium models we consider are essentially simple and leave out many important factors, such as gravity and fine structure, that are present in real prominences. This simplicity of our model allows us to obtain analytical expressions for the order of magnitude estimates of the periods of oscillations. Moreover, it enables us to draw on analogies with the modes of vibration of some classical oscillatory systems, thus providing an insight into the physical nature of the modes. The order of magnitude of the periods we calculate are expected to be unchanged even in the case of more realistic prominence models, although precise numerical values may alter somewhat in these more complex situations. Our calculations with simple prominence models are therefore offered in the hope that they will serve as useful guides even in such complicated and (presumably) entirely numerical calculations for the modes of oscillation of realistic magnetohydrostatic prominence equilibria.

Before we proceed further with our discussion of the magnetohydrodynamic modes of oscillation in prominences, it is convenient to summarize the important properties of MHD waves in a uniform medium, and also highlight some of the important works that have been done on the applications of the MHD wave theory in more complicated inhomogeneous plasmas as are commonly found in both solar and astrophysical situations. Only a brief overview is given in the following subsection. More detailed discussions on the recent advances in MHD wave theory can be found in the reviews by Roberts (1984, 1985, 1989, 1990a,b; 1991a,b,c; 1992).

1.3 Magnetohydrodynamic waves

1.3.1. Basic equations: The macroscopic state of an energetically isolated, perfectly conducting fluid in a magnetic field is generally described by the single-fluid, ideal magnetohydrodynamic (MHD) equations (eg. Alfven, 1950; Cowling, 1957; Roberts, 1967; Parker, 1979; Priest, 1982). For the static equilibrium (steady) state of a gravitationally stratified fluid, these MHD equations take the following forms.
The magneto-hydrostatic force balance equation is:

$$-\nabla p_0 - \rho_0 g \hat{\mathbf{z}} + \frac{1}{4\pi}(\nabla \times \mathbf{B_0}) \times \mathbf{B_0} = 0, \qquad (1.1)$$

the divergence-free condition for the applied magnetic field is:

$$\nabla . \mathbf{B_0} = 0, \tag{1.2}$$

and the adiabatic equation of state of the fluid is:

$$p_0 = \text{constant } \rho_0^{\gamma} . \tag{1.3}$$

In (1.1)-(1.3), p_0 (x,y,z), ρ_0 (x,y,z) and $\mathbf{B_0}$(x,y,z) are the pressure, density, and the magnetic field of the plasma in equilibrium, and γ is the ratio of specific heat of the gas, whose value is taken to be 5/3 throughout in this thesis. The acceleration due to gravity, $-g\hat{\mathbf{z}}$, is taken as constant with the unit vector $\hat{\mathbf{z}}$ pointing vertically upwards.

To investigate the propagation of linear hydromagnetic waves in such a fluid, we consider the linearized form of the MHD equations that represent small amplitude perturbations about the equilibrium state described in Eqs. (1.1)-(1.3). The linearized equations are as follows. The equations describing the conservation of mass, momentum and energy are

$$\frac{\partial \rho}{\partial t} + (\mathbf{v}.\nabla)\rho_0 + \rho_0(\nabla.\mathbf{v}) = 0, \tag{1.4}$$

$$\rho_0 \frac{\partial \mathbf{v}}{\partial t} = - \nabla p + \frac{1}{4\pi}(\mathbf{b}.\nabla)\mathbf{B_0} + \frac{1}{4\pi}(\mathbf{B_0}.\nabla)\mathbf{b} - \nabla\left(\frac{\mathbf{B_0}.\mathbf{b}}{4\pi}\right) - \rho g \hat{\mathbf{z}}, \tag{1.5}$$

and

$$\frac{\partial p}{\partial t} + (\mathbf{v}.\nabla)p_0 - c_s^2\left\{\frac{\partial \rho}{\partial t} + (\mathbf{v}.\nabla)\rho_0\right\} = 0. \tag{1.6}$$

The induction equation is

$$\frac{\partial \mathbf{b}}{\partial t} = \nabla \times (\mathbf{v} \times \mathbf{B_0}), \tag{1.7}$$

and the divergence-free condition for the perturbed magnetic field yields

$$\nabla.\mathbf{b} = 0. \tag{1.8}$$

Here $\mathbf{v} = (v_x, v_y, v_z)$ is the velocity perturbation, $\mathbf{b} = (b_x, b_y, b_z)$ is the magnetic field perturbation, $c_s(x,y,z) = \left(\gamma p_0(x,y,z)/\rho_0(x,y,z)\right)^{1/2}$ is the sound speed, and p and ρ are the perturbations in the gas pressure and the mass density, respectively, at time t. We are using the cgs system of units.

In the following, we consider the simplest case of an unstratified medium (g=0). We further assume that the medium is uniform ($\mathbf{B_0}$, p_0 and ρ_0 are constants) and is of infinite extent in y and z-directions. For small amplitudes of the perturbations, we can also express the perturbations as the superposition of independent Fourier components or modes, each of which can be written in the form

$$\Psi(x,y,z,t) = \Psi(x) \exp\left\{ i\omega t + ik_y y + ik_z z \right\}, \tag{1.9}$$

with ω being the frequency, and k_y and k_z being the y and the z components of the wavevector of the Fourier mode.

In terms of Fourier components, we can rewrite Eqs.(1.4)-(1.8) as

$$i\omega\rho + \rho_0\left\{\frac{dv_x}{dx} + ik_y v_y + ik_z v_z\right\} = 0 , \tag{1.10}$$

$$i\omega\rho_0 v_x = -\frac{dp}{dx} + \frac{1}{4\pi}\left(B_{0x}\frac{d}{dx} + iB_{0y}k_y + iB_{0z}k_z\right) b_x - \frac{d}{dx}\left(\frac{\mathbf{B_0}\cdot\mathbf{b}}{4\pi}\right), \tag{1.11a}$$

$$i\omega\rho_0 v_y = -ik_y p + \frac{1}{4\pi}\left(B_{0x}\frac{d}{dx} + iB_{0y}k_y + iB_{0z}k_z\right) b_y - ik_y\left(\frac{\mathbf{B_0}\cdot\mathbf{b}}{4\pi}\right), \tag{1.11b}$$

$$i\omega\rho_0 v_z = -ik_z p + \frac{1}{4\pi}\left(B_{0x}\frac{d}{dx} + iB_{0y}k_y + iB_{0z}k_z\right) b_z - ik_z\left(\frac{\mathbf{B_0}\cdot\mathbf{b}}{4\pi}\right), \tag{1.11c}$$

$$p = c_s^2\rho , \tag{1.12}$$

$$i\omega b_x = ik_y\left(v_x B_{0y} - v_y B_{0x}\right) - ik_z\left(v_z B_{0x} - v_x B_{0z}\right) , \tag{1.13a}$$

$$i\omega b_y = ik_z\left(v_y B_{0z} - v_z B_{0y}\right) - \left(B_{0y}\frac{dv_x}{dx} - B_{0x}\frac{dv_y}{dx}\right), \tag{1.13b}$$

$$i\omega b_z = \left(B_{0x}\frac{dv_z}{dx} - B_{0z}\frac{dv_x}{dx}\right) - ik_y\left(v_y B_{0z} - v_z B_{0y}\right), \qquad (1.13c)$$

and

$$\frac{db_x}{dx} + ik_y b_y + ik_z b_z = 0. \qquad (1.14)$$

1.3.2 MHD wavemodes in an infinitely uniform medium: For an infinite medium, we can substitute ik_x for $\frac{d}{dx}$, and write the magnitude of the total wavevector $\mathbf{k}$ as $k = |\mathbf{k}| = \left(k_x^2 + k_y^2 + k_z^2\right)^{1/2}$. Eqs. (1.10), (1.11), (1.13) and (1.14) then become

$$\omega\rho + \rho_0(\mathbf{k}.\mathbf{v}) = 0, \qquad (1.15)$$

$$\omega\rho_0\mathbf{v} = -\mathbf{k}p + \frac{1}{4\pi}(\mathbf{B_0}.\mathbf{k})\mathbf{b} - \mathbf{k}(\mathbf{B_0}.\mathbf{b}), \qquad (1.16)$$

$$\omega\mathbf{b} = \mathbf{k} \times (\mathbf{v} \times \mathbf{B_0}), \qquad (1.17)$$

and

$$\mathbf{k}.\mathbf{b} = 0. \qquad (1.18)$$

Equations (1.15)-(1.18), together with Eq.(1.12), allows three distinct types of hydromagnetic wavemodes for an infinite uniform medium. These modes are (a) the *Alfven mode*, and (b) the *(slow and fast) magnetoacoustic modes.*

(a) *Alfven mode.* Alfven waves are transverse ($\mathbf{k}.\mathbf{v} = 0$) in character. From Eqs. (1.15) and (1.12) we find that these waves are also incompressible with $\rho = p = 0$. Taking the vector product of equations (1.16) and (1.17) with the total wavevector $\mathbf{k}$, we obtain (for $|\mathbf{k} \times \mathbf{v}| \neq 0$)

$$\omega^2 = \frac{(\mathbf{k}.\mathbf{B_0})^2}{4\pi\rho_0} = k^2 v_A^2 \cos^2\theta, \qquad (1.19)$$

which is the dispersion relation for Alfven modes. Here $v_A = \frac{B_0}{(4\pi\rho_0)^{1/2}}$ is the Alfven speed and θ is the angle subtended by the propagation vector $\mathbf{k}$ with the magnetic field $\mathbf{B_0}$. The Alfven waves have a constant field-aligned phase propagation speed given by the Alfven speed v_A. With the help of the dispersion relation (1.19), Eqs. (1.16) and (1.17) further yield

$$\mathbf{v}.\mathbf{B_0} = 0 \tag{1.20}$$

and

$$\mathbf{v} = \pm \frac{\mathbf{b}}{(4\pi\rho_0)^{1/2}}, \tag{1.21}$$

showing that the velocity perturbation $\mathbf{v}$ and the magnetic field perturbation $\mathbf{b}$ pertaining to the Alfven modes are in the same direction, both being perpendicular to the plane containing the wavevector $\mathbf{k}$ and the unperturbed magnetic field vector $\mathbf{B_0}$.

(b) *Magnetoacoustic modes.* When $\mathbf{k}.\mathbf{v} \neq 0$, elimination of p, ρ, and $\mathbf{b}$ from Eqs.(1.12) and (1.15)-(1.18) yields

$$\omega^2\mathbf{v} = c_s^2\mathbf{k}\,(\mathbf{k}.\mathbf{v}) + \frac{1}{4\pi\rho_0}\{(\mathbf{k}.\mathbf{B_0})\mathbf{a} - \mathbf{k}(\mathbf{B_0}.\mathbf{a})\}, \tag{1.22a}$$

where we have written

$$\mathbf{a} = (\mathbf{k}.\mathbf{B_0})\mathbf{v} - (\mathbf{k}.\mathbf{v})\mathbf{B_0}. \tag{1.22b}$$

The scalar products of Eq.(1.22) with $\mathbf{k}$ and $\mathbf{B_0}$ lead to the dispersion relation for the magnetoacoustic waves. This magnetoacoustic dispersion relation is

$$\omega^4 - \omega^2k^2\,(c_s^2+v_A^2) + k^2c_s^2\,\frac{(\mathbf{k}.\mathbf{B_0})^2}{4\pi\rho_0} = 0\,; \tag{1.23a}$$

we may rewrite this in the form

$$\omega^4 - \omega^2 k^2 c_f^2 + k^4 c_s^2 v_A^2 \cos^2\theta = 0, \qquad (1.23b)$$

where $c_f = (c_s^2 + v_A^2)^{1/2}$ is the so-called 'fast speed' of the medium. Eq. (1.23) may be solved thus:

$$\frac{\omega^2}{k^2} = \frac{1}{2} c_f^2 \left\{ 1 \pm \left(1 - \frac{4 c_T^2}{c_f^2} \cos^2\theta \right)^{1/2} \right\}, \qquad (1.24)$$

where $c_T = \frac{c_s v_A}{c_f}$ is the 'cusp speed'. The two solutions in Eq.(1.24) correspond to the *fast* and *slow magnetoacoustic modes*, respectively.

For propagation along the magnetic field, $\theta = 0$ and $\omega^2 = k^2 c_s^2, k^2 v_A^2$. Propagation perpendicular ($\theta = \pi/2$) to the field direction yields $\omega^2 = k^2 c_f^2$ for the fast mode and $\omega^2 = 0$ for the slow mode. In fact, the field-aligned phase speed $\omega/(k\cos\theta)$ of the slow mode approaches the cusp speed c_T as $\theta \to \pi/2$. The slow waves, like Alfven waves, have therefore highly anisotropic propagation characteristics and cannot propagate across the magnetic field.

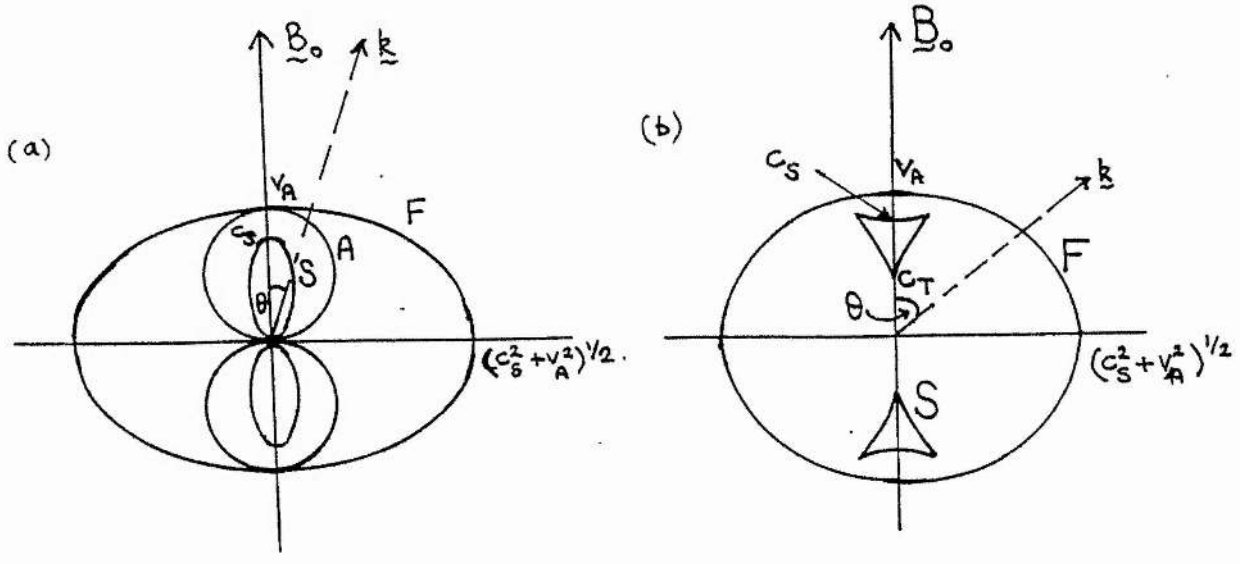

Fig. 1.2. The (a) phase speed and (b) group velocity of magnetohydrodynamic waves in the case $v_A > c_s$.

On the other hand, the fast waves acquire their greatest phase-speed ($c_f > c_s, v_A$) when propagating across the field. These propagation characteristics of the three MHD wavemodes are shown in polar form in Fig. 1.2, where we sketch both the phase speeds ω/k and the group velocity $\mathbf{c_g} \equiv \partial\omega/\partial\mathbf{k}$ of the three MHD waves in the particular case $v_A > c_s$. In Table 1.3, we also reproduce a useful summary of the properties of these modes given by Roberts (1985).

Table 1.3. *Properties of the three MHD waves of infinite, uniform medium (after Roberts, 1985).*

Wave	Characteristics
Alfven	Driven by tension forces; no pressure or density variations; motions transverse to both the applied magnetic field and the direction of propagation. Anisotropic, unable to propagate across the field; energy flows along the field at the Alfven speed.
slow magnetoacoustic	Driven by tension and pressure forces; involves pressure and density variations; gas and magnetic pressure variations are out of phase. Anisotropic, unable to propagate across the field; energy flow confined to near the magnetic field.
fast magnetoacoustic	Driven by tension and pressure forces; involves pressure and density variations; gas and magnetic pressure variations are in phase. Roughly isotropic, propagating fastest across the field. Forms an orthogonal triad with the other two modes.

1.3.3 MHD waves in inhomogeneous media: The apparently simple picture of the MHD waves in an infinitely uniform medium becomes highly complicated whenever the plasma medium is inhomogeneous or the magnetic field strength is dependent on the spatial co-ordinates. In the general case of a continually structured magnetic plasma, the linearized magnetohydrodynamic equations possess regular mobile singular points

that correspond to continuous spectra in MHD (eg. Appert et al. 1974; Adam, 1982, 1986; Goedbloed, 1983; Goossens et al. 1984, 1985). In fact, generally there are two continuous spectra, one associated with the Alfven wave (Alfven continuum) and the other associated with the slow magnetoacoustic wave (cusp continuum), both of which share the property in a uniform medium of being unable to propagate across the magnetic field (see Table 1.3). Continuous spectra, therefore, signal an anisotropic behaviour in disturbances, with the component of motion perpendicular to the magnetic field behaving differently from the component in the direction of the field. Small spatial scales are rapidly built up in disturbances and efficient damping (with subsequent heating) is likely to take place (Roberts, 1992; see also detailed discussions in Sedlacek, 1971; Uberoi, 1972; Chen and Hasegawa, 1974; Rae and Roberts, 1982; Heyvaerts and Priest, 1983; Noccera et al., 1984; Lee and Roberts, 1986; Davila, 1987; Hollweg, 1987a,b, 1990; Grossmann and Smith, 1988; Hollweg and Yang, 1988; Cally, 1991; Goossens, 1991; Goossens and Hollweg, 1993).

In several astrophysical situations, plasma inhomogeneities in the magnetic field appear in the form of well-defined, almost discrete structures rather than a slow, gradual variation of the magnetic field and plasma density, such as in the case of the large scale structures in the solar coronal plasma. While studying such structures, it may sometimes be useful to ignore the large but finite variation of the magnetic field or the plasma properties at the edges of these structures, and thus to consider their gradients to be infinite. The idealized sharply discontinuous structures can then be subjected to a normal mode analysis, thus revealing some of the important properties of the global oscillations of these structures. Such investigations of the magnetohydrodynamic modes of oscillation of discrete magnetic plasma structures are the subject of considerable interest in solar physics, see for example, the reviews in Roberts (1991b,c; 1992). An appreciable amount of work has therefore been done on the MHD oscillations of a single magnetic interface (eg. Wenzel, 1979; Roberts, 1981a; Uberoi, 1982; Somasundaram and Uberoi, 1982; Joarder et al., 1987; Miles and Roberts, 1989), and the waves in a magnetic slab or a cylindrical tube (eg. Roberts and Webb, 1978,1979; Wilson, 1980; Uberoi and Somasundaram, 1980, 1982; Roberts, 1981b; Spruit, 1982; Edwin and Roberts, 1982, 1983; Rae and Roberts, 1983; Roberts, Edwin and Benz, 1984; Cally, 1985, 1986; Davila, 1985; Abdelatif, 1988; Evans and Roberts, 1990a). We will discuss some of these results in

Chapter II. The effect of gravitational stratification on the MHD modes has also been examined, either in a plane parallel atmosphere with a horizontal magnetic field (eg. Yu, 1965; Nye and Thomas, 1974, 1976a, b; Thomas, 1982, 1983; Roberts and Campbell, 1986; Roberts, 1989; Campbell and Roberts, 1989; Evans and Roberts, 1990b, 1991; Miles and Roberts, 1992; Miles et al. 1992) or a vertical field (eg. Antia and Chitre, 1979; Zhugzhda, 1979; Scheur and Thomas, 1981; Leroy and Schwartz, 1982; Zhugzhda and Dzhalilov, 1982, 1984a,b; Hasan and Sobouti, 1987; Hasan and Abdelatif, 1990; Hasan and Christensen-Dalsgaard, 1992), or in a thin magnetic flux tube (eg. Defouw, 1976; Roberts and Webb, 1978, 1979; Webb and Roberts, 1978; Spruit, 1981, 1982; Spruit and Roberts, 1983; Rae and Roberts, 1982).

1.4. Elementary models of prominence oscillations

1.4.1. Oscillations in loop prominences: We now briefly discuss some of the earlier theoretical models that were proposed to explain the periodicities observed in prominence oscillations. Most of these models were developed to explain either the oscillatory motions in active loop prominences, or to explain the so-called 'winking phenomenon', which is the oscillation excited in prominences by the disturbances created by a solar flare; cf. Section 1.2.2.

Among the theoretical models of the oscillations in cylindrical loop prominences, Malville and Schindler (1981) provided an explanation of an observed 75s periodicity of the coupled torsional and longitudinal oscillations of an active prominence in terms of the marginally stable m=1 kink mode (eg. Kruskal and Tuck, 1958; Spicer, 1979; Hasan, 1979; Hood, 1985; 1990) in a current carrying, twisted flux tube. Also, Solovjev (1985) argued that the observed long period (about 1 hr, see Section 1.2.3) oscillations in quiescent prominences may also be due to the shear Alfven motions in a twisted flux rope supporting and surrounding the prominence.

A detailed and unified model of the oscillations, instability and eruption of active loop prominences is, however, provided by Vrsnak and his collaborators. Like Malville and Schindler (1981), these authors also calculated the stability properties of a twisted flux tube carrying an uniform line current at its centre (Vrsnak, 1984, 1990a,b; Vrsnak et al. 1988, 1990, 1991), but including the effects of curvature of the flux tube and also the photospheric boundary conditions in their model. The

predicted periods of oscillations (in the range 4 to 10 min) were found to be in good general agreement with the observations of oscillations in the pre-eruptive or post-eruptive phase of a loop prominence (Section 1.2.3). In a rigorous analysis, Vrsnak (1990b) also showed that the prominence eruption is dependent on its height. Beyond a certain height of the loop prominence above the photosphere, some crucial physical parameters such as the twist in the flux-tube and the ratio of the total current to the total mass of the loop attain their critical values at which non-equilibrium sets in. This description of prominence eruption is in qualitative agreement with the observations of Zirin (1988, see also Demoulin and Vial, 1992), who concluded that virtually every prominence that rises above 50, 000 km will erupt in 48 hours.

In this thesis we concentrate on the stable quiescent prominences that are traditionally thought to have a sheet-type structure rather than the twisted loop-type geometry considered by Malville and Schindler, Solovjev and Vrsnak et al. The helical structures seen occasionally in Hα emission lines from quiescent prominences (Malville, 1969; Anzer and Tandberg-Hanssen, 1970; Tandberg-Hanssen and Anzer, 1970; see also Tandberg-Hanssen, 1974), which might be an indication of the existence of twisted flux loops, is often observed clearly in the erupting (or dispartition brusque) phase of such prominences (eg. Tandberg-Hanssen, 1974; Wang, 1985; Kurokawa et al., 1987; Schmieder, 1989; Schmieder et al. 1985; Vrsnak, 1990a, b; Vrsnak et al. 1988) though rarely, if ever, observed in the stable, quiescent phase of a prominence (cf. Zirker, 1989). It may be of some relevance to note that the recent giant flux tube model of a prominence by Priest, Hood and Anzer (1989) (see section 1.1.3 and Fig. 1.1(c)) is an attempt to incorporate both the cylindrical and the sheath-like structure in a single model. In its stable phase, the giant flux tube supporting and surounding the prominence, is not visible because of the low density and, therefore, low emissivity of the flux tube. The flux tube structure of the magnetic field reveals itself only when increasing twist makes the prominence unstable and the prominence material fills up the flux tube in its erupting phase (Priest, 1990). The Priest et al. model will not be discussed further in this thesis. Apart from the mathematical difficulty of analyzing such a complicated model, it has a drawback in that it does not include the internal structure of the prominence sheet and only predicts a dip in the magnetic field geometry that supports the prominence.

1.4.2. Models of winking filaments: Quiescent prominences may be set in damped oscillations due to the impact of shock waves generated by solar flares. Such oscillations may be either in the vertical or in the lateral direction, and are commonly referred to as the 'winking' phenomenon (cf. Section 1.2.2). Winking filaments have been investigated theoretically by Athay and Moreton (1961), Malville (1961), Anderson (1966), Hyder (1966), Meyer (1968), Uchida (1968, 1970) and Kleczek and Kuperus (1969). Two principal models of such oscillations have thus emerged. They are: (a) model for vertical oscillations by Hyder (1966), and (b) model for horizontal oscillations by Kleczek and Kuperus (1969). We briefly discuss these two models in the following.

(a) *Model for vertical oscillations.* Hyder (1966) assumed that the vertical component B_z of the supporting magnetic field of a prominence sheet increases due to a downward displacement δz of the prominence according to the linear relationship

$$\delta B_z = - \frac{B_z \delta z}{H}, \tag{1.25}$$

with $H \approx 10^4$ km being the height of the prominence. Under such a condition, the vertical oscillations of a prominence sheet of mass $M_{prom} \approx 10^{15}$ g can be described by the equation of motion of a damped harmonic oscillator, the frequency of which may be written as:

$$\nu_{osc} = \frac{1}{2\pi} \left(\frac{K_z}{M_{prom}} - \gamma_v^2 \right)^{1/2}, \tag{1.26}$$

where K_z is the restoring force per unit length and γ_v is a damping constant due to the viscous forces in the ambient corona. In Eq. (1.26), the ratio K_z/M_{prom} can be expressed in terms of the tension force, which, under the condition (1.25), takes the form

$$\frac{K_z}{M_{prom}} = \left(\frac{B_z}{H} \right)^2 \frac{1}{\pi \rho_0}, \tag{1.27}$$

with $\rho_0 \approx 10^{-11}$ gcm^{-3} being the density inside the prominence sheet. The damping constant γ_v in Eq. (1.26) may be expressed in terms of the coronal coeffecient of viscosity η as:

$$\gamma_v = \frac{\eta A}{2Md} \cdot \tag{1.28}$$

Here, $A \approx 10^{20}$ cm^2 is the area of the large face of the prominence and $d \approx 10^9$ cm is an assumed distance perpendicular to A over which the magnetic shear exists in the coronal plasma (due to the vertical oscillation of the prominence).

Hyder substituted the observed values of $\nu_{osc} \approx 10^{-3}$ s^{-1} and $\gamma_v \approx 10^{-3}$ s^{-1} in Eqs. (1.27) and (1.28) to obtain $B_z \approx 10$G for the vertical component of the magnetic field strength in the prominence, and $\eta \approx 30$ cgs (dyne.s cm^{-2}) for the coeffecient of viscosity in the ambient corona. To derive the value of the coronal magnetic field strength (B_c) from the oscillation data, Hyder further substituted the value of η in a formula (cf. Linhart,1960)

$$\eta = 4.8\ 10^{-16} \frac{n_e^2}{B_c^2 T_c^{1/2}} \cdot \tag{1.29}$$

For a coronal electron density $n_e \approx 10^9$ cm^{-3} and a coronal temperature $T_c \approx 10^6$ K, Eq. (1.29) ultimately gives a value $B_c \approx .13$G for the magnetic field strength in the coronal environment of a prominence.

The coronal and prominence magnetic field strengths derived from Hyder's model are far from the values that may be inferred from modern observations. However, Hyder was the first to indicate the potential seismological value of the study of prominence oscillations.

It may be of some interest here to note that Roberts (1991c, see also Joarder and Roberts,1992a) has suggested a simple analogy of the vertical oscillations of a prominence with the gravitational oscillations of a point mass M_{prom} that is supported by an elastic string of natural length ℓ_0 and tension T_0. Although viscous damping is not included in this model, it is essentially similar to the model proposed by Hyder (1966). In the following, we consider this model in some detail.

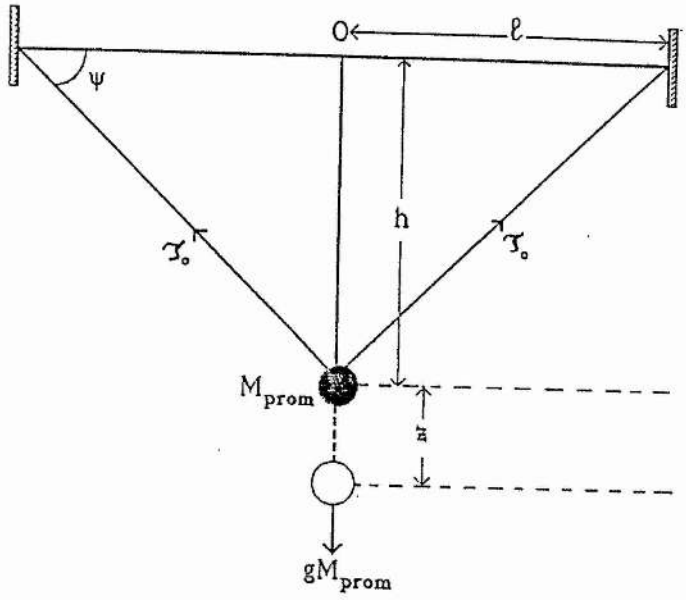

Fig. 1.3. The gravitational oscillation of a stretched string loaded with a heavy point-mass M_{prom} at its centre.

Consider the mass M_{prom} to be in equilibrium under gravity when a distance h below the horizontal, the string then subtending an angle Ψ to the horizontal (see Fig. 1.3). The distance between the end points of the string is $2\mathfrak{l}$. In such an equilibrium state

$$2\mathcal{T}_0 \sin\Psi = gM_{prom}\,, \tag{1.30}$$

giving

$$gM_{prom} = 2\lambda h\left[1 - \frac{\mathfrak{l}_0}{\left(\mathfrak{l}^2+h^2\right)^{1/2}}\right] \approx \frac{2\lambda h}{\mathfrak{l}}[\,\mathfrak{l} - \mathfrak{l}_0], \tag{1.31}$$

where λ is the elastic constant of the string of a natural length $\mathfrak{l}_0$, and $h << \mathfrak{l}$.

If a small vertical displacement z is applied to the mass, then the equation of motion is approximately

$$z'' + \frac{2\lambda z}{M_{prom}}\left[1 - \frac{\mathfrak{l}^2\mathfrak{l}_0}{\left(\mathfrak{l}^2+h^2\right)^{3/2}}\right] = 0. \tag{1.32}$$

The frequency ω of oscillation is thus given by

$$\omega^2 \approx \frac{2\lambda}{M_{prom}}\left[1 - \frac{\ell_0}{\ell}\right] \approx \left(\frac{g}{h}\right), \tag{1.33}$$

giving a period of

$$\tau_{gravity} \approx 2\pi\left[\frac{\ell}{g}\tan\Psi\right]^{1/2}. \tag{1.34}$$

Eq. (1.33) is, in fact, also similar to the frequency of oscillation calculated for prominences by Kuperus and Raadu (1974), in which the distance h is the height of the prominence mass over the solar photosphere (Fig. 1.1(b)). Considering an end-point separation distance $2\ell \approx$ 50,000 - 150,000 km, a solar gravity g=0.274 kms^{-2}(eg. Priest, 1982), and a field-line angle of about 10^o we again obtain, from Eq. (1.34), a $\tau_{gravity} \approx$ 20-30 min that is similar to the periods given by Hyder (1966) and Kuperus and Raadu (1974).

In this thesis we have mainly confined ourselves to the non-gravitational, magnetohydrodynamic calculations. It would, of course, be of some interest to see whether the improvements of our magnetohydrodynamic slab model, that we mainly discuss in this thesis, can indeed provide a periodicity similar to Eq. (1.34) for any of the modified fundamental MHD modes in the presence of gravity. Such a calculation, of course, faces an obvious difficulty of finding a simple magnetostatic equilibrium model that can be investigated in an analytical way.

(b) *Models for horizontal oscillations.* Kleczek and Kuperus (1969) provided a model for the horizontal vibrations of a prominence sheet that are excited by external sources, such as the shock waves generated by a solar flare. The vibrations discussed by Kleczek and Kuperus, are essentially due to the 'leaky magnetoacoustic wavemodes' (Roberts and Webb, 1979; Spruit, 1982; Davila, 1985; Cally, 1985, 1986) that would have been excited initially in a prominence-coronal system due to flare disturbances, provided the corona were of infinite extent on either side of the prominence slab; see detailed discussions in Chapter II.

In their original model, Kleczek and Kuperus considered the vertical prominence sheet to be hit broadside by the flare disturbance and displaced horizontally from its equilibrium position. They approximated

the supporting magnetic field of the prominence by an effective field **B** along the long axis of the prominence and anchored in fixed positions. The horizontal restoring force per unit displacement K_x is then given by the magnetic tension force per unit length $\frac{1}{4\pi}(\mathbf{B}.\nabla)\mathbf{B}V \approx (B^2/\pi L^2)V$, with L being the length and V the volume of the prominence. The motion of the prominence can again be described by the equation of motion of a damped harmonic oscillator, the damping now being due to the radiation of acoustic (or more precisely, magnetoacoustic) waves that propagate into the coronal plasma at the expense of the kinetic energy of oscillation of the prominence sheet. If we ignore the effect of this damping on the frequency of the prominence, the period of oscillation is simply given by

$$\tau \approx 2\pi L B^{-1}\sqrt{\pi\rho_0}. \qquad (1.35)$$

Kleczek and Kuperus considered $L \approx 10^5$ km, $\rho_0 \approx 10^{-14}$ gcm^{-3} and a magnetic field strength $B \approx 9$G, giving a value of about 20 min for the period τ. For the damping constant γ_R, they considered Rayleigh's model for the acoustic radiation from a circular piston (Lindsey, 1960) to obtain

$$\gamma_R = \frac{\rho_0 c_s A}{M_{prom}}\left[1 - \frac{J_1(2ka)}{ka}\right], \qquad (1.36)$$

where $J_1(x)$ is the Bessel function of first order (eg. Abramowitz and Stegun, 1964), $c_s \approx 1.5\ 10^7$ cms^{-1} is the acoustic speed in the corona (say), $A = \pi a^2 = LH$ is the surface area of the large face of the prominence and k is the wavenumber of the acoustic wave radiated in the ambient corona. For acoustic waves of period 20 min, Kleczek and Kuperus thus obtained a value of $\gamma_R \approx 4\ 10^{-4}$ s^{-1}.

It is of some interest here to note a somewhat similar, (though non-damping) model of prominence oscillations proposed recently by Roberts (1991c) and Joarder and Roberts (1992a,c). In this model, the prominence oscillations are viewed as the vibrations of an elastic rectangular sheet, with its magnetic field lying essentially along the long axis of the sheet. The period of the (m,n)-th mode of the thin sheet can be written by following Rayleigh (1877) as

$$\tau_{m,n} = 2/\left(\frac{m^2}{L^2} + \frac{n^2}{H^2}\right)^{1/2} c\,, \qquad (1.37)$$

where c, the elastic speed within the sheet, is identified with the fast magnetoacoustic speed $c_f = (c_s^2 + v_A^2)^{1/2}$ (see Section 1.3.2) within the prominence plasma. The mode numbers m,n (=1,2,3.....) describe the various geometrical patterns of vibration of the sheet.

A quiescent prominence is characterized by $H^2 << L^2$; for example, the height H=5 10^4 km and the length L=2 10^5 km. Thus the period τ tends to be determined principally by the integer n describing the vertical structure of the modes. To illustrate, with c_f = 27 kms^{-1} (consistent with a sound speed c_s = 15 kms^{-1} and an Alfven speed v_A=23 kms^{-1}) we obtain

$$\tau = 60.7/\left(n^2 + \frac{m^2}{16}\right)^{1/2} \text{ minutes.} \qquad (1.38)$$

Thus, the n=1 mode gives τ = 59-34 minutes for harmonics with m=1-6; the n=2 mode gives 30-24 minutes for m=1-6. We again find modes with periods of the order of an hour, consistent with the long-period oscillations observed in quiescent prominences.

In Chapter II of this thesis, we calculate in detail the modes of oscillation of a thin sheet-like structure that is subjected to a three-dimensional perturbation (see also Joarder and Roberts, 1992a). The sheet is taken to be permeated by an uniform longitudinal magnetic field. We show that the magnetic sheet can sustain *fast magnetoacoustic surface modes* that are somewhat similar to the long period modes discussed by Kleczek and Kuperus (1969) and Roberts (1991c). The presence of fast magnetoacoustic surface waves in slab geometries has been discussed in Roberts (1981a,b), Edwin and Roberts (1982) and Rae and Roberts (1983), though without reference to prominence oscillations.

1.4.3. Importance of the transverse magnetic field component: The magnetic field in a prominence is, however, not purely longitudinal but is inclined at a fine angle of approximately 20° to the long axis of the prominence (see section 1.1.2). With an average magnetic field strength of about 12G (Jensen and Wiik, 1990; see Table 1.1), this produces a dominant longitudinal component of about 10-11G and a weaker

transverse field component of about 3-5G. The presence of this weaker magnetic field component transverse to the slab axis qualitatively changes the oscillatory modal structure of the thin magnetic slab from that found when the magnetic field is purely longitudinal. In particular, the order of the governing differential equation is raised, as was first indicated by Schwartz and Bel (1984a,b) in a somewhat different context. The increased order of the differential equation gives rise to the need for additional boundary conditions, and this is where the effects of *photospheric line-tying* of the prominence magnetic field come in.

The physical processes involved in line-tying are not completely clear. It is generally agreed, that the magnetic field supporting and surrounding the prominence (such as a coronal magnetic arcade in the direct-polarity, Kippenhahn-Schluter-type prominence model of Fig. 1.1a) must be, in some way, anchored in the underlying photosphere, where the extremely dense photospheric material with $\rho_{corona}/\rho_{photosphere} < 10^{-8}$ should restrict the free movements of the field lines. Considerable contoversy, however, remains on the exact nature of such constraining forces (eg. Bray et al. 1991). A weak constraint, advocated by Van Hoven et al. (1981) is to demand that the displacement perpendicular to the magnetic field, $\xi_{\perp}$, vanish. This choice has been criticized by An (1984), Rosner et al. (1984) and Hood (1985, 1986a,b, 1989, 1990) who argue that as both the sound speed c_{sp} ($\approx$ 10 kms^{-1}) and the Alfven-speed v_{Ap} ($\approx$ .01-10 kms^{-1}) in the photosphere are much less than the corresponding speeds ($c_{se} \approx$ 100-200 kms^{-1}, $v_{Ae} \approx 10^3$-10^4 kms^{-1}) in the corona, the photosphere is likely to take a long time to respond to coronal disturbances, and therefore, displacements that are either perpendicular (supposedly governed by Alfven travel time) or parallel (supposedly governed by sound travel time) to the magnetic field, and are generated in the corona, will vanish at the photospheric interface. According to this argument, the correct line-tying boundary condition should thus read $\xi = 0$, where ξ is the net displacement of the footpoints of the magnetic field-lines. This choice for the line-tying boundary condition was considered by Raadu (1972) and Hood and Priest (1979).

In the remainder of this thesis, we consider the boundary condition of Raadu (1972) and Hood and Priest (1979) without any further justification, inspite of the fact that the above time-scale arguments given in favour of this condition may not be entirely satisfactory and therefore an examination of the effects of different photospheric boundary

conditions on the modes of oscillation of a prominence would form a topic for future investigation.

Coming back to our discussion of the magnetohydrodynamic modes of oscillation of the prominence slab, the detailed nature of the new type of oscillation spectrum of the magnetic slab, that arises in the presence of a magnetic field component that is transverse to the prominence axis, and also constrained by photospheric line-tying, is the subject matter of our discussion in Chapter III and onwards (see also Joarder and Roberts, 1992b, 1993b; Roberts and Joarder, 1993). We may, however, gain some insight into the nature of the (non-gravitational) MHD modes of oscillation of a two dimensional slab (sheet) in a purely transverse, line-tied magnetic field from an elementary analogy of a vibrating mass M in a taut elastic string of length 2ℓ under tension $\mathcal{T}$ (Roberts, 1991c; Joarder and Roberts, 1992b). The frequency ω of the fundamental vibration of such an elastic string is given by Rayleigh (1877). In the case where the mass of the string can be ignored compared to the mass M, this frequency is determined by

$$\omega^2 = \left(\frac{2\mathcal{T}}{M\ell}\right). \tag{1.39}$$

If we now consider the mass M to be uniformly distributed over a length 2a with a mass density ρ_0 per unit length, the period of oscillation $\tau = 2\pi/\omega$ is given by (see Lamb, 1910)

$$\tau = \pi\left(\frac{2M\ell}{\mathcal{T}}\right)^{1/2} = \frac{2\pi}{c}(\ell a)^{1/2}, \tag{1.40}$$

where $c = (\mathcal{T}/\rho_0)^{1/2}$ is a natural wave speed of the system. Considering a prominence width 2a = 5000 km, a string length 2ℓ = 50,000-150,000 km, an acoustic speed c_s = 15 kms^{-1} and Alfven speed v_A =23 kms^{-1} inside the prominence, we then obtain a period $\tau_s \approx$ 55-96 min for the slow mode, and a period $\tau_f \approx$ 40-60 min for the fast mode, the propagation vector of both the modes being in the direction of the field lines. The periods presented by these two modes are thus well within the range of the observed long period oscillations in prominences (see section 1.2). In this elastic string analogy of prominence oscillations, the long period fast mode

produces a transverse (vertical) oscillation of the prominence, whereas, the long period slow mode produces a lateral (compressional) oscillation in the direction of the magnetic field.

The above analogy of the vibration of a mass attached to a stretched elastic string has proved to be particularly useful in our analysis of the magnetohydrodynamic modes of oscillation of a prominence-sheet, as will be shown in Chapters III and V. It will there be demonstrated that modes similar to those described by Eq.(1.40) are present in the plasma sheet, even when the magnetic field threading the sheet is not purely transverse, but makes a very small angle to the long axis of the plasma sheet, as is the situation in quiescent prominences.

1.5 A non-gravitating MHD slab model of prominence oscillations.

Finally, in this section we describe the principal model of a solar quiescent prominence that we examine in this thesis to describe the magnetohydrodynamic modes of oscillation of a prominence. The idealized prominence model that we here analyze is, in fact, derived through a series of simplifications over a more realistic description of a quiescent prominence. In Fig. 1.4, we present a standard description of quiescent prominences, that represents reasonably well the situations observed in prominences with simplest magnetic topology, namely, the direct-polarity prominences; cf. Section 1.1.3. This figure is, in fact, a generalization of the two-dimensional Kippenhahn-Schlüter-type model of a quiescent prominence that was given in Fig. 1.1(a).

In Fig. 1.4, the arch-like prominence is imbedded in a hot corona, and also overlies an inversion line of the photospheric magnetic field. The prominence-arch is generally connected to the photosphere by several feet. The prominence material is supported against gravity by the electromagnetic Lorentz force ($\mathbf{F} = \mathbf{J}\times\mathbf{B}$), that arise due to the interaction of the large scale current-sheath (resulting from the inversion of the line-of-sight photospheric magnetic field) with the almost horizontal magnetic field lines at the top of a coronal magnetic arcade threading the prominence. The arcade magnetic field is also supposed to possess a small dip at the site of the prominence, see Section 1.1.2. This three-dimensional magnetic arcade is considered to be almost semi-circular in cross section, with its footpoints being anchored in the opposite magnetic polarity regions of the dense photosphere. The coronal arcade is also somewhat

sheared, with its field lines lying in planes that are inclined at a small angle $\phi \approx 20^{o}$ with the prominence-axis (Y-axis), see Fig. 1.4.

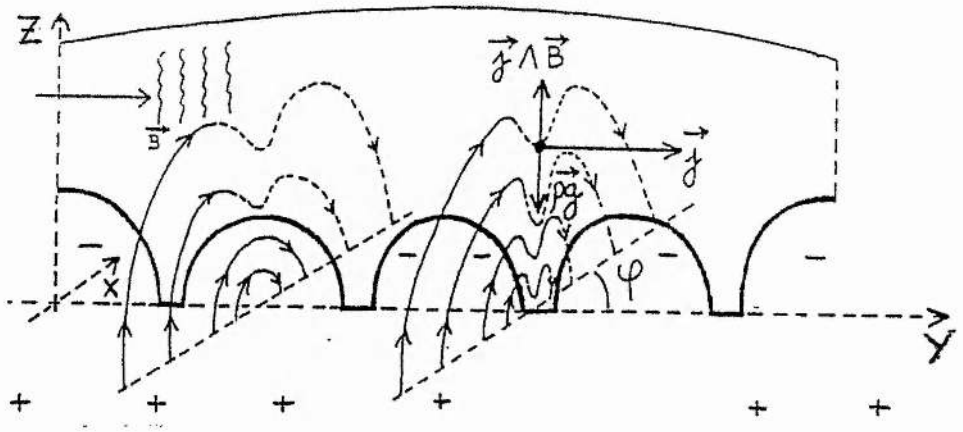

Fig. 1.4 Schematic of a prominence embedded in the corona overlying an inversion line of the photospheric magnetic field (+/-). Solid lines represent the arch boundaries of the filament, while dashed lines represent magnetic field-lines supporting the prominence (*After Schmieder, 1989*).

In our idealized, non-gravitating prominence model displayed in Fig. 1.5, we ignore the curvature of the prominence-arch (Fig. 1.4), thus approximating the prominence as a plane-parallel, uniform magnetic plasma slab embedded in a hotter and rarer coronal medium. Here, we also ignore the existence of the feet that connect the prominence material to the photosphere. The prominence slab is taken to be of thickness 2a in the X-direction, of length L in the Y-direction, and of height H in the Z-direction. The dimensions of the slab satisfies the condition $2a << H, L$. This condition allows us to consider the further simplification of one-dimensionality in our equilibrium configuration, where we treat all the equilibrium quantities to be independent of Y and Z. The effect of finite edges of the slab in these two directions are considered through a three dimensional perturbation; see Chapter II.

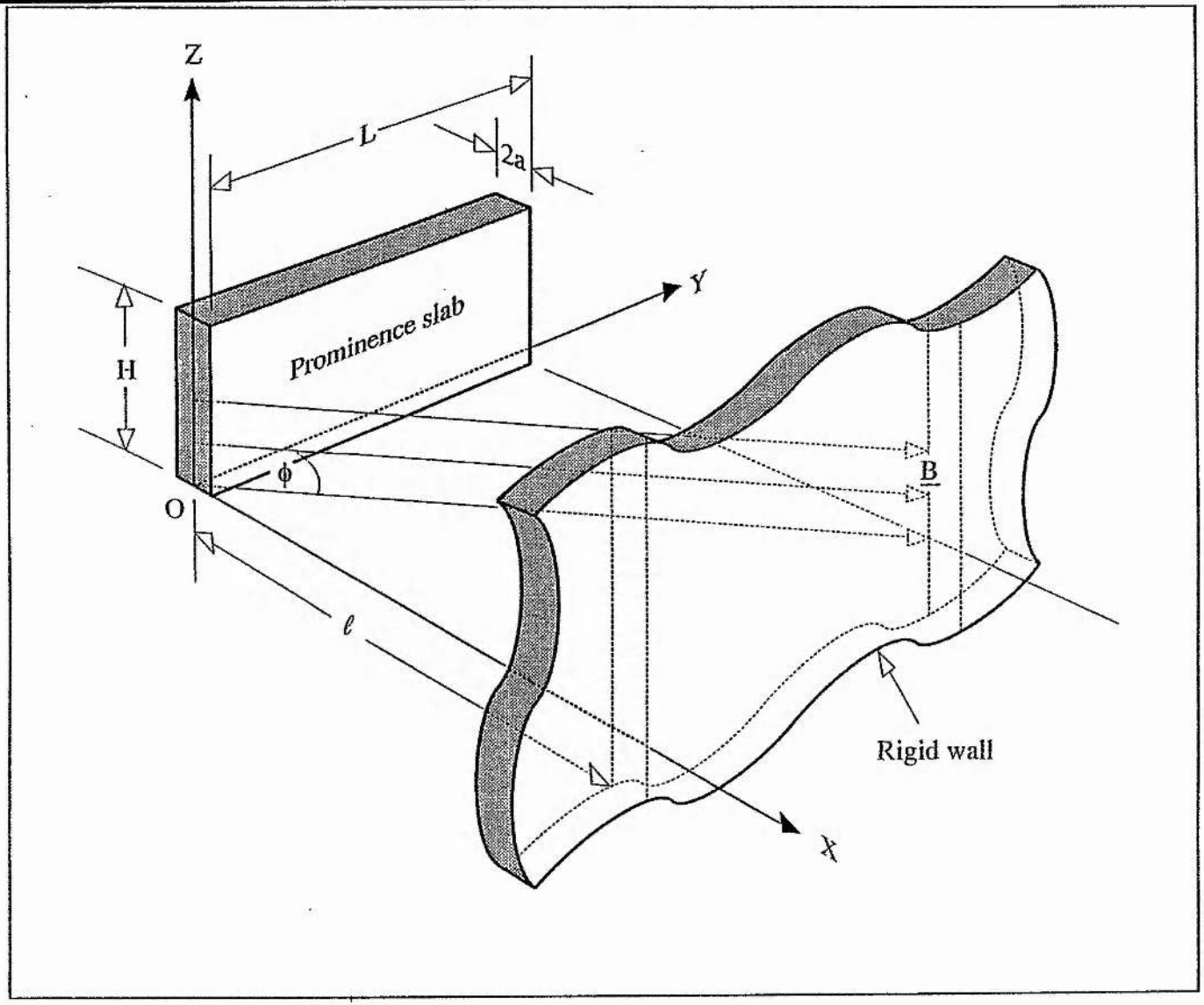

Fig. 1.5. The non-gravitating, plane-parallel magnetic slab model of a prominence.

In this non-gravitational prominence model of Fig. 1.5, we ignore the dip at the top of the magnetic arcade that supports the prominence material against gravity (see Fig. 1.4). As the field lines pertaining to the magnetic arcade are nearly horizontal in the neighbourhood of the prominence, we here approximate the arcade magnetic field as a planar, uniform magnetic field $\mathbf{B}=(B_x, B_y, 0)$ that is inclined at an angle ϕ to the Y-axis, thus giving $\tan\phi = \frac{B_x}{B_y}$.

The density and temperature inside and outside the prominence slab are taken to be ρ_0, T_0 and ρ_e, T_e respectively, that are related by the condition of the continuity of gas pressure, namely, $\rho_0 T_0 = \rho_e T_e$. We here ignore the difference in the mean molecular weight (μ) inside and outside the prominence (Jensen and Wiik,1990; Table 1.1) and consider $\mu=1/2$ in both the prominence and the coronal media. This difference in the values of μ in the two media can hardly affect the approximate estimate of the periods of the magnetohydrodynamic modes that are provided by our simple model.

Finally, we consider the magnetic field to be anchored at rigid walls placed at a distance ℓ from the prominence centre on either side of the prominence slab, representing the photospheric line-tying effect (see Section 1.4.3).

We analyze the various aspects of this simple slab model in the remainder of this thesis. In Chapter II, we consider the magnetic field to be purely longitudinal ($\phi=0$), and calculate the magnetohydrodynamic modes of oscillation of such a magnetic slab. The effect of photospheric line-tying of the field lines is ignored in Chapter II. The model considered in Chapter II is, in fact, an improved version of the model proposed by Kleczek and Kuperus (1969), where we also consider the effect of the external corona on the structure of the oscillatory modes of the model prominence slab.

In view of the limitations of a purely longitudinal field model and the importance of the weaker transverse component of the magnetic field (see Section 1.4.3), we consider the case of a purely transverse field in Chapter III. The effect of the line-tying boundary conditions on the oscillations is also included in this chapter. For the sake of simplicity, we confine ourselves to a two-dimensional geometry in Chapter III, thus ignoring the Alfven modes.

In both Chapters II and III, we ignore the effects of gravity. Accordingly, in Chapter IV, we discuss the possible effects of gravity on the magnetoacoustic modes of oscillation of a prominence by considering an elementary, isothermal and two-dimensional magnetohydrostatic model, namely Menzel's (1951) prominence model. The modes of oscillation of a generalized Kippenhahn-Schlüter (1957)-type prominence model is also briefly described in this chapter. We compare the results obtained from these more realistic prominence models with those found in Chapter III, thus indicating that the structures and the periods of the magnetohydrodynamic modes of a more realistic prominence model are not likely to change appreciably from those obtained in our simple slab models.

In Chapter V we again turn to our simple slab model and consider a prominence slab that is threaded by a line-tied, skewed magnetic field that possesses both a longitudinal and a transverse component; see Figure 1.5. It is to be hoped that the modes described in this chapter are able to provide an approximate idea of the actual global magnetohydrodynamic modes in a quiescent prominence. The simplicity of our model allows us to provide approximate scaling laws for the periods of the modes of oscillation, and these may in principle be verified by future observations of prominence oscillations.

Finally, in Chapter VI, we discuss briefly some limitations of the theoretical model considered in the present study of prominence oscillations, and also indicate some possible projects that may be investigated in future to improve upon the theoretical models of prominence oscillations that are presented here.

Chapter II

The slab with a purely longitudinal magnetic field

2.1 Introduction

In this chapter, we consider a simple theoretical model of prominence oscillations in terms of the magnetoacoustic modes of oscillation of a thin plasma slab. The slab is embedded in a hotter and rarer coronal plasma. The effects of gravity are ignored. We assume that both the prominence slab and its coronal environment are permeated by a uniform magnetic field that is aligned along the long axis of the slab. Such an assumption regarding the magnetic field of a prominence was, in fact, considered by Kleczek and Kuperus (1969) to explain the so-called 'winking phenomenon' observed in quiescent prominences. A similar model of prominences has also been proposed recently by Roberts (1991c; see also Joarder and Roberts, 1992a) to explain the observed long period (of about an hour) oscillations in quiescent prominences. The models by Kleczek and Kuperus (1969) and Roberts (1991c) are described in Chapter I.

The model we examine in this chapter forms a natural extension of the earlier models of Kleczek and Kuperus (1969) and Roberts (1991c). Here, we examine the effect of a finite thickness of prominence slab, and also the effect of the external coronal medium on the oscillation frequencies and modes of the model prominence.

In reality, a prominence magnetic field is not longitudinal, but is inclined at a fine angle of approximately 20° with the long axis of the prominence; see the observational discussion in Section 1.1.2. With an average magnetic field strength of 12 G in prominences (see Table 1.1 in Chapter I), this produces a dominant longitudinal component of field strength 10-11 G and a weaker transverse component of strength 3-5 G. In this chapter, we consider the dominant longitudinal field component, ignoring the transverse component altogether. The weaker transverse component of the magnetic field ignored in this discussion, is traditionally believed to pertain to the coronal magnetic arcade that threads the prominence plasma transversely, providing it with the necessary support against gravity; see, for example, Kippenhahn-Schluter model (Fig. 1.1(a)) in Chapter I for a traditional description of prominences. The footpoints of this magnetic arcade are anchored in the regions of opposite magnetic

polarity in the photosphere, thus producing a line-tying effect (Section 1.4.3). We ignore this photospheric line-tying effect in the present model and consider the coronal plasma to be of infinite extent on either side of the prominence slab.

With these simplifying assumptions regarding the prominence and its coronal environment, the equilibrium that we examine in this chapter is then easily constructed from Fig.1.5 (see Section 1.5, Chapter I) by substituting $\phi=0$ and $\ell \to \infty$. Here ϕ is the angle of inclination of the magnetic field to the slab axis and 2ℓ is the anchor point separation distance of the magnetic field lines. For convenience, the modified equilibrium configuration is sketched in Fig. 2.1.

The model that we are considering falls far short of satisfying the situation actually observed in quiescent prominences. The normal modes considered here, cannot therefore be compared directly with the observations of prominence oscillations. Nonetheless, it is useful to consider the modes of oscillation for this model as it provides a basis for

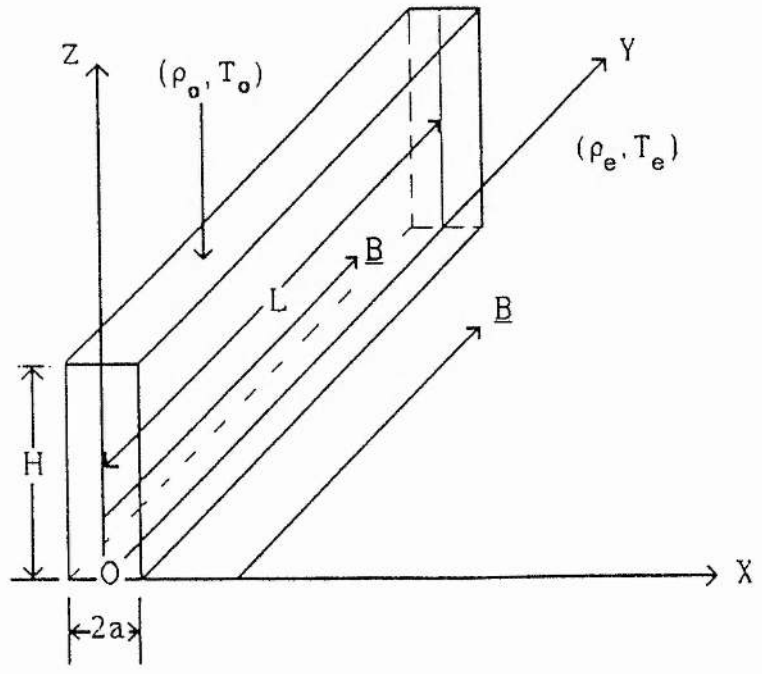

Fig. 2.1. A schematic diagram showing the model prominence slab with a longitudinal magnetic field.

the understanding of the modes of oscillation that arise in the more complex models investigated in later chapters.

The normal modes we here describe are in fact the three dimensional counterparts of the hydromagnetic modes of oscillation of a two dimensional plasma slab discussed in Roberts (1981b) and Edwin and Roberts (1982), and in this context are of some interest for various solar and astrophysical phenomena. The modes are also similar in nature to the hydromagnetic modes of a straight, uniform cylindrical plasma tube with a magnetic field that is aligned to the axis of the tube; see Edwin and Roberts (1983), Roberts (1985). The study of such modes has a wide range of applications in the energy transport mechanisms in sunspots and thin photospheric flux tubes, as well as in coronal loops; see the discussion in Edwin and Roberts (1983), Roberts et al. (1984), Roberts, (1991a,b,c, 1992).

The equilibrium state in the particular case of a purely longitudinal (ϕ=0) magnetic field is described by the condition of continuity of the gas pressure across the plasma slab, namely, $\rho_o T_o = \rho_e T_e$, where ρ_o, ρ_e and T_o, T_e are the equilibrium densities and temperatures inside and outside the slab. The mean molecular weight (μ=1/2) is assumed to be the same inside and outside the prominence slab.

The characteristic MHD speeds that enter in our description of the modes of oscillation of the plasma slab are the Alfven speeds v_{Ao} and v_{Ae} inside and outside the slab, the sound speeds c_{so} and c_{se}, and the magnetoacoustic cusp speeds c_{To} and c_{Te}. Here the suffix 'o' stands for the properties inside the slab (the object), whereas the suffix 'e' (the exterior) is used for the properties of the slab's environment. We also define two critical speeds for non-parallel propagation in each of the uniform media inside and outside the plasma slab. These are

$$v_{co}^{\pm} = \left\{ \frac{1}{2}\left(c_{so}^2+v_{Ao}^2\right)\sec^2\theta \pm \frac{1}{2}\left[\left(c_{so}^2+v_{Ao}^2\right)^2\sec^4\theta - 4v_{Ao}^2 c_{so}^2\sec^2\theta\right]^{1/2} \right\}^{1/2}, \qquad (2.1a)$$

$$v_{ce}^{\pm} = \left\{ \frac{1}{2}\left(c_{se}^2+v_{Ae}^2\right)\sec^2\theta \pm \frac{1}{2}\left[\left(c_{se}^2+v_{Ae}^2\right)^2\sec^4\theta - 4v_{Ae}^2 c_{se}^2\sec^2\theta\right]^{1/2} \right\}^{1/2}, \qquad (2.1b)$$

where θ is the angle of inclination between the direction of propagation of the wave mode and the magnetic field **B**. The speeds $v_{co}^{\pm}$ and $v_{ce}^{\pm}$ are simply the magnetoacoustic speeds along the magnetic field **B**, with '+'

referring to the fast wave and '- ' referring to the slow wave (see Section 1.3). Note that as $\theta \to 0$, $v_{co}^{-} \to \min(v_{Ao},c_{so})$ and $v_{ce}^{-} \to \min(v_{Ae},c_{se})$, whereas $v_{co}^{+} \to \max(v_{Ao},c_{so})$ and $v_{ce}^{+} \to \max(v_{Ae},c_{se})$. Also, as $\theta \to \frac{\pi}{2}$, $v_{co}^{-} \to c_{To}$, $v_{ce}^{-} \to c_{Te}$, whereas $v_{co}^{+} \to \infty$ and $v_{ce}^{+} \to \infty$. These limits are consistent with the phase speeds of the magnetoacoustic modes given in Section 1.3.2 (see Fig. 1.2a, b). For intermediate values of the angle of propagation, we have $v_{co}^{+} > v_{co}^{-} > c_{To}$ and $v_{ce}^{+} > v_{ce}^{-} > c_{Te}$.

2.2 Basic equations and the dispersion relation

We now consider small perturbations of the form (1.9) about the equilibrium configuration displayed in Fig. 2.1. In each of the three uniform media inside and outside the slab, the linearized MHD equations governing small perturbations can be obtained from Eqs. (1.10)-(1.14) of Chapter I after substituting $B_y = B = |\mathbf{B}|$ and $B_x = B_z = 0$. Elimination of the pressure perturbation p and the density perturbation ρ from the linearized MHD equations leads to three coupled ordinary differential equations in the components of the velocity perturbation (v_x,v_y,v_z). These equations are (see Roberts, 1981a)

$$(\omega^2-k_y^2v_A^2)v_x + v_A^2\left(\frac{d^2v_x}{dx^2}\right) + ik_zv_A^2\left(\frac{dv_z}{dx}\right) + \frac{i\omega^2}{k_y}\left(\frac{dv_y}{dx}\right) = 0, \qquad (2.2a)$$

$$(k_y^2c_s^2-\omega^2)v_y + ik_yc_s^2\left(\frac{dv_x}{dx}\right) + k_yk_zc_s^2v_z = 0, \qquad (2.2b)$$

and

$$\left\{\omega^2-(k_y^2 + k_z^2)v_A^2\right\}v_z - \omega^2\left(\frac{k_z}{k_y}\right)v_y + iv_A^2k_z\left(\frac{dv_x}{dx}\right) = 0. \qquad (2.2c)$$

Further elimination in favour of v_x yields a second order ordinary

differential equation (Roberts, 1981a; Rae and Roberts, 1983)

$$(k_y^2 v_A^2 - \omega^2)\left\{\frac{d^2 v_x}{dx^2} - (m^2+k_z^2)v_x\right\} = 0, \tag{2.3a}$$

where

$$m^2 = \frac{\left(k_y^2 c_s^2 - \omega^2\right)\left(k_y^2 v_A^2 - \omega^2\right)}{\left(c_s^2 + v_A^2\right)\left(k_y^2 c_T^2 - \omega^2\right)} . \tag{2.3b}$$

The first bracketed () term in Eq.(2.3a) simply represents an Alfven wave propagating along the field and it is completely decoupled from the magnetoacoustic waves. The second term in parenthesis {}, gives the governing differential equation for the magnetoacoustic waves.

In the following, we do not discuss further the Alfven modes of the slab. Apart from the trivial nature of these modes in the particular case of a purely longitudinal magnetic field, these modes are highly anisotropic and incompressible in character.(see Section 1.3.2) and are therefore not likely to play any significant role in the global motion of the prominence slab, but instead may produce localized disturbances in the individual magnetic field lines. In this chapter, we confine attention to the magnetoacoustic modes of the slab.

It is convenient to rewrite Eq. (2.3a) in terms of the critical speeds $v_c^{\pm}$ as defined in Eq. (2.1). For the magnetoacoustic waves, we obtain (Rae and Roberts, 1983; Joarder and Roberts, 1992a)

$$\frac{d^2 v_x}{dx^2} = k_y^2 M^2 v_x , \tag{2.4a}$$

where

$$M^2 = \frac{\left(v_c^{+2} - c^2\right)\left(v_c^{-2} - c^2\right)}{\left(v_A^2 + c_s^2\right)\left(c_T^2 - c^2\right)} = \frac{m^2}{k_y^2} + \tan^2\theta \tag{2.4b}$$

and $c \equiv \omega/k_y$ is the field-aligned phase speed.

The linearized MHD equations also give expressions for the various important perturbations in terms of the component of velocity perturbation v_x. These expressions are:

$$v_y(x) = \frac{ic_s^2\left(k_y^2v_A^2-\omega^2\right)}{\left(c_s^2+v_A^2\right)\left(k_y^2c_T^2-\omega^2\right)k_y^2M^2}\left(\frac{dv_x}{dx}\right), \tag{2.5}$$

$$v_z(x) = \frac{ik_z\left(c_s^2+v_A^2\right)}{k_y^2M^2}\left(\frac{dv_x}{dx}\right), \tag{2.6}$$

$$p(x) = \frac{-i\rho_{(o,e)}\omega c_s^2\left(k_y^2v_A^2-\omega^2\right)}{\left(c_s^2+v_A^2\right)\left(k_y^2c_T^2-\omega^2\right)k_y^2M^2}\left(\frac{dv_x}{dx}\right) \tag{2.7}$$

and

$$p_T(x) = \frac{i\rho_{(o,e)}\left(k_y^2v_A^2-\omega^2\right)}{\omega k_y^2M^2}\left(\frac{dv_x}{dx}\right). \tag{2.8}$$

Here $p(x)$ and $p_T(x)$ are the perturbation amplitudes in gas pressure and in the total (gas+ magnetic) pressure, respectively.

Eqs. (2.2)-(2.8) apply inside ($|x| \leq a$) the slab with $c_s = c_{so}$, $v_A = v_{Ao}$, $c_T = c_{To}$, $v_c^{\pm} = v_{co}^{\pm}$, $m^2 = m_o^2$, $M^2 = M_o^2$, and outside ($|x| > a$) the slab where $c_s = c_{se}$, $v_A = v_{Ae}$, $c_T = c_{Te}$, $v_c^{\pm} = v_{ce}^{\pm}$ and $m^2 = m_e^2$, $M^2 = M_e^2$.

In their model of prominence oscillations, Kleczek and Kuperus (1969) assumed that the hydromagnetic modes of oscillation of the prominence slab excited magnetoacoustic waves in the external corona that propagated away from the slab, causing the modes to decay in time. Such modes are here characterized by $M_e^2 < 0$ and correspond to propagating wave-like solutions of Eq. (2.4a) in the medium external ($|x| > a$) to the slab. Such

waves are known as 'leaky modes' in the terminology of MHD wave theory, and may be excited by external sources placed at large distances from the slab, perhaps by a solar flare in the case of a winking filament; see the discussion of leaky modes in Roberts and Webb (1979), Spruit (1982), Davila (1985), and Cally (1985, 1986).

We may note, however, that the magnetic slab examined here may also support internal normal modes (Rae and Roberts, 1983) that have a purely oscillating temporal behaviour and do not decay in time due to the excitation of external waves. In what follows we restrict attention to such normal modes of oscillation of the slab, with their velocity amplitude $v_x(x)$ supposed evanescent away from the slab (in $|x| > a$), implying $M_e^2 > 0$. A discussion of such normal modes is perhaps more relevant in the context of the recent observations (see Section 1.2.3) of oscillatory motions in quiescent solar prominences, as no external source of energy, such as a solar flare, have so far been identified to excite such motions in prominences. In the case of such normal modes, the general solution of Eq.(2.4) can be written as (Roberts, 1981b; Edwin and Roberts, 1982)

$$v_x(x) = \begin{cases} A_1 \exp\{-k_y M_e (x-a)\}, & x > a \ , \\ B_1 \sinh(k_y M_o x) + B_2 \cosh(k_y M_o x), & |x| < a \ , \\ A_2 \exp\{k_y M_e (x+a)\}, & x < -a \ , \end{cases} \tag{2.9}$$

where A_1, A_2, B_1, B_2 are arbitrary constants. Following Roberts (1981a,b), solutions with $M_o^2 > 0$ are termed *surface modes* and those with $M_o^2 < 0$ are termed *body modes*.

The arbitrary constants in Eq. (2.9) can be eliminated by requiring that both v_x and the perturbation of the total (gas + magnetic) pressure p_T (see Eq. (2.8)) are continuous across the interfaces $x = \pm a$ of the slab (Roberts, 1981b; Edwin and Roberts, 1982). For a nontrivial solution under such conditions, we obtain the dispersion relation (Rae and Roberts, 1983, Joarder and Roberts, 1992a)

$$\left(\frac{\rho_e}{\rho_o}\right)(v_{Ae}^2 - c^2) M_o \begin{bmatrix} \tanh \\ \coth \end{bmatrix} (k_y a M_o) + (v_{Ao}^2 - c^2) M_e = 0, \tag{2.10}$$

where the choice of the tanh function represents the antisymmetric (B_2=0) solution of Eq. (2.9) and the choice of the coth function represents the symmetric (B_1=0) solutions. These are the *sausage* and *kink* modes, respectively. We note that Rae and Roberts (1983) have provided 'existence diagrams' for some specific orderings of the parameters, as an intuitive way of classifying the normal mode solutions of Eq.(2.10) according to the locations of their phase speeds in different regions of the parameter space.

2.3 Properties of the dispersion relation

The condition of lateral evanescence of the normal modes demands that $M_e^2 > 0$. As $v_{ce}^+ > v_{ce}^- > c_{Te}$, solutions of Eq.(2.10) that satisfy this condition must have their field-aligned phase speed c ($\equiv \omega/k_y$) such that either $c < c_{Te}$ or $v_{ce}^- < c < v_{ce}^+$. Similarly, Eq. (2.4b) shows that modes with $c > v_{co}^+$ or $c_{To} < c < v_{co}^-$ are body modes, whereas modes with $v_{co}^- < c < v_{co}^+$ are surface modes.

It is convenient to introduce two critical angles of propagation, θ_{c1} and θ_{c2}, given as solutions of the equations

$$v_{co}^+(\theta) = c_{Te}, \quad (\theta=\theta_{c1}) \tag{2.11}$$

and

$$v_{co}^+(\theta) = v_{ce}^-(\theta), \quad (\theta=\theta_{c2}). \tag{2.12}$$

When the media inside and outside the slab are such that $v_{Ae} >> c_{se} > v_{Ao}$ and $c_{so} \approx 0$, then Eq. (2.1a, b) gives $v_{co}^+ \approx v_{Ao}\cos\theta$ and $v_{ce}^- \approx c_{se}$, so that the solutions of Eqs. (2.11) and (2.12) reduce to

$$\theta_{c1} \approx \theta_{c2} \approx \cos^{-1}\left(\frac{v_{Ao}}{c_{se}}\right). \tag{2.13}$$

For an arbitrary choice of parameters, Eq. (2.11) and (2.12) are most

conveniently solved numerically, giving $\theta_{c2} > \theta_{c1}$. The physical significance of these critical angles will be shortly made clear.

To discuss the behaviour of the solutions of the dispersion relation (2.10), we consider the ordering of physical speeds as $c_{To} < c_{so} < v_{Ao} < c_{Te} < c_{se} < v_{Ae}$. This is the situation normally found in quiescent prominences. For example, with a prominence temperature of $T_o = 8\ 10^3$ K and an average density of $\rho_o = 2.5\ 10^{-13}$ gcm^{-3} (corresponding to a particle density that is slightly above 10^{11} cm^{-3}) in a corona with $T_e = 10^6$ K and $\rho_e = 2\ 10^{-15}$ gcm^{-3}, our various physical speeds are $c_{To} = 12$ kms^{-1}, $c_{so} = 15$ kms^{-1}, $v_{Ao} = 23$ kms^{-1}, $c_{Te} = 139$ kms^{-1}, $c_{se} = 166$ kms^{-1} and $v_{Ae} = 252$ kms^{-1} for a magnetic field of 4 G. For a magnetic field of 12 G, our physical speeds are $c_{To} = 15$ kms^{-1}, $v_{Ao} = 68$ kms^{-1}, $c_{Te} = 163$ kms^{-1} and $v_{Ae} = 757$ kms^{-1}, with c_{so} and c_{se} unchanged, of course. With this ordering of parameters, the nature of the solutions of Eq. (2.10) are shown schematically in Fig. 2.2a-c, for three different angles of propagation θ, namely (a) for $\theta = 0^o$, (b) for an angle $\theta < \theta_{c1}$, and (c) for an angle $\theta > \theta_{c2}$. Note that Fig. 2.2a, describing the situation at $\theta = 0^o$, is qualitatively similar to Fig. 8 of Edwin and Roberts (1983), which is a corrected version of Fig. 7 of Edwin and Roberts (1982).

Figure 2a-c shows that the normal mode solutions of Eq. (2.10) exist only in three "propagation windows" in parameter space, namely for (i) $c_{To} < c < v_{co}^-$, (ii) $v_{Ao} < c < c_{Te}$, and (iii) $v_{ce}^- < c < v_{ce}^+$. No normal mode exists for $c < c_{To}$ or $v_{co}^- < c < v_{Ao}$ as both the terms of Eq. (2.10) are positive definite for such values of the field-aligned phase speed c, and therefore the dispersion relation is not satisfied. We now proceed to discuss the nature of the modes in the three propagation windows mentioned above.

(i) $c_{To} < c < v_{co}^-$. The solutions of Eq.(2.10) in this band of phase propagation are the *slow body sausage modes* and the *slow body kink modes* . Consider, for example, the sausage modes. For these modes, Eq. (2.10) can be written as

$$k_y a N_o = \tan^{-1}\left[\left(\frac{\rho_o}{\rho_e}\right)\frac{(v_{Ao}^2-c^2)M_e}{(v_{Ae}^2-c^2)N_o}\right] + j\pi\,, \qquad (2.14a)$$

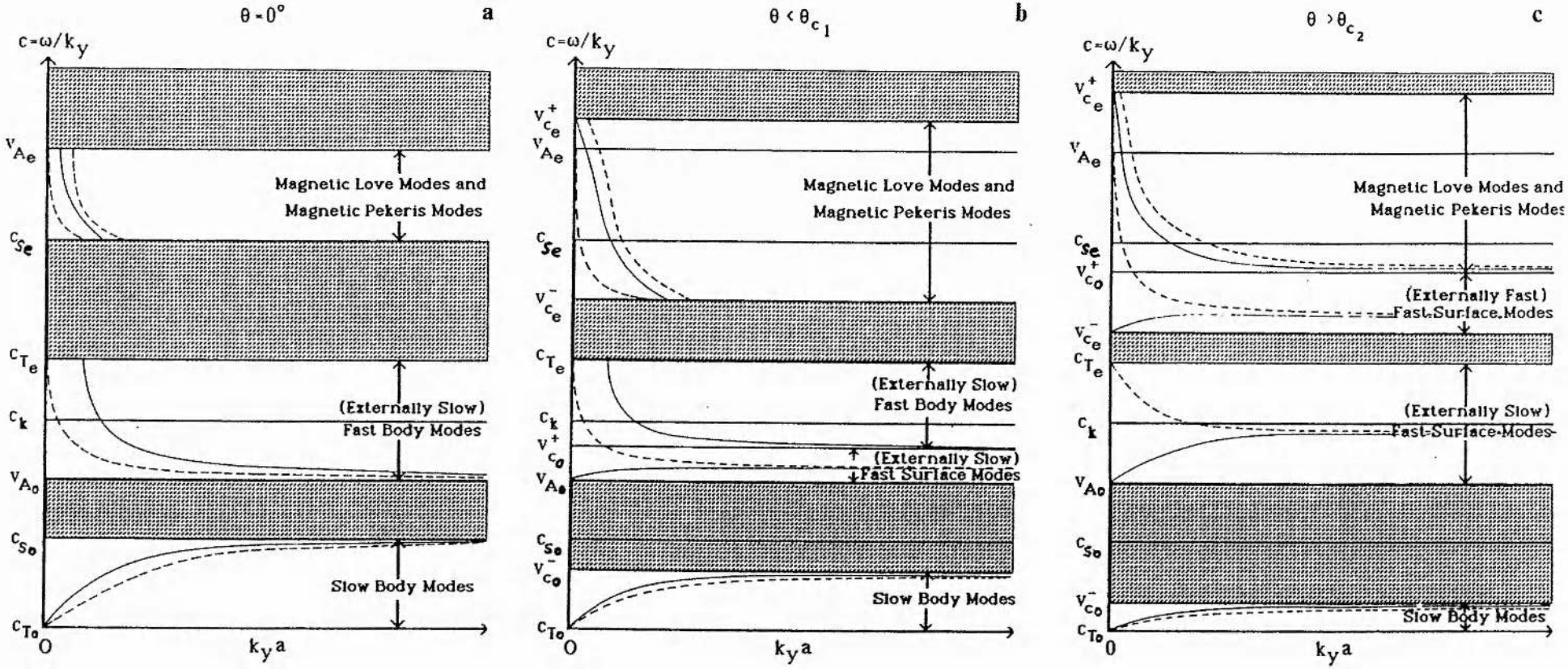

Fig. 2.2a-c. Schematic diagram showing the variation of the field-aligned phase speed c of the normal modes of oscillation of the plasma slab with the dimensionless wavenumber $k_y a$. (**a**) to (**c**) represent the situations for three different angles of propagation, namely (**a**) $\theta = 0^o$, (**b**) for $\theta < \theta_{c1}$, and (**c**) $\theta > \theta_{c2}$. In all three diagrams, a continuous line (_____) denotes sausage modes and a dashed line (-------) denotes kink modes. The hatched ( ) zones denote regions where no normal mode exists. Note that these figures are not drawn to scale.

where

$$N_o^2 = -M_o^2 = \frac{\left(v_{co}^{+2} - c^2\right)\left(v_{co}^{-2} - c^2\right)}{\left(v_{Ao}^2 + c_{so}^2\right)\left(c^2 - c_{To}^2\right)} > 0 \qquad (2.14b)$$

and j= 0,1, 2, 3.... In the long wavelength limit ($k_y a \to 0$) the field-aligned phase speed c for these slow body sausage modes approaches the value c_{To}, the cusp speed inside the slab, thus giving $k_y a N_o \to j\pi$ in this long wavelength extreme. On the other hand, in the short wavelength limit ($k_y a \to \infty$) the phase speed c approaches the field-aligned slow speed v_{co}^- for the internal medium, thus giving $k_y a N_o \to (j+1/2)\pi$ for these slow sausage modes. A similar analysis applies to the slow body kink modes, showing that the longitudinal phase speed varies with $k_y a$ in a similar way for these modes also.

The propagation of these slow modes are not particularly influenced by the critical angles of propagation θ_{c1} and θ_{c2}, as can be seen from Fig. 2a-c. But as the propagation vector (0, k_y, k_z) tends towards the normal to the magnetic field B, the propagation band for the slow modes collapses to a single line $c = c_{To}$, showing the highly anisotropic propagation characteristics of slow modes (see also Roberts, 1985).

(ii) $v_{Ao} < c < c_{Te}$. The solutions lying in this region of parameter space are the fast modes of the slab. However, since these fast modes have their longitudinal phase speed c below the field aligned slow speed v_{ce}^- of the external medium, we can refer to them as the *(externally slow) fast modes* (see Cally, 1985, 1986 and Abdelatif, 1988 for alternative nomenclatures).

For purely field-aligned propagation ($\theta = 0^o$), illustrated in Fig.2a, $v_{co}^+ = v_{Ao}$ and we obtain two types of body modes, namely, *fast body sausage modes* and *fast body kink modes* (Edwin and Roberts, 1982).

For a small angle of propagation $\theta < \theta_{c1}$ (illustrated in Fig.2b), we find $v_{Ao} < v_{co}^+ < c_{Te}$. The fast body modes still exist with their field-aligned phase speed c in the domain $v_{co}^+ < c < c_{Te}$, and have very similar characteristics as for the case of parallel ($\theta = 0^o$) propagation. Note the upper cut-offs in wavelength (frequency) in the fast body sausage modes

and the harmonics of the fast body kink modes. At such cut-offs the normal mode is transformed into a leaky mode that drives external magnetoacoustic waves and therefore decays in time; see Section 2.2. However, detailed calculations with prominence parameters suggest that the existence of such cut-offs is not likely to greatly influence the normal modes of the slab at a wavelength interesting for prominence oscillations, this is discussed further in the next section.

In addition to the above body modes, we now gain two *fast surface modes (externally slow)* with $v_{Ao} < c < v_{co}^{+}$. The appearance of such fast surface modes (externally slow), for even a small non-zero angle of propagation with respect to the direction of the magnetic field-vector, is a special feature of the calculations presented in this chapter. These fast surface modes owe their existence to the particular ordering of the physical speeds considered here. The characteristics of the fast surface modes can easily be derived from Eq. (2.10). For example, the phase speed c of the sausage surface mode approaches the Alfven speed v_{Ao} in the limit of long wavelengths ($k_y a \rightarrow 0$). For the kink surface mode, Eq. (2.10) seems to suggest that $c \rightarrow c_{Te}$ in the limit of vanishingly small $k_y a$. In fact, this kink surface mode merges with the fundamental of the fast body kink modes present in the band $v_{co}^{+} < c < c_{Te}$ at some finite value of $k_y a$.

When the angle of propagation exceeds the critical angle θ_{c1}, so that $v_{co}^{+} > c_{Te}$, the fast body modes disappear completely, leaving only two fast surface (externally slow) modes (see Fig. 2c). When $v_{Ae} >> c_{se} \approx c_{Te}$ and $c_{so} \approx c_{To} \approx 0$, the frequencies of these sausage and kink surface modes, for small $k_y a$, are given by the following approximate formulae:

$$\omega^2 \approx k_y^2 v_{Ao}^2 [1 + (k_y a) \tan\theta] \tag{2.15}$$

for sausage modes, and

$$\omega^2 \approx k_y^2 \left[c_{Te}^2 - \frac{\left(c_{Te}^2 - v_{Ao}^2\right)^2 \left(c_{se}^2 - c_{Te}^2\right) (k_y a)^2}{v_{Ao}^4} \sec^2\theta \right] \tag{2.16}$$

for kink modes. On the other hand, for large $k_y a$ and for a nearly normal

propagation ($\theta \approx \pi/2$) the field-aligned phase speed c of both these surface modes approaches the limit

$$c_k = \left\{ \frac{\rho_o v_{Ao}^2 + \rho_e v_{Ae}^2}{\rho_o + \rho_e} \right\}^{1/2} , \qquad (2.17)$$

which is the longitudinal phase speed for magnetohydrodynamic surface waves in an incompressible medium (cf. Wenzel, 1979; Uberoi and Somasundaram, 1980; Roberts, 1981a, 1985, 1991a; Somasundaram and Uberoi, 1982). We may note that a similar asymptotic behaviour is also found for the slow surface waves, that exist in a plasma slab for certain orderings of the physical speeds (different from the ordering of the speeds considered in this chapter); see, for example, Edwin and Roberts (1982), Roberts (1985).

(iii) $v_{ce}^+ > c > v_{ce}^-$. The longitudinal phase speed c for the modes appearing in this band lie above the field-aligned slow speed v_{ce}^- of the external medium. We therefore refer to these modes as the *(externally fast) fast modes* of the slab (see also Cally, 1985, 1986; Abdelatif, 1988). For $\theta < \theta_{c2}$, as illustrated in Fig. 2b, the *fast body sausage and kink modes* are similar to the body modes obtained for the case of parallel propagation ($\theta = 0^o$, $v_{ce}^+ = v_{Ae}$, $v_{ce}^- = c_{se}$). In the case of parallel propagation, and also when both the media inside and outside the slab possess extremely high or low plasma-beta values, the dispersion relations for these fast body sausage and kink modes are similar to the dispersion relations obtained respectively for the Pekeris waves in oceanography and the Love waves in seismology (cf. Edwin and Roberts, 1982, 1983, 1988; Roberts et al. 1984; Edwin et al. 1986). Accordingly, these fast body sausage and kink modes are sometimes referred to as the *magnetic Pekeris modes* and the *magnetic Love modes*. We here retain these terminologies, in spite of the fact that the analogies for the modes are not immediately apparent in the more complicated situation of the non-parallel propagation considered in the present discussion.

Note that unlike the case of parallel propagation, the upper cut-offs in

wavelength (frequency) for the fundamental Pekeris mode is removed even for a slightly inclined angle of propagation, allowing this mode to propagate for arbitrarily long wavelengths with its phase speed c asymptotically approaching the critical speed v_{ce}^{+}. However, the harmonics of both the Pekeris and Love modes still possess upper cut-offs.

The periods of the magnetic Love and Pekeris modes at the cut-off wavelengths can be calculated from Eq. (2.10). For the harmonics of the magnetic Pekeris modes, this equation reads

$$k_y a N_o - j\pi = -\tan^{-1}\left\{\left(\frac{\rho_o}{\rho_e}\right)\frac{\left(c^2-v_{Ao}^2\right)M_e}{\left(c^2-v_{Ae}^2\right)N_o}\right\}, \qquad (2.18a)$$

with

$$N_o^2 = \frac{\left(c^2-v_{co}^{+\,2}\right)\left(c^2-v_{co}^{-\,2}\right)}{\left(c_{so}^2+v_{Ao}^2\right)\left(c^2-c_{To}^2\right)}, \qquad (2.18b)$$

and j=1,2,3....., thus giving

$$k_{yc}^{P} = \left(\frac{\rho_e}{\rho_o}\right)^{1/2}\frac{j\pi}{a}\cos\theta \quad , \quad \text{and} \quad \tau_c^{P} = \frac{2a}{jv_{Ao}} \qquad (2.19)$$

for the approximate values of the wavenumbers and the periods at the upper cut-offs ($c = v_{ce}^{+}(\theta)$) of the magnetic Pekeris modes. The cut-off wavenumbers and periods of the magnetic Love modes can be found similarly. These are given by

$$k_{yc}^{L} = \left(\frac{\rho_e}{\rho_o}\right)^{1/2}\frac{(2j-1)\pi}{2a}\cos\theta \quad , \qquad \tau_c^{L} = \frac{4a}{(2j-1)v_{Ao}} \quad , \; j=1,2,3,..... \qquad (2.20)$$

Note the angular dependence of the cut-off wavenumbers in Eqs. (2.19) and (2.20).

At a small angle of propagation ($\theta < \theta_{c2}$), all the magnetic Love and Pekeris modes possess lower cut-offs at a wavelength where the field-

aligned phase speed attains the value $v_{ce}^{-}(\theta)$. The lower cut-offs are removed when the propagation angle θ exceeds its critical value θ_{c2} (see Fig. 2c). Instead, the phase speed c for these modes asymptotically approaches $v_{co}^{+}(\theta)$ at arbitrarily short wavelengths. In addition, we also gain two *(externally fast) fast surface modes.* The existence of such fast surface waves, with a phase speed c below a critical value v_{co}^{+} , has been noted earlier by Uberoi (1982) for a single surface of discontinuity separating two extremely low-beta plasmas, whereas the existence of a critical angle of propagation for such fast surface waves has been suggested by Rae and Roberts (1983). We also note that the kink surface mode merges with the fundamental magnetic Love mode at some intermediate value of the wave number k_y.

The (approximate) asymptotic formulae for the frequencies of these fast modes are presented below in the limit of long wavelength of propagation and for a large angle of propagation $\theta \approx \pi/2$. We have

$$\omega^2 \approx k_y^2 v_{Ae}^2 \sec^2\theta \left[1-(k_y a)^2 \tan^2\theta \ \sin^2\theta\right] \tag{2.21}$$

for the fundamental Pekeris mode;

$$\omega^2 \approx k_y^2 c_{Te}^2 \left[1+\frac{v_{Ao}^4 (k_y a)^2 \left(c_{se}^2-c_{Te}^2\right)}{\left(c_{Te}^2-v_{Ao}^2\right)c_{Te}^2}\sec^2\theta\right] \tag{2.22}$$

for the fast sausage surface mode; and

$$\omega^2 \approx k_y^2 v_{Ae}^2 \left[1-\left(\frac{\rho_o}{\rho_e}\right)(k_y a)\tan\theta\right] \tag{2.23}$$

for the fundamental Love mode. In deriving formulae (2.21)-(2.23), we have assumed for simplicity that $v_{Ae} \gg c_{se}$ and $c_{so} \approx c_{To} \approx 0$. We further note that Eq. (2.23) suggests a rapid exponential decay for the behaviour of the phase speed c of the fundamental Love mode with dimensionless wavenumber $k_y a$ (see Fig.2b, c). For this behaviour of the mode, an estimate of the frequency of the (externally fast) fast surface mode which

is an extension of the fundamental magnetic Love mode for large angle of propagation θ ($> \theta_{c2}$; see discussion above) cannot be given from Eq. (2.23) at a wavelength interesting for prominence oscillations. For example, with $\rho_e/\rho_o = .008$ and $\theta \approx 76^o$, Eq. (2.23) predicts an imaginary frequency for this mode even for $k_y a$ as small as 0.04. Due to such difficulties, an estimate of the frequency of this fast surface mode is best given by the frequency interval in which the surface mode exists; thus

$$k_y v_{co}^{+} \approx k_y v_{Ao} \sec\theta > \omega > k_y v_{ce}^{-} \approx k_y c_{Te} . \qquad (2.24)$$

2.4 Periods of oscillations of the model prominence

Having discussed the general problem of non-parallel propagation in a plane-parallel plasma slab, we now turn to a discussion of the characteristics of the eigenmodes that may be present in the slab. To model the effect of the finite extent of the prominence slab in the Y and Z directions, we impose periodic boundary conditions, namely that

$$\Psi(x, 0, z, t) = \Psi(x, L, z, t) \text{ and } \Psi(x, y, 0, t) = \Psi(x, y, H, t). \qquad (2.25)$$

Equation (1.9) then takes the form

$$\Psi(x, y, z, t) = \Psi(x)\, e^{i\omega t} \begin{pmatrix} \sin k_y y & \sin k_z z \\ \cos k_y y & \cos k_z z \end{pmatrix}, \qquad (2.26)$$

representing, respectively, the odd and even parts of the real eigenfunction with

$$k_y = \frac{m\pi}{L}\,,\; k_z = \frac{n\pi}{H}\;;\; m, n = 1,2,3,\ldots\ldots, \qquad (2.27)$$

where the integers m and n describe the modal structure along the length and the height of the model prominence slab. This representation of the stationary eigenmodes of the prominence slab is similar to the representation of the modes of vibration of a rectangular elastic membrane (cf. Roberts, 1991c; Joarder and Roberts, 1992a,b,c; 1993a,b) that is clamped at its edges, and for which only the odd parts of the

eigenfunctions (2.26) are allowed, as the disturbances vanish at all points on the edges of such an elastic membrane; see, for example, Rayleigh, (1877), Coulson (1955).

In what follows, we concentrate on the m=n=1 oscillations, as such principal eigenmodes of oscillation are expected to have maximum energy densities in prominences. Taking 2a= 5000 km, L = 2 10^5 km and H = 5 10^4 km (see, Section 1.1.2), we then obtain $k_y a \approx 0.04$, and $\theta = \tan^{-1}\left(\frac{L}{H}\right) \approx 76^\circ$ for the principal eigenmode of the model prominence. It is important to note that the angle of phase propagation θ does not have any strictly physical significance in the context of the stationary eigenmodes of the plasma slab. However, it is convenient to retain this notation as a way to describe the ratio of the two wavenumbers along the length and height of the model prominence.

For the plasma parameters inside and outside the prominence, we choose the illustrative values of Section 2.3, namely, c_{so} = 15 kms^{-1}, and c_{se} = 166 kms^{-1}. We consider two different magnetic field strengths, namely B = 4 G and B = 12 G, the second choice representing a field strength in an average prominence situation and the first choice representing a minimum field strength observed in prominences (see Jensen and Wiik, 1990, Table 1.1). Calculations carried out with a much higher magnetic field strength (say, B=20 G) lead to much the same conclusions as for B =12 G, though the numerical values of the periods are reduced.

For the above choice of physical parameters, the properties of the principal modes of oscillation of the prominence slab are summarized in Table 2.1 (see also Joarder and Roberts, 1992a). Along with the numerically calculated values of the periods, we give also an order-of-magnitude estimate for the periods in this table. We may also note that the nature and the numbers of the eigenmodes that may be present in the prominence slab change somewhat as we increase the field strength from its low (B = 4 G) to high(12 G) values. This is because the critical angles θ_{c1} and θ_{c2} ($> \theta_{c1}$) decrease with increasing magnetic field strength [see Eq.(2.13)]. As a result, the magnetic Love mode turns into a fast kink surface mode in the high magnetic field strength case. In addition, we obtain one more fast sausage surface mode (see Section 2.3) in the case of the prominence slab with a high magnetic field strength. Our numerical calculations with prominence parameters further suggest that the existence of the cut-off frequencies, that may, in principle, be present for

Table 2.1. *The periods of the principal (m=n=1) eigenmodes of the slab prominence for $\theta=\tan^{-1}(L/H) \approx 76^{o}$, and for two different values of the magnetic field strength.*

Name of the mode	Periods	
	$\|B\|$ = 4.0 G $\theta_{c1} \approx \theta_{c2} \approx 80^{o}$	$\|B\|$ = 12.0 G $\theta_{c1} \approx \theta_{c2} \approx 65^{o}$
Fundamental slow body sausage mode ($\tau \approx 2L/c_{To}$)	9 hr	8 hr
Fundamental slow body kink mode ($\tau \approx 2L/c_{To}$)	9 hr	8 hr
(Externally slow) Fast sausage surface mode ($\tau \approx 2L/v_{Ao}$)	5 hr	90 min
(Externally slow) Fast kink surface mode ($2L/c_{Te} < \tau < 2L/c_{k}$)	110 min	40 min
(Externally fast) Fast sausage surface mode ($\tau \approx 2L/c_{Te}$)	———	40 min
(Fundamental Love mode) or (Externally fast) Fast kink surface mode $\left(\frac{2L}{v_{Ao}}\cos\theta < \tau < 2L/c_{Te}\right)$	48 min	35 min
Fundamental Pekeris mode $\left(\tau \approx \frac{2L}{v_{Ae}}\cos\theta\right)$	6 min	3 min

Table 2.1 (contd.)

Name of the modes	Periods	
1st Harmonic Love modes $\left(\tau \approx \tau_c \approx \frac{4a}{v_{Ae}}\right)$	5 min	2 min

certain fast body modes of the plasma slab (see discussion in Section 2.2), are not likely to alter the oscillatory properties of at least the principal (fundamental) normal modes of the slab for wavelengths interesting for prominence oscillations (as is typically shown in Table 2.1).

2.5 Discussions

We note that the periods of some of the normal modes displayed in Table 2.1 show an interesting similarity with the periodicities actually found in the observations of prominence oscillations (Table 1.2(a)-(c)). For example, the (externally slow or fast) fast sausage and kink surface modes, or the fundamental magnetic Love mode (in the case of the slab with weaker magnetic field strength) typically show periods that are in the range of 1/2-2 hr. Such periodicities are consistent with the observed long period oscillations in prominences. Similarly, the fundamental of the magnetic Pekeris modes and the 1st harmonic of the magnetic Love modes present periodicities that are similar to the short periodicities (1-5 min) observed in prominence oscillations. Intermediate periodicities in the range of 10-20 minutes are not obtained in this calculation for a model prominence slab with a purely longitudinal magnetic field, at least for the range of values of the prominence parameters considered here.

The existence of the (externally slow) fast kink surface mode and either of the fundamental magnetic Love mode (in the case of a weak magnetic field) or the (externally fast) fast kink surface mode (in the case of average or strong magnetic field) is, however, of some interest. Eqs. (2.5), (2.6) and (2.9) suggest that for these modes, the amplitudes of velocity perturbations at either of the two interfaces ($x = \pm a$) of the prominence slab satisfy the condition

$$\left|\frac{v_y}{v_x}\right| \approx \left|\frac{v_z}{v_x}\right| \approx C.|\tanh(k_y a\, M_o)|, \qquad (2.28)$$

where the quantity C depends on the frequencies of the modes. For $k_y a \ll 1$ (as is the case for prominences), both M_o and C are of order of unity, thus giving $\left|\frac{v_y}{v_x}\right| \approx \left|\frac{v_z}{v_x}\right| \ll 1$ in the limit of long wavelengths (with their numerical values being ≤ 0.2 for our specific prominence parameters; see Joarder and Roberts,1992a). The amplitudes of the velocity perturbation pertaining to these fast kink modes are then predominantly in the x-direction. The modes pertain to lateral, symmetric oscillations of the interfaces of the prominence slab, and are therefore somewhat analogous to the modes of vibration of an elastic membrane (see Section 1.4.2, Chapter I) with their the periods (see Table 2.1) being consistent with the approximate estimates given in Section 1.4.2 [see Eq.(1.35)], although their numerical values are now changed somewhat due to the more complicated situation considered here. The appearance of two such kink modes is, of course, due to the inclusion of the external coronal medium in our calculation. Similarly, the appearance of the long period (externally slow or fast) fast sausage surface modes is due to the consideration of a finite width to the prominence slab, and therefore, cannot be predicted from the infinitely thin sheet-type models of prominences presented by Kleczek and Kuperus (1969) and Roberts (1991c).

In our description of the oscillatory motion of a model prominence slab, we have confined ourselves to the normal modes of the slab. The investigation of such normal modes is of primary interest in the observations of oscillatory motions in prominences. Apart from such normal modes of oscillation, we may, however, also obtain leaky modes in the prominence slab. Leaky modes correspond to the propagating solutions ($M_e^2 < 0$) of Eq.(2.4) outside the prominence slab ($|x| > a$), and decay in times that are comparable to their periods of oscillation; see Section 2.2. In their model of winking filaments, Kleczek and Kuperus (1969) predicted a period of about 20 minutes for such intermittent modes in prominences (see Eq. 1.35, Section 1.4.2). In our calculations, such leaky modes appear with frequencies in the range $k_y c_{Te} < \omega < k_y v_{ce}$, thus presenting a period of about 40-50 min. However, as with the long period normal modes (see Table 2.1) of the slab, the periods of leaky modes scale roughly with the

length (L) of the prominence slab, thus decreasing to about 20 min if the length of the prominence is reduced by a factor of two or so.

Finally, we may here note that, in spite of their apparent similarity to the observed oscillations in prominences, the modes described in this chapter do not represent a true picture of the realistic situation present in quiesecent prominences. The small transverse component of the magnetic field ignored in this present calculation may, in fact, completely change the modal structure of the plasma slab. In the next chapter, we therefore go on to a consideration of this weak transverse magnetic field component alone, neglecting the dominant longitudinal magnetic field component in prominences. A consideration of a transverse magnetic field, along with the condition of line-tying, introduces new modes that are not present in the simple slab model with a longitudinal field.

Chapter III

The slab with a purely transverse magnetic field

3.1 Introduction

In Chapter II we described our first attempt to develop a theoretical model of the oscillations in quiescent prominences in terms of the vibrations of a dense plasma slab within which is embedded a longitudinal magnetic field. Such a representation of a prominence was also used by Kleczek and Kuperus (1969) - see Section 1.4.2, Chapter I- and gives emphasis to the dominant component of the magnetic field that threads a prominence. However, observations show that the magnetic field in a quiescent prominence makes a small angle of approximately 20° with the long axis of the prominence; see discussions in Chapter I, Section 1.1.2. With a resultant magnetic field of magnitude 4-20 G in quiet regions (Table 1.1, Chapter I), this produces a longitudinal component with a field strength of 3.8-18.8 G, and a weaker transverse component of 1-7 G. In Chapter II we discussed the consequences of a longitudinal field, ignoring the weaker transverse component. Here, we turn to a consideration of the effect of a transverse component, now ignoring the effect of the longitudinal field (see also Joarder and Roberts, 1992b,c). The combined effect of both components is reserved for Chapter V.

We found in Chapter II that in the case of a longitudinal field, long-period (about 1 hour) oscillations were principally given by the fast surface modes of the slab. Some of these fast surface modes (the fast kink surface modes) are somewhat analogous to the classical modes of vibration of an elastic membrane (Roberts, 1991c; Joarder and Roberts, 1992a, c). Shorter period oscillations, in the range 3-5 minutes, were produced in this model by magnetic Pekeris modes and magnetic Love modes (Joarder and Roberts, 1992a, c) which are ducted fast body waves; see Edwin and Roberts (1982, 1983), Roberts et al. (1984) and Edwin et al. (1986). Intermediate periodicities, in the range 10-20 minutes, that are observed in prominence oscillations (cf. Table 1.2(b), Section 1.2.3), were absent in the model investigated in Chapter II.

Here we consider the influence of a transverse field, which corresponds to the case $\phi = \frac{\pi}{2}$ in Fig. 1.5 of Chapter I. We show that in this model oscillations with periods of the order of 10 min are in fact produced.

Such periods result from trapped magnetoacoustic modes (fast or slow, depending on the relative magnitude of the sound speed to the Alfven speed in the transverse component of the field) in prominences that have a period of twice the acoustic travel time across the prominence slab.

We find too that there are modes with periods in the range 1/2-1 hour. These are produced by waves that reflect off the boundaries at which the magnetic field is anchored. The magnetic field of a prominence is anchored in the dense photosphere, producing a line-tying effect (see Sections 1.4.3 in Chapter I). Line-tying is represented in our model by walls placed on either side of the prominence slab. It results in an oscillation of period τ given approximately by (Section 1.4.3, Chapter I)

$$\tau \approx \frac{2\pi}{v}\sqrt{\ell a}, \tag{3.1}$$

where v is the field-aligned (fast or slow) magnetoacoustic speed within the prominence sheet of width 2a and line-tied at a distance ℓ on either side of the prominence centre. In Chapter I we saw that such modes are analogous to the fundamental modes of vibration of a mass-loaded stretched elastic string and present long periodicities of about an hour for parameter values that are relevant to the observations of solar quiescent prominences (see also Roberts, 1991c; Joarder and Roberts, 1992b, c).

Motivated by this analogy, we model the prominence by a plasma slab of infinite extent in the y-direction, of dimension H in the z-direction, and of width 2a ($<<$ H) in the x-direction. The effect of gravity is ignored. The slab of density ρ_o and temperature T_o is embedded in a uniform plasma of density ρ_e and temperature T_e. Pressure balance demands that $\rho_o T_o = \rho_e T_e$, for μ to be taken the same inside and outside the prominence. The plasmas inside and outside the slab are permeated by a uniform magnetic field $\mathbf{B} = B\hat{\mathbf{x}}$ in the x-direction. The equilibrium we consider here corresponds to the case $\phi = \pi/2$ of Fig. 1.5 of Chapter I, with $L \rightarrow \infty$. This equilibrium configuration is shown in Fig. 3.1. The magnetic field lines are considered to be anchored at rigid walls located at $x = \pm \ell$ on either side of the prominence slab, and representing the effect of inertial line-tying of the field lines in the photosphere.

The prominence model we are considering is thus somewhat similar to the classical Kippenhahn-Schluter (1957)-type equilibrium models (described in Section 1.1.3 of Chapter I), where the two- dimensional

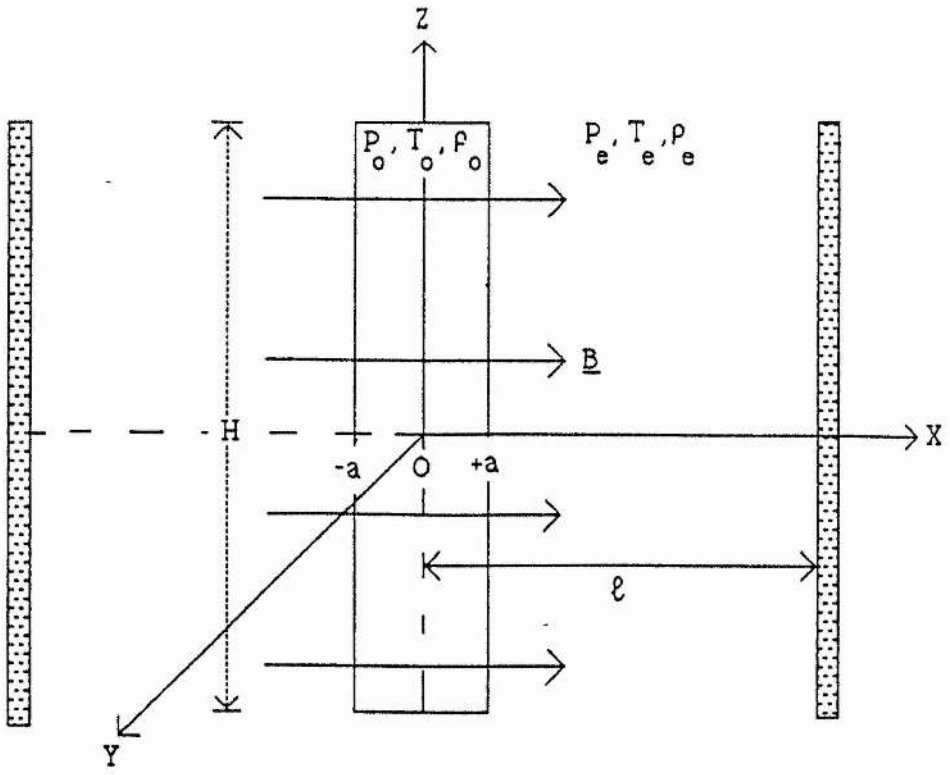

Fig. 3.1. A schematic diagram showing the model prominence slab with a transverse magnetic field.

prominence slab is assumed to reside in a magnetic arcade (cf. Fig. 1.1(a)), the foot-points of which are tightly anchored at the opposite line-of-sight magnetic polarity regions of the photosphere. As a first approximation, we here consider the magnetic field lines of the arcade to be flat (horizontal). As we are confining ourselves to a zero gravity model, we here also ignore a small dip at the top of the magnetic arcade , at the site of the prominence, that is present in the Kippenhahn-Schlüter equilibrium model and provides the prominences with the necessary support against gravity. We may note that, apart from producing a small dip of about 10^{o} in the magnetic field lines (cf. Section 1.1.2, Chapter I), gravity plays an otherwise passive role in the Kippenhahn-Schlüter-type prominence model, where the prominence is assumed to be essentially unstratified in the vertical (z) direction. The periods of the modes of oscillation that are present in the calculations of this chapter are, therefore, expected to be similar to those periods that may be present in models of the Kippenhahn-Schlüter-type. Recent results of Oliver et al. (1992c) confirm this supposition. We examine this similarity in greater detail in Chapter IV.

3.2 Derivation of the dispersion relation

3.2.1 Basic equations: The linearized MHD equations representing small perturbations about the equilibrium configuration of Fig. 3.1 can be obtained from Eqs. (1.10)-(1.14) of Chapter I on substituting $B_y = B_z = 0$, $B_x = B = |\mathbf{B}|$, $k_y = 0$ and $v_y = 0$. The continuity equation then takes the form

$$i\omega\rho + \rho_o\left(\frac{dv_x}{dx} + ik_z v_z\right) = 0, \tag{3.2}$$

while the momentum equation yields

$$i\omega\rho_o v_x + \frac{dp}{dx} = 0, \tag{3.3a}$$

$$i\omega\rho_o v_z + ik_z p + \frac{B}{4\pi}\left(ik_z b_x - \frac{db_z}{dx}\right) = 0. \tag{3.3b}$$

The induction equation gives

$$b_x = \frac{Bk_z v_z}{\omega}, \quad b_z = \frac{B dv_z}{i\omega\, dx}, \tag{3.4}$$

and the adiabatic equation is

$$p = c_s^2\rho. \tag{3.5}$$

From Eqs. (3.2)-(3.5) we may obtain the relationships between the various perturbations:

$$v_z = \frac{-i}{k_z\left(\omega^2 - k_z^2 c_f^2\right)}\left\{v_A^2\frac{d^3v_x}{dx^3} + \left(k_z^2 c_s^2 + \omega^2\frac{v_A^2}{c_s^2}\right)\frac{dv_x}{dx}\right\}, \tag{3.6}$$

$$p = \frac{i\rho_o}{\omega\left(\omega^2 - k_z^2 c_f^2\right)}\left\{ v_A^2 c_s^2 \frac{d^3 v_x}{dx^3} + c_f^2\left(\omega^2 - k_z^2 c_T^2\right)\frac{dv_x}{dx}\right\}, \tag{3.7}$$

$$b_z = \left(\frac{B}{k_z \omega}\right)\left\{\frac{d^2 v_x}{dx^2} + \frac{\omega^2}{c_s^2} v_x\right\}. \tag{3.8}$$

Elimination of the pressure perturbation p, density perturbation ρ and the perturbation in the magnetic field $(b_x, 0, b_z)$ from Eqs. (3.2)-(3.5) yields two coupled, second order ordinary differential equations in the velocity perturbation $(v_x, 0, v_z)$. These are

$$c_s^2\left\{\frac{d^2 v_x}{dx^2} + ik_z \frac{dv_z}{dx}\right\} + \omega^2 v_x = 0, \tag{3.9}$$

and

$$v_A^2 \frac{d^2 v_z}{dx^2} + \left(\omega^2 - k_z^2 c_f^2\right) v_z + ik_z c_s^2 \frac{dv_x}{dx} = 0, \tag{3.10}$$

where $c_f = \left(c_s^2 + v_A^2\right)^{1/2}$ is the magnetoacoustic fast speed (cf. Section 1.3.2, Chapter I). Further elimination from Eqs. (3.9) and (3.10) in favour of the component of velocity perturbation v_x yields the following fourth order ordinary differential equation (cf. Joarder and Roberts, 1992b)

$$c_T^2 \frac{d^4 v_x}{dx^4} + \left(\omega^2 - k_z^2 c_T^2\right)\frac{d^2 v_x}{dx^2} + \left(\frac{\omega^2}{c_f^2} - k_z^2\right)\omega^2 v_x = 0. \tag{3.11}$$

Here $c_T = \frac{c_s v_A}{c_f}$ is the magnetoacoustic cusp speed (cf. Section 1.3.2, Chapter I). Eqs. (3.2)-(3.11) apply both inside ($|x| \leq a$) the slab (where the unperturbed density is ρ_o and $c_s = c_{so}$, $v_A = v_{Ao}$, $c_f = c_{fo}$, and $c_T = c_{To}$) and outside ($a < |x| \leq \ell$) the slab (where the density is ρ_e and $c_s = c_{se}$, $v_A = v_{Ae}$, $c_f = c_{fe}$, and $c_T = c_{Te}$).

For a uniform unbounded medium, we can substitute $dv_x/dx = ik_x v_x$ in Eq. (3.11) to give ($v_x \neq 0$)

$$\omega^4 - \omega^2 c_f^2 \left(k_x^2 + k_z^2\right) + k_x^2 \left(k_x^2 + k_z^2\right) c_s^2 v_A^2 = 0. \tag{3.12}$$

This is the standard dispersion relation for magnetoacoustic waves in a uniform medium with $k_y = 0$, $k_x = k\cos\theta$ and $k^2 = \left(k_x^2 + k_z^2\right)$; see Section 1.3.2, Chapter I. We note that the Alfven waves, having a velocity perturbation in a direction normal to both the unperturbed magnetic field and the direction of propagation, are absent in this case due to our assumption of $k_y = v_y = 0$.

The symmetry of the basic equilibrium configuration in Fig. 3.1 suggests that the solutions of Eq. (3.11) may be divided into even and odd solutions. As in Chapter II, the eigenmodes represented by these two groups of solution will be called *kink* and *sausage* modes. This is a geometrical classification of the modes (see Roberts, 1981b; Edwin and Roberts, 1982, 1983), centred on the distortion of the slab as seen from the side. A symmetrical compression or rarefaction resembles the kink mode of a magnetic slab (or tube) and disturbs the centre (x=0) of the slab; an anti-symmetrical distortion resembles the sausage mode of a slab (or tube) and leaves the centre of the slab undisturbed.

The solutions of Eq. (3.11) for the regions inside the slab ($|x| \leq a$) can thus be written in the alternative forms

$$v_x(x) = \begin{cases} B_1 \cos k_o^+ x + B_2 \cos k_o^- x \\ B_1 \sin k_o^+ x + B_2 \sin k_o^- x \end{cases}, \quad 0 \leq x \leq a, \tag{3.13}$$

where the symmetric (cosine) solution corresponds to the kink modes, and the anti-symmetric (sine) solution corresponds to the sausage modes. Here B_1, B_2 are arbitrary constants and the wavenumbers k_o^+ and k_o^- are given by

$$\left(k_o^{\pm}\right)^2 = \frac{1}{2}\left(\frac{\omega^2}{c_{To}^2} - k_z^2\right) \pm \frac{1}{2}\left\{\left(\frac{\omega^2}{c_{To}^2} + k_z^2\right)^2 - 4\frac{\omega^4}{c_{To}^2 c_{fo}^2}\right\}^{1/2}. \tag{3.14}$$

The solutions outside the slab can be written in the general form

$$v_x(x) = A_1\exp\left\{ik_e^+(x-a)\right\} + A_2\exp\left\{-ik_e^+(x-a)\right\} + A_3\exp\left\{ik_e^-(x-a)\right\} + A_4\exp\left\{-ik_e^-(x-a)\right\}, \qquad a \leq x \leq \ell\ , \tag{3.15}$$

where

$$\left(k_e^{\pm}\right)^2 = \frac{1}{2}\left(\frac{\omega^2}{c_{Te}^2} - k_z^2\right) \pm \frac{1}{2}\left\{\left(\frac{\omega^2}{c_{Te}^2} + k_z^2\right)^2 - 4\frac{\omega^4}{c_{Te}^2 c_{fe}^2}\right\}^{1/2} \tag{3.16}$$

and A_1, A_2, A_3, A_4 are arbitrary constants.

The quantities $k_{o,e}^{\pm}$ are simply the field-aligned wavenumbers of the magnetoacoustic waves inside and outside the slab, with '+' representing the slow waves and '-' representing the fast waves (note the diffrence in notation from that given in Eq. (2.1) of Chapter II). For each of the media inside and outside the slab, these wavenumbers are given by the two solutions of the quadratic (in k_x) equation (3.12). The normal modes of the equilibrium configuration (Fig. 3.1) associated with these wavenumbers will accordingly be referred to as the *(slow or fast) internal modes* and the *(slow or fast) external modes*, respectively. The former group of modes arise principally from the magnetoacoustic properties of the plasma slab, though they are also somewhat influenced by the external plasma because of the presence of the free interfaces of the slab. The external group of modes are, on the other hand, influenced principally by the magnetoacoustic properties of the medium outside the plasma slab. Note that $k_{o,e}^+$ are real and positive, whereas $k_{o,e}^-$ may be real or pure imaginary depending on whether $\omega^2 > k_z^2 c_{fo,e}^2$ or $\omega^2 < k_z^2 c_{fo,e}^2$ (cf. Schwartz and Bel, 1984a). Neither of these four quantities can, however, be complex as Eqs. (3.14) and (3.16) then demand that $c_{To,e}^2 > c_{fo,e}^2$, which is not possible.

3.2.2. Boundary conditions: The six arbitrary constants in Eqs. (3.13) and (3.15) are determined by the appropriate choice of boundary conditions. At the free interfaces $x = \pm a$ of the slab, we impose the MHD

boundary conditions given by Goedbloed (1983). The linearized form of these boundary conditions, obtained by integrating the MHD equations (1.1)-(1.5) [cf. Section 1.3.1, Chapter I] across arbitrary surface of discontinuity in the plasma, are:

$$\left[\mathbf{n}_0.\mathbf{v}\right] = 0\,, \tag{3.17}$$

$$\left[\mathbf{n}_0.\mathbf{b} + \mathbf{n}_1.\mathbf{B}\right] = 0\,, \tag{3.18}$$

$$\left[p + \frac{1}{4\pi}(\mathbf{B}.\mathbf{b})\right] = \left[p_T\right] = 0\,, \tag{3.19}$$

$$\mathbf{n}_0.\mathbf{B}\left[\mathbf{n}_0\times \mathbf{b} + \mathbf{n}_1\times \mathbf{B}\right] + \left(\mathbf{n}_1.\mathbf{B} + \mathbf{n}_0.\mathbf{b}\right)\left[\mathbf{n}_0\times \mathbf{B}\right] = 0\,, \tag{3.20}$$

$$\mathbf{n}_0.\mathbf{B}\left[\mathbf{n}_0\times \mathbf{v}\right] = 0\,, \tag{3.21}$$

and

$$\mathbf{n}_0.\mathbf{B}\left[\mathbf{v}.\mathbf{B}\right] = 0\,. \tag{3.22}$$

Here $\mathbf{n}_0$ and $\mathbf{n}_1$ are the unit vectors normal to the unperturbed and the perturbed boundaries, respectively. The quantity $[f] = f^+ - f^-$ represents the jump of a function f(x) across the boundary. The normal vector $\mathbf{n}_1$ is given by the condition

$$(\mathbf{n}_0 + \mathbf{n}_1).\left\{\mathbf{dl}_0 + (\mathbf{dl}_0.\nabla)(\mathbf{v}\delta t)\right\} = 0, \tag{3.23}$$

where $\mathbf{dl}_0$ is any line element on the unperturbed interface.

For the specific situation considered here, these conditions imply that

$$v_x,\ v_z,\ p \text{ and } b_z \text{ are continuous across } x = a. \tag{3.24}$$

For the remaining two boundary conditions, we impose the 'line-tying boundary conditions' at the walls $x = \pm \ell$, representing the chromospheric-photospheric boundaries at which the field lines are anchored. We thus obtain (see Section 1.4.3, Chapter I)

$$v_x(x) = v_z(x) = 0 \text{ at } x = \pm \ell\,. \tag{3.25}$$

3.2.3. The dispersion relation: Application of the boundary conditions (3.24) and (3.25) to the solutions (3.13) and (3.15) leads to the governing dispersion relations.

Write

$$X = k_z^2 c_s^2 + \omega^2 \left(\frac{v_A^2}{c_s^2} \right) - k^{+2} v_A^2, \tag{3.26}$$

$$Y = k_z^2 c_s^2 + \omega^2 \left(\frac{v_A^2}{c_s^2} \right) - k^{-2} v_A^2, \tag{3.27}$$

$$E = c_f^2 \left(\omega^2 - k_z^2 c_T^2 \right) - k^{+2} v_A^2 c_s^2, \tag{3.28}$$

$$F = c_f^2 \left(\omega^2 - k_z^2 c_T^2 \right) - k^{-2} v_A^2 c_s^2, \tag{3.29}$$

where these quantities have their appropriate values, X_o, Y_o, E_o and F_o and X_e, Y_e, E_e and F_e, in the regions "o" and "e", respectively. We further define the following quantities:

$$Q_1 = \frac{\left(\frac{1}{\eta} - 1 \right) \omega^2 + c_{se}^2 \left(k_e^{+2} - k_o^{-2} \right)}{c_{se}^2 \left(k_o^{+2} - k_o^{-2} \right)}, \tag{3.30}$$

$$Q_2 = \frac{\left(\frac{1}{\eta} - 1 \right) \omega^2 + c_{se}^2 \left(k_e^{-2} - k_o^{-2} \right)}{c_{se}^2 \left(k_o^{+2} - k_o^{-2} \right)}, \tag{3.31}$$

$$R_1 = \frac{i \left(\omega^2 - k_z^2 c_{fo}^2 \right) k_e^{+} \left(\eta X_o E_e - X_e E_o \right)}{\left(\omega^2 - k_z^2 c_{fe}^2 \right) k_o^{-} \left(X_o F_o - Y_o E_o \right)}, \tag{3.32}$$

$$R_2 = \frac{\left(\omega^2 - k_z^2 c_{fo}^2\right) k_e^- \left(\eta X_o F_e - Y_e E_o\right)}{\left(\omega^2 - k_z^2 c_{fe}^2\right) k_o^- \left(X_o F_o - Y_o E_o\right)}, \tag{3.33}$$

$$S_1 = \frac{i\left(\omega^2 - k_z^2 c_{fo}^2\right) k_e^+ \left(\eta Y_o E_e - X_e F_o\right)}{\left(\omega^2 - k_z^2 c_{fe}^2\right) k_o^+ \left(Y_o E_o - X_o F_o\right)}, \tag{3.34}$$

$$S_2 = \frac{\left(\omega^2 - k_z^2 c_{fo}^2\right) k_e^- \left(\eta Y_o F_e - F_o Y_e\right)}{\left(\omega^2 - k_z^2 c_{fe}^2\right) k_o^+ \left(Y_o E_o - X_o F_o\right)}, \tag{3.35}$$

$$Z_1 = \frac{\left(\frac{1}{\eta} - 1\right)\omega^2 + c_{se}^2 \left(k_e^{+2} - k_o^{+2}\right)}{\left(k_o^{-2} - k_o^{+2}\right) c_{se}^2}, \tag{3.36}$$

$$Z_2 = \frac{\left(\frac{1}{\eta} - 1\right)\omega^2 + c_{se}^2 \left(k_e^{-2} - k_o^{+2}\right)}{\left(k_o^{-2} - k_o^{+2}\right) c_{se}^2}, \tag{3.37}$$

$$\chi = \frac{i k_e^+ X_e}{k_e^- Y_e}, \quad \eta = \frac{\rho_e}{\rho_o}. \tag{3.38}$$

The dispersion relation for the *kink* modes can then be written as (see also Joarder and Roberts, 1992b)

$$(iQ_2Z_1-iQ_1Z_2)\left[\sin\left\{k_e^+(\ell-a)\right\}\cos\left\{k_e^-(\ell-a)\right\}+i\chi\sin\left\{k_e^-(\ell-a)\right\}\cos\left\{k_e^+(\ell-a)\right\}\right]$$

$$x\tan(k_o^+a)\tan(k_o^-a)+\left[\sin\left\{k_e^+(\ell-a)\right\}\sin\left\{k_e^-(\ell-a)\right\}-i\chi\cos\left\{k_e^+(\ell-a)\right\}\cos\left\{k_e^-(\ell-a)\right\}\right]$$

$$x\left[iS_2Z_1\tan(k_o^-)-iQ_1R_2\tan(k_o^+)\right]+(Q_1R_1+\chi Q_2R_2)\tan(k_o^+a)-(S_1Z_1+\chi S_2Z_2)\tan(k_o^-a)+$$

$$(R_2S_1-R_1S_2)\left[\cos\left\{k_e^+(\ell-a)\right\}\sin\left\{k_e^-(\ell-a)\right\}+i\chi\sin\left\{k_e^+(\ell-a)\right\}\cos\left\{k_e^-(\ell-a)\right\}\right]-$$

$$\left[Q_2R_1\tan(k_o^+a)-S_1Z_2\tan(k_o^-a)\right]\left[\cos\left\{k_e^+(\ell-a)\right\}\cos\left\{k_e^-(\ell-a)\right\}+i\chi\sin\left\{k_e^+(\ell-a)\right\}\sin\left\{k_e^-(\ell-a)\right\}\right]$$

$$= 0. \qquad (3.39)$$

The dispersion relation for the sausage modes follow from Eq. (3.39) on replacing "tan" by "- cot".

3.3. Solution of the dispersion relation

3.3.1. String analogies in the long wavelength limit: The dispersion relation (3.39) governing the various modes of oscillation of the plasma slab is too complicated to permit us to immediately draw any conclusions as to the nature of the modes it describes. However, we examine its properties in the extreme of small $k_z\ell$. In this limit of long wavelengths ($k_z\ell \ll 1$), Eqs. (3.14) and (3.16) take the following simplified forms:

$$k_o^+ = \frac{\omega}{\min(v_{Ao},c_{so})}, \quad k_e^+ = \frac{\omega}{\min(v_{Ae},c_{se})},$$

$$k_o^- = \frac{\omega}{\max(v_{Ao},cso)}, \quad k_e^- = \frac{\omega}{\max(v_{Ae},c_{se})}. \qquad (3.40)$$

With these simplified forms, the dispersion relation for the kink modes reduces to (see also Joarder and Roberts, 1992b)

$$\left[\left(\frac{\rho_e}{\rho_o}\right)^{1/2}\cot\frac{\omega(\ell-a)}{c_{se}} - \tan\frac{\omega a}{c_{so}}\right]\left[\left(\frac{\rho_e}{\rho_o}\right)^{1/2}\tan\frac{\omega a}{v_{Ao}} + \tan\frac{\omega(\ell-a)}{v_{Ae}}\right] = 0. \qquad (3.41)$$

The dispersion relation for the *sausage* modes in the long wavelength extreme follows by replacing $\tan(\omega a/c_{so})$ by - $\cot(\omega a/c_{so})$ and $\tan(\omega a/v_{Ao})$ by - $\cot(\omega a/v_{Ao})$ in Eq. (3.41).

It is of interest to note that the two square bracketed terms in Eq.(3.41) are in fact identical to the dispersion relations for the even and odd modes of vibration of a two density elastic string (Oliver et al. 1992c) with v_{Ae} , c_{se} and v_{Ao}, c_{so} replaced by the elastic speeds c_e and c_o in the two density regions of the string. The analogy of Eq.(3.41) to the dispersion relation of the vibratory modes of a mass loaded elastic string was pointed out earlier by Roberts (1991c) and Joarder and Roberts (1992b, c). To appreciate further this analogy, we consider the limit $2a \to 0$, $\rho_o \to \infty$ such that $2a\rho_o \to M$. The dense slab reduces to a point mass M in this limit, and the first square bracketed term in Eq. (3.41), representing the even modes of vibration of the string, reduces to the form (see Roberts, 1991c)

$$\frac{\omega \ell}{c_e} \tan\left(\frac{\omega \ell}{c_e}\right) = \frac{2\rho_e \ell}{M} . \qquad (3.42)$$

This is the dispersion relation for the vibratory modes of a point mass M attached to the centre of a stretched string of mass density ρ_e (Rayleigh, 1877).

In the case of a point mass M, the dispersion relation for the odd modes [obtained from the second square bracketed expression of Eq.(3.41)], yields $\tan\left(\frac{\omega \ell}{c_e}\right) = 0$, thus giving $\frac{\omega \ell}{c_e} = \nu'\pi$ ($\nu' = 1,2,3\ldots$). This is because, the odd modes have no displacement at x=0, and so in the point mass analogy these are external modes of the string, rather than the modes of the mass M itself.

Eq. (3.41) affords us with a means of classifying the various modes of the plasma slab in their long wavelength extreme. To shed further light on this classification, we discuss separately two cases of interest, namely, (i) when both the acoustic speeds internal and external to the slab are less than the respective Alfven speeds in the two media (so that $c_{so} < v_{Ao}$ and $c_{se} < v_{Ae}$); and (ii) when both the acoustic speeds are greater than the corresponding Alfven speeds (so that $c_{so} > v_{Ao}$ and $c_{se} > v_{Ae}$).

(i) $c_{so} < v_{Ao}$, $c_{se} < v_{Ae}$. In this case the two square bracketed terms in Eq. (3.41) represent the *slow* and *fast magnetoacoustic kink* modes in their

long wavelength ($k_z\ell << 1$) extreme. These long wavevelength kink modes can also be obtained directly from the differential equations (3.9) and (3.10). In the limit of long wavelengths ($k_z\ell << 1$), these two equations take the forms

$$\left[\frac{d^2}{dx^2} + \frac{\omega^2}{c_s^2}\right] v_x = 0 \qquad (3.43)$$

and

$$\left[\frac{d^2}{dx^2} + \frac{\omega^2}{v_A^2}\right] v_z = 0 \,. \qquad (3.44)$$

In both the regions "o" and "e", the long wavelength, decoupled, slow and fast waves then satisfy the simple harmonic wave equation. Eq. (3.43) shows that the velocity perturbation for the slow waves is predominantly in the x-direction in this limit of long wavelengths. Accordingly, the dispersion relation for the slow modes of the slab, in the limit $k_z\ell << 1$, can be obtained from the even (cosine) or odd (sine) solutions of Eq. (3.43) after imposing the boundary conditions (3.24) and (3.25) on v_x and p ($\equiv \frac{dv_x}{dx}$ in the limit $k_z\ell << 1$). For the kink (even) slow modes this dispersion relation is identical to the first square bracketed expression in Eq.(3.41).

For the fast waves, Eq.(3.44) shows that the velocity perturbation pertaining to these waves is predominantly in the z-direction (in the limit $k_z\ell << 1$). The relationship between the two components (v_x and v_z) of the velocity perturbation is given in Eq. (3.6). This equation shows that an even (cosine) functional behaviour of $v_x(x)$ implies an odd (sine) functional behaviour of $v_z(x)$. Accordingly, the dispersion relation for the fast kink mode is given by the odd (sine) solutions of Eq. (3.44) after the application of the boundary conditions (3.24) and (3.25) on v_z and b_z [$\equiv \frac{dv_z}{dx}$; see Eq.(3.4)]. This dispersion relation is identical to the second square bracketed expression in Eq.(3.41).

Eq. (3.41) can be simplified further in the case when the plasma slab is much denser than it surroundings, so that $\rho_e/\rho_o << 1$; see also Joarder and Roberts (1992b). Such a situation is normally found in solar quiescent

prominences. In this case, the frequencies of the slow kink modes are given by

$$\frac{\omega a}{c_{so}} = \nu\pi, \tag{3.45}$$

for the harmonics (ν=1,2,3.....) of the internal slow kink ($\equiv IS^k$) modes; and

$$\frac{\omega(\ell-a)}{c_{se}} = \nu'\pi, \tag{3.46}$$

for the harmonics (ν'=1,2,3.....) of the external slow kink ($\equiv ES^k$) modes.

The fundamental ($\nu = \nu'=0$) of the slow kink modes is of particular interest. This mode is given by the lowest frequency solution of Eq.(3.41). In both the cases a=0 and a=ℓ, this fundamental mode presents the fundamental slow kink mode of a uniform bound medium, thus giving $\frac{\omega\ell}{c_{se}} = \frac{\pi}{2}$ and $\frac{\omega a}{c_{so}} = \frac{\pi}{2}$, respectively. For small a/ℓ, we can, however, rewrite the dispersion relation for the slow kink modes as

$$\tan\left(\frac{\omega\ell}{c_{sc}}\right)\tan\left[\left(\frac{\omega\ell}{c_{se}}\right)\left(\frac{a}{\ell}\right)\left(\frac{\rho_o}{\rho_e}\right)^{1/2}\right] = \left(\frac{\rho_e}{\rho_o}\right)^{1/2}. \tag{3.47}$$

When both $\frac{\omega\ell}{c_{se}}$ and $\left[\left(\frac{\omega\ell}{c_{se}}\right)\left(\frac{a}{\ell}\right)\left(\frac{\rho_o}{\rho_e}\right)^{1/2}\right]$ are small, we obtain, from Eq. (3.47), the following formula for the frequency of the fundamental slow kink mode (see also Joarder and Roberts, 1992b, c)

$$\frac{\omega\ell}{c_{se}} \approx \left(\frac{\rho_e}{\rho_o}\right)^{1/2} \Big/ \left(\frac{a}{\ell}\right)^{1/2}; \tag{3.48a}$$

thus

$$\omega = \frac{c_{so}}{(\ell a)^{1/2}}. \tag{3.48b}$$

While deriving Eq. (3.48a, b), we have assumed $\left(\frac{\rho_e}{\rho_o}\right) << \left(\frac{a}{\ell}\right) << 1$. However, Eq.(3.48a, b) provides a good approximation to the actual (numerically determined) frequency of this fundamental mode, provided a/ℓ lies in the range $\left(\frac{\rho_e}{\rho_o}\right)$ to $\left(\frac{\rho_e}{\rho_o}\right)^{1/2}$; see also Joarder and Roberts (1993b). This fact is demonstrated in Table 3.1, where we compare the numerically determined values of $\frac{\omega\ell}{c_{se}}$ for the fundamental slow kink mode with those given by Eq. (3.48a). The numerical values are obtained by solving Eq. (3.41) for various values of the anchor point separation distance 2ℓ (and hence for various values of the ratio $\frac{a}{\ell}$). We considered a slab of width 2a = 5000 km in an environment with temperature $T_e = 10^6$ K (giving a sound speed $c_{se} \approx$ 166 kms^{-1}), and a density ratio $\frac{\rho_o}{\rho_e} \approx$ 125. Table 3.1 shows that Eq. (3.48) gives a good estimate for the actual frequency of the fundamental mode for values of the anchor point separation distance 2ℓ lying approximately in a range of 5 10^4 km (corresponding to $\frac{a}{\ell} = \left(\frac{\rho_e}{\rho_o}\right)^{1/2} = 0.09$) to 6 10^5 km (corresponding to $\frac{a}{\ell} = \left(\frac{\rho_e}{\rho_o}\right) = 0.008$). Even for a value of 2ℓ as small as 1.7 10^4 km, corresponding to an $\frac{a}{\ell} = \left(\frac{\rho_e}{\rho_o}\right)^{1/4} = 0.3$, the actual frequency lies only slightly above the value estimated from Eq.(3.48). However, Table 3.1 shows that for arbitrarily large values of the anchor point separation distance 2ℓ, such that $\frac{a}{\ell} << \frac{\rho_e}{\rho_o} << 1$, the approximation (3.48) breaks down with the dimensionless frequency $\frac{\omega\ell}{c_{se}}$ of the fundamental mode approaching asymptotically to a value of $\frac{\pi}{2}$; see the discussion above.

We may here note that Eq. (3.48) for the frequency of the fundamental slow kink mode is, in fact, the same as the frequency derived intuitively by Lamb (1910) for the fundamental vibration of a mass loaded stretched string; see also Eq. (1.40) in Section 1.4.3, chapter I. To

emphasize this analogy to the fundamental vibrations of an elastic string, we refer to the fundamental slow kink mode as the *slow string* ($\equiv S_{string}$) mode.

Table 3.1. *The frequency of the 'slow string' mode (ie. fundamental slow kink mode) in the limit $k_z \ell << 1$ for various values of the anchor point separation distance 2ℓ, with $c_{se} \approx 166$ kms^{-1}, $a = 2500$ km and $\rho_o/\rho_e = 125$.*

2ℓ in km	$\frac{a}{\ell}$	$\frac{\omega\ell}{c_{se}}$	$\left(\frac{\rho_e}{\rho_o}\right)^{1/2} / \left(\frac{a}{\ell}\right)^{1/2}$
$1.\ 10^{12}$	$5.\ 10^{-09}$	1.5708	$1.26\ 10^{3}$
$6.25\ 10^{5}$	$8\ 10^{-3}$	0.8650	1.0
$5.6\ 10^{4}$	$8.9\ 10^{-2}$	0.3045	0.2991
$1.67\ 10^{4}$	0.30	0.1821	0.1636
$5\ 10^{3}$	1.0	0.1405	0.0894

Having thus discussed the behaviour of the long wavelength slow kink modes of the plasma slab, in a case where both the sound speeds internal and external to the slab are less than the respective Alfven speeds in the two media, we now investigate the nature of the long wavelength *fast magnetoacoustic kink* modes of the model prominence slab. The dispersion relation of such modes were given by the second square bracketed [] expression of Eq. (3.41). When the density ratio ρ_e/ρ_o is arbitrarily small, we can classify the asymptotic solutions pertaining to these fast magnetoacoustic kink modes in their long wavelength extreme as

$$\frac{\omega a}{v_{Ao}} = (2\mu+1)\frac{\pi}{2} \quad \text{and} \quad \frac{\omega(\ell-a)}{v_{Ae}} = (\mu'+1)\pi \ ; \ \mu, \mu'=0,1, 2...., \tag{3.49}$$

corresponding to the internal fast kink ($\equiv IF^k$) modes and the external fast kink ($\equiv EF^k$) modes, respectively.

Turning now to the *sausage* modes, the fundamental ($\mu, \mu'=0$) of the fast sausage modes is similar in character to the fundamental vibration of a mass loaded elastic string. For small ρ_e/ρ_o and for small a/ℓ the frequency of this mode is therefore given by Eq. (3.1), with now v replaced

by the Alfven speed v_{Ao} inside the slab. Accordingly, we refer to the fundamental fast sausage mode as the *fast string* ($\equiv F_{string}$) *mode*.

The other sausage modes may be considered in a similar fashion. In the limit of long wavelength and for an extremely dense plasma slab, we find that

$\frac{\omega a}{v_{Ao}} = \mu\pi$, for the harmonics ($\mu$=1, 2, 3,...) of the internal fast sausage ($\equiv IF^s$) modes; (3.50a)

$\frac{\omega(\ell-a)}{v_{Ae}} = \mu'\pi$ for the harmonics (μ'=1, 2, 3,...) of the external fast sausage ($\equiv EF^s$) modes; (3.50b)

$\frac{\omega a}{c_{so}} = (2\nu+1)\frac{\pi}{2}$, ν =0, 1, 2, ... for internal slow sausage ($\equiv IS^s$) modes; (3.50c)

and

$\frac{\omega(\ell-a)}{c_{se}} = (\nu'+1)\pi$, ν' = 0, 1, 2,.....for external slow sausage ($\equiv ES^s$) modes. (3.50d)

As before, the first letter (I or E) denotes internal or external modes, the second letter (S or F) represents slow or fast, and the superscript (^{k} or ^{s}) represents kink or sausage modes.

(ii) $c_{so} > v_{Ao}$, $c_{se} > v_{Ae}$. Consider now the situation where both the sound speeds internal and external to the slab are greater than the corresponding Alfven speeds. The normal modes in this situation may be identified much as in case (i) with the names "slow" and "fast" interchanged in Eqs. (3.45)-(3.50).

3.3.2. Numerical solutions of the full dispersion relation: The investigation of the dispersion relation (3.41) for the slab modes in their long wavelength extreme ($\kappa\ell << 1$) provides us with a means of identifying all the modes of oscillation of the plasma slab that appear in the numerical solution of the general dispersion relation (3.39) in the case when the

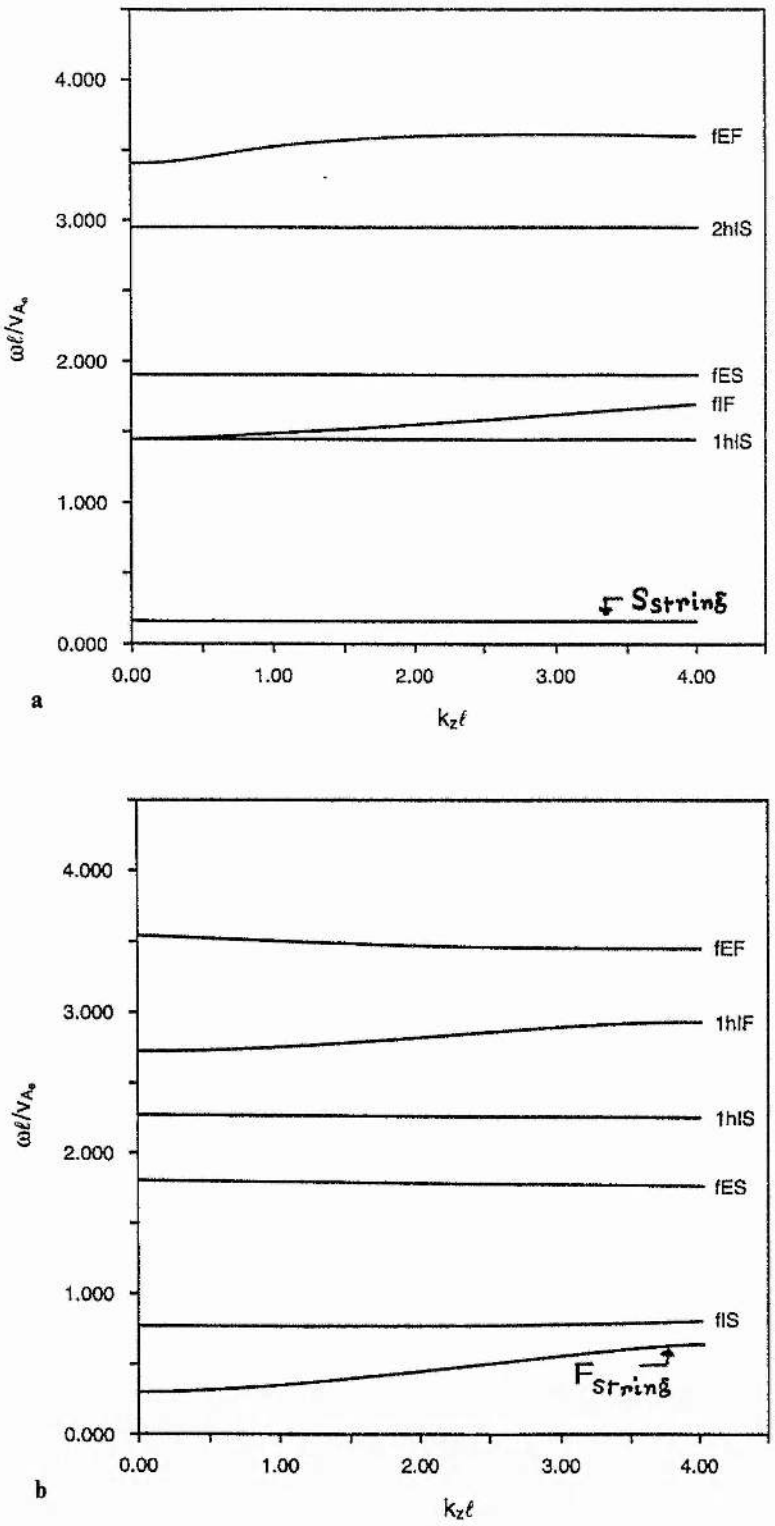

Fig. 3.2a,b. Dimensionless frequency vs. dimensionless wavenumber for (a) kink and (b) sausage modes of the plasma slab and its environment, in a case when $c_{so} = 15$ kms^{-1}, $v_{Ao} = 28$ kms^{-1}, $c_{se} = 166$ kms^{-1} and $v_{Ae} = 315$ kms^{-1}. The modes are identified as fast (F) and slow (S) magnetoacoustic modes, with 'I' denoting an internal mode and 'E' denoting an external mode. The string modes are denoted by a subscript 'string'. The first letter in the name of a mode indicates whether it is a fundamental (f) or a higher harmonic (first harmonic 1h; second harmonic 2h, etc.)

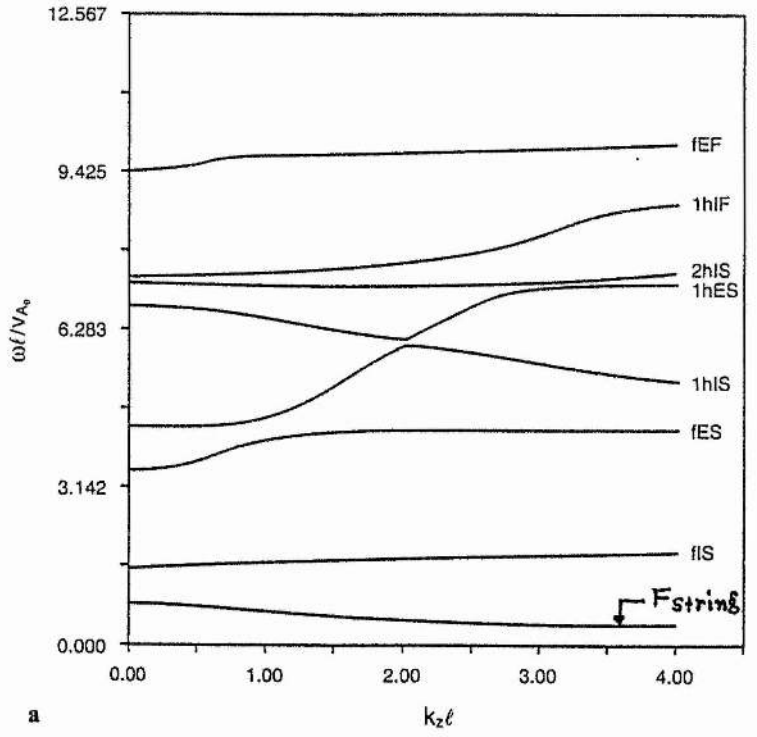

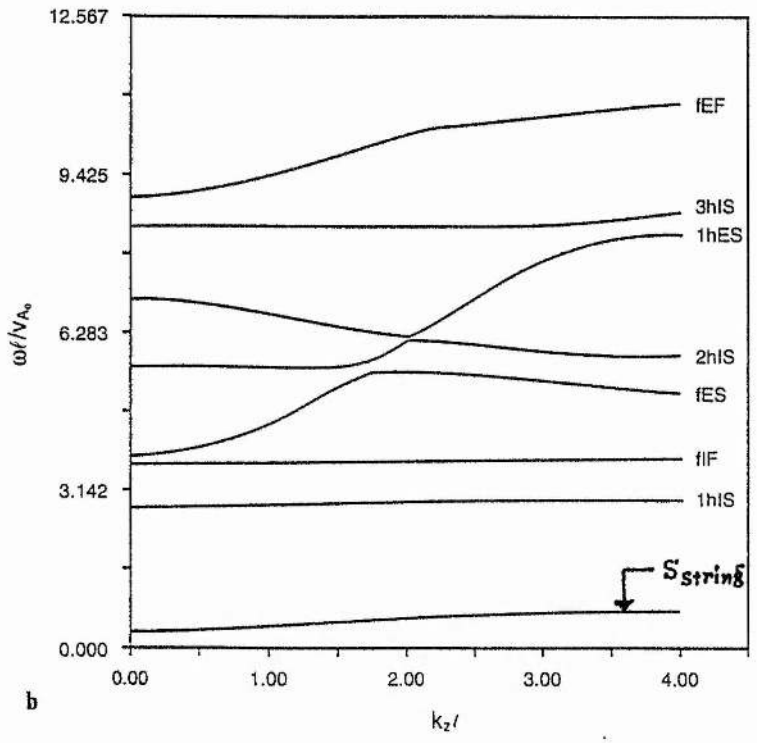

Fig. 3.3a,b. Frequency vs. wavenumber for (a) kink and (b) sausage modes of the plasma slab and its environment in the case when c_{so} = 15 kms^{-1}, v_{Ao} = 6 kms^{-1}, c_{se} = 166 kms^{-1}, and v_{Ae} = 63 kms^{-1}. The symbols representing the various modes are the same as in Fig. 3.2.

dimensionless wavenumber $\kappa\ell$ of the modes is of the order of unity or even larger. Such numerical solutions of the full dispersion relation (3.39) are shown in Figs. (3.2) and (3.3). Fig. 3.2(a,b) shows the various kink and sausage modes that are present in the plasma slab in the case when the acoustic speeds of both the media inside and outside the slab are less than the respective alfven speeds ($c_{so} < v_{Ao}$, $c_{se} < v_{Ae}$). The diagrams 3.2(a) and 3.2(b) are computed for a slab (prominence) density of $\rho_o = 2.5\ 10^{-13}$ gcm^{-3}, temperature $T_o = 8000$ K, and magnetic field B=5 G, giving $c_{so} = 15$ kms^{-1}, $v_{Ao} = 28$ kms^{-1}, $c_{se} = 166$ kms^{-1} and $v_{Ae} = 315$ kms^{-1}. The plasma slab is taken to be of width 2a = 5000 km and is anchored at a distance $\ell = 10a$ on either side of the centre of the slab.

In Fig. 3.3(a,b), we present our numerical results for the various kink and sausage modes of the prominence slab, choosing the parameters to be the same as in Fig. 3.2, except for the magnetic field strength. Here we choose a transverse field of B=1 G, giving the Alfven speeds inside and outside the slab as $v_{Ao} = 6$ kms^{-1} and $v_{Ae} = 63$ kms^{-1}; the acoustic speeds c_{so} and c_{se} are unchanged, of course. Fig.3.3 thus represents the case when both the acoustic speeds inside and outside the slab are greater than the respective Alfven speeds (ie. $c_{so} > v_{Ao}$, $c_{se} > v_{Ae}$).

In both the Figs. 3.2 and 3.3 the normal modes show strong signatures of "avoided crossing" or "mode coupling" near certain wavenumbers of these modes at which the asymptotic dispersion (frequency vs. wavenumber) curves of the modes intersect each other. As a result of such avoided crossing, a splitting in the frequencies of the coupled modes takes place at the point of crossover, generally in a hyperbolic fashion. Avoided crossings of normal modes have been discussed by many authors in various contexts; see, for example, Jones (1970) for a description of avoided crossings in the context of ionospheric oscillations, Pippard (1978) in the context of the coupled electrical resonant circuits, Christensen-Dalsgaard (1980) for the coupling between the acoustic (p) modes and gravity (g) modes in asteroseismology, Leibacher and Stein (1981) in the case of the resonant excitation of the 3 min oscillations in solar chromosphere due to their couplings with the photospheric 5 min oscillations, and Hasan (1991), Hasan and Christensen-Dalsgaard (1992) in the context of the mode couplings of the magnetoacoustic-gravity modes in sunspots.

At the region of avoided crossing, the coupled modes exchange kinetic energy between themselves, permiting a resonant excitation of one

mode due to the coupling with another more energetic mode. Such coupled modes also share some common properties among themselves, and therefore, a distinction between the coupled modes according to their dominant restoring forces, or according to the behaviour of the eigenfunctions pertaining to the modes, may no longer be possible around a region where such avoided crossings take place. We may, however, note that the detailed nature of the coupling between different modes is sensitive to the choice of the particular equilibrium configuration pertaining to these modes. To draw any definite conclusions about the nature of such mode coupling in solar prominences, it is therefore required that we examine other, perhaps more realistic, magnetostatic prominence equilibrium models than those considered in this thesis. The models of prominences that we examine are all somewhat elementary in nature, and so we here avoid any detailed discussion of the mode coupling between various normal modes that pertain in these basic models of prominences. The simple models we here examine can only give us rough estimates for the periods of the fundamental modes that may exist in solar prominences. In the next section, we accordingly confine ourselves to a discussion of the periods of the fundamental modes for wavelengths relevant to prominence oscillations.

3.4. Eigenfrequencies of prominence oscillations

Having thus solved our dispersion relation, we now examine the eigenfrequencies of the normal modes that may be present in quiescent prominences. As in Chapter II, we consider the prominence as a rectangular elastic membrane. The wavenumber of the normal modes of such an elastic membrane can be expressed as (cf. Section 1.4.2, Chapter I)

$$k_{m,n} = \pi \sqrt{\frac{m^2}{L^2} + \frac{n^2}{H^2}}, \tag{3.51}$$

where m and n are integers describing the modal structure along the length L and the height H of the prominence. The case m= n=1 gives the principal (fundamental) mode of oscillation.

In this chapter, we consider the prominence to be of infinite length, implying $L \rightarrow \infty$ and $k_y = 0$. In this particular case, Eq. (3.51) can be written as

$$k_{m,n} \approx k_n = k_z = \pi \frac{n}{H}. \qquad (3.52)$$

With a typical prominence height $H \approx 4\text{-}5\ 10^4$ km (see Section 1.1.2, Chapter I) and a mean separation distance of $2\ell = 50{,}000$ km (say) between the anchor points of the field-lines, Eq. (3.52) then yields a value of $k_n\ell = k_z\ell \approx 1.6\text{-}2.0$ for the principal (n=1) eigenmode. We choose $k_z\ell = 1.75$ for the numerical calculations of the periods of prominence oscillations.

For the plasma parameters inside the prominence, we choose the illustrative values of Section 3.3, namely a temperature $T_o = 8000$ K and a density $\rho_o = 2.5\ 10^{-13}$ gcm^{-3}; these values are representative of the situation normally found in quiescent prominences (see Table 1.1, Chapter I). With a coronal temperature of 10^6 K, pressure balance then gives a density of $\rho_e = \rho_o(T_o/T_e) = 2\ 10^{-15}$ gcm^{-3} for the coronal environment of a prominence. Such a value of the mass density corresponds to a particle density of $n_p \approx 10^9$ cm^{-3}. This is somewhat larger than the particle density of about 10^8 particles per cm^3 (Engvold et al. 1990) generally observed for the coronal environment of prominences. The larger value for the coronal mass density implied by pressure balance in our model is perhaps an artefact of the model's simplicity. In any case, the precise value of ρ_e does not greatly influence our calculations for the periods of the modes of oscillation of a prominence; periods are principally influenced by the Alfven speed and the acoustic speed inside the prominence.

In the present case of a prominence slab with a transverse magnetic field, the significant oscillatory modes of the prominence would seem to be the two (slow and fast) string modes and also the fundamental internal modes of the slab. These modes are expected to have appreciable kinetic energy densities. The periods of these modes in a prominence slab of width $2a = 5000$ km are displayed in Table 3.2 for two values of the transverse field strength, namely B = 5G and B =1G. The case of B = 5G represents an average prominence situation, whereas the case of B = 1G is included as possibly representative of prominences with much weaker transverse field-strengths (see Section 3.1).

Along with the numerical values of the periods of the various modes in the prominence slab, we also display the formulae for these periods in

their long wavelength extreme; cf. Section 3.3. These simple mathematical relations provide us with an order of magnitude estimate for the periods and also shed some light on the physical nature of the modes of oscillation. Table 3.2 shows that, except for the case of the magnetoacoustic string modes in a slab with a very weak magnetic field strength, the actual numerical values of the periods deviate only slightly from these simple order of magnitude estimates of the periods calculated in the limit of long wavelengths, even when the dimensionless wavenumber $k_z\ell$ for the modes is of the order of unity or larger.

Table 3.2. *Numerically determined periods of the fundamental vibrations of a prominence slab for two different values of the transverse magnetic field strength* $\boldsymbol{B}$, *with* $\rho_o = 2.5\ 10^{-13}\ gcm^{-3}$, $T_o = 8000\ K$, $a = 2500\ km$, $\ell = 10a$, *and* $H = 4.5\ 10^4\ km$.

Names of the modes	Periods	
	B = 5.0 G $v_{Ao} \approx 28\ kms^{-1}$, $c_{so} \approx 15\ kms^{-1}$	B = 1.0 G $v_{Ao} \approx 6\ kms^{-1}$, $c_{so} \approx 15\ kms^{-1}$
Slow string mode (S_{string})	56 min $\left(\tau \approx \frac{2\pi(\ell a)^{1/2}}{c_{so}} \approx 55\ min\right)$	73 min $\left(\tau \approx \frac{2\pi(\ell a)^{1/2}}{v_{Ao}} \approx 138\ min\right)$
Fast string mode (F_{string})	20 min $\left(\tau \approx \frac{2\pi(\ell a)^{1/2}}{v_{Ao}} \approx 30\ min\right)$	86 min $\left(\tau \approx \frac{2\pi(\ell a)^{1/2}}{c_{so}} \approx 55\ min\right)$
Internal slow mode	11 min (fIS^s) $\left(\tau \approx \frac{4a}{c_{so}} \approx 11\ min\right)$	26 min (fIS^k) $\left(\tau \approx \frac{4a}{v_{Ao}} \approx 28\ min\right)$
Internal fast mode	6 min (fIF^k) $\left(\tau \approx \frac{4a}{v_{Ao}} \approx 6\ min\right)$	11 min (fIF^s) $\left(\tau \approx \frac{4a}{c_{so}} \approx 11\ min\right)$

It is encouraging to note that the frequencies of the various modes displayed in Table 3.2 are in reasonable agreement with the observed frequencies of prominence oscillations (see Section 1.2, Chapter I, for discussion of observational results). However, considering the simplicity of

the model presented here, we concentrate only on those modes which are of particular interest.

As discussed in the Introduction, intermediate periodicities (of the order of 10-20 min) that have been detected in prominences (see Table 1.2(b)) were absent in the model calculations for a prominence slab within which is embedded a purely longitudinal magnetic field (Chapter II). Here we find the occurrence of such periodicities in a mode that is essentially a trapped magnetoacoustic wave reflected off the boundaries of the prominence slab. This mode has a period of the order of twice the sound travel time across the width of the prominence. In our simple slab model of a prominence with a purely transverse, line-tied, magnetic field, this mode is an internal sausage mode, being slow or fast depending on the magnitude of the transverse magnetic field threading the prominence. Much shorter periodicities, in the range of 3-5 min, that are observed in prominence oscillations, also appear in the present model of a prominence, although only in the case of an intermediate to strong transverse magnetic field. For a magnetic field strength of 5G, such a periodicity of 6 min is presented by an internal fast mode of the slab; see Table 3.2.

The existence of the low frequency kink and sausage modes with periods of the order of 1/2-1 hr is of particular interest. These modes owe their existence to the effect of photospheric line-tying on the foot points of the magnetic arcades threading a prominence. The modes arise from waves that are reflected off the boundaries where the field lines are anchored; they are analogous to the fundamental vibrations of a mass loaded elastic string. Accordingly, we refer to these modes as the (slow or fast) string modes. For a prominence slab with a transverse field of 5G, these modes correspond to a slow kink mode and a fast sausage mode of the slab; see Fig. 3.2a, b. However, for a prominence slab with a much weaker (1G, say) transverse field, the slow (S_{string}) mode corresponds to a sausage mode, whereas the fast (F_{string}) mode corresponds to a kink mode of the plasma slab (see Fig.3.3a,b).

3.5 Conclusions

In this chapter, we have considered the magnetohydrodynamic modes of vibration of a two-dimensional, non-gravitating prominence slab embedded in a purely transverse and line-tied magnetic field. Such a consideration of the transverse field component and its photospheric line-

tying introduce a new structure in the magnetohydrodynamic modes of oscillation of a prominence that could not be expected from the slab with a purely longitudinal magnetic field. This is clear from a comparison of the present results with those presented in Chapter II. Despite the fact that we have ignored gravity, the prominence model we have investigated in this chapter is somewhat similar to certain classical, two-dimensional models of quiescent prominences, such as the Menzel (1951) or the Kippenhahn-Schlüter (1957) prominence models. The results presented in this chapter are therefore expected to serve as a useful guide to the modes of oscillation of these more complicated magnetostatic models of prominences, as we will see in the next chapter.

It is, however, important to note that, like most of the classical models of quiescent prominences, the model of a prominence slab investigated in this chapter suffers from a serious drawback, namely that it completely excludes a discussion of the dominant longitudinal component of the magnetic field that threads a prominence. The magnetic field in a prominence makes a fine angle of approximately 20^{o} with the prominence-axis. This orientation of the magnetic field is so typical in quiescent prominences that it is sometimes considered to play a significant role in the mechanism of formation of such prominences; cf. Zirker (1989). A theoretical model of prominence oscillations that excludes a discussion of this field-orientation cannot therefore be considered to provide a very realistic description of the oscillatory modes in quiescent prominences and is, perhaps, not entirely suitable for any direct comparison with the observational results. Nevertheless, the present model reveals, in its simplest form, the basic structure of the magnetohydrodynamic modal spectrum that may possibly exist in quiescent prominences, and also gives us clues as to how these simple results are expected to be modified in the case the more realistic skewed-field geometry actually observed in quiescent prominences. We return to this topic in Chapter V.

Chapter IV

Oscillations in simple gravitational prominence models

4.1 Introduction

We have so far explored (in Chapters II and III) the nature of oscillatory motions in simple magnetohydrodynamic slab models, assumed representative of prominences. The complications of a real prominence, with its inhomogeneous density and temperature structure in gravitational balance with the curved magnetic field that threads the structure, is of course not represented by such simple models. Nonetheless, one may expect that the periods of the fundamental modes of a prominence model are given, to a reasonable approximation, by such models, in so far as gravitational forces and magnetic curvature play subsidiary roles. In such a case, the study of a simple model leads to a clearer insight into the principal factors that determine the periods of oscillation than could readily be gained from an analysis - no doubt largely numerical - of a complex structure. This was the basis for Chapters II and III.

Of course, a study of simple models, such as those of Chapters II and III, must ultimately be complemented by studies of complex models that are more closely representative of observed prominences. Such detailed studies are indeed vital if one is to use oscillations as a probe of prominence-coronal conditions. But a full understanding of the nature of a prominence's modes of oscillation will no doubt need the insights provided by an analysis of simple models.

Here (see also Joarder and Roberts, 1993a), as a first step towards investigating the modes of oscillation of a complex prominence model, we consider the influence of gravity and field line curvature on a simple prominence-like structure. We examine the modes of oscillation of an isothermal, two-dimensional prominence equilibrium model commonly referred to as Mènzel's model. Menzel's (1951) model is not a good representation of a prominence, for it fails to allow either for non-isothermality or for a component of magnetic field along the principal axis of the prominence-sheet. Nonetheless, Menzel's model has a simplicity that allows us to study its modes of oscillation. This provides some insight into the roles of gravity and field line curvature and furthermore allows a close comparison with the simple model of Chapter III.

Complementary studies have recently been done for the modes of oscillation of an isothermal Kippenhahn-Schlüter (1957) prominence model (Oliver et al. 1992a, b), and also of a generalized, non-isothermal version of the Kippenhahn-Schlüter equilibrium model, as obtained from the calculations of Poland and Anzer (1971) by ignoring the effects of non-adiabaticity that were present in their model; see Oliver et al. (1993a). In this chapter, we also describe the investigations of Oliver et al. in some detail in order to show that, as for the Menzel's model, the modes obtained from these complementary prominence models can also be readily interpreted by using a simple slab-type model, such as the one presented in Chapter III.

4.2 Menzel's model

4.2.1 The basic magnetostatic equilibrium equation: Following Brown (1958), we here consider the solutions of the magneto-hydrostatic force balance equation (1.1) along with the divergence-free condition (1.2) for the magnetic field; see Section 1.3.1 in Chapter I. We also consider an isothermal (T_0=constant) atmosphere. The pressure scale-height H_0 in such an atmosphere is defined as

$$H_0 = \frac{p_0}{\rho_0 g} = \frac{RT_0}{\mu g}, \tag{4.1}$$

where R is the gas constant and μ is the mean molecular weight of the plasma.

We confine ourselves to the (x, z) plane of a rectangular coordinate system. The magnetic field can then be given in terms of a flux function F(x, z) as

$$\mathbf{B_0} = \left(-\frac{\partial F}{\partial z}, 0, \frac{\partial F}{\partial x} \right) \tag{4.2}$$

thus satisfying Eq. (1.2) of Chapter I. The lines of force are given by F(x, z) = constant for any plane y = constant.

With the help of Eqs. (4.1) and (4.2), we can rewrite Eq. (1.1) as

$$\nabla\left\{p_0 \exp\left(\frac{z}{H_0}\right)\right\} = -\frac{1}{4\pi}\left\{\nabla^2 F \exp\left(\frac{z}{H_0}\right)\right\}\nabla F. \tag{4.3}$$

Eq. (4.3) shows that $p_0 \exp\left(\frac{z}{H_0}\right)$ is a function of F, which we denote by G(F), say, and then

$$\frac{d}{dF}G(F) = -\frac{1}{4\pi}\nabla^2 F \exp\left(\frac{z}{H_0}\right). \tag{4.4}$$

Thus $(\nabla^2 F) \exp\left(\frac{z}{H_0}\right)$ must also be a function of F that satisfies the condition (cf. Menzel, 1951; Dungey, 1953; Cowling, 1957; Brown, 1958)

$$\nabla^2 F = \Phi(F) \exp\left(-\frac{z}{H_0}\right), \tag{4.5}$$

where $\Phi(F) = -4\pi\ (dG/dF)$ is any arbitrary function of F.

Eq. (4.5) is, in fact, the basic equation for static equilibrium in the two-dimensional ($B_y = 0$) case. Any function F(x, z) that is a solution of Eq. (4.5) will give a possible model for the magnetic field. A wide range of such solutions are considered by various authors (cf. Menzel, 1951; Dungey, 1953; Kippenhahn and Schluter, 1957; Hood and Anzer, 1990). Two choices for the function $\Phi(F)$ are of particular interest. They are

$$\Phi(F) = A_1 F^{\left(1-\frac{2H_B}{H_0}\right)}, \tag{4.6a}$$

with

$$F(x, z) = f(x)\exp\left(-\frac{z}{2H_B}\right), \tag{4.6b}$$

for the Menzel's (1951) model, and

$$\Phi(F) = A_2 \exp\left\{\frac{F(x, z)}{A_3 H_0}\right\}, \tag{4.7a}$$

with

$$F(x, z) = A_3 z + F_1(x) , \quad A_3 < 0 , \tag{4.7b}$$

for the Kippenhahn-Schluter (1957) model. Here A_1, A_2, A_3 are constants, and $f(x)$, $F_1(x)$ are arbitrary functions. In Eq. (4.6), we have assumed that the presence of the magnetic field modifies the state of stratification of the isothermal plasma that prevailed under ordinary hydrostatic force balance condition in the absence of the magnetic field. This effect of the magnetic field may simply be described by replacing H_0 (Eq. (4.1)) by a magnetically modified pressure scale-height H_B that depends on the curvature of the magnetic field lines, and on the value of the plasma-beta of the material. For a prominence-type equilibrium, where dense material is supported against gravity by the magnetic field lines, we must have $H_B > H_0$. The numerical value of H_B is, however, specified arbitrarily in the simple equilibrium model of Menzel (1951); see discussions below.

We here note that more generalized forms of the magnetostatic equilibrium equation have also been constructed, and its various exact solutions, involving two-dimensional flux-functions that correspond to various field geometries and also allow for a continuous temperature variation of the plasma, have been obtained; see, for example, Parker (1968, 1979), Lerche and Low (1977, 1980), Low (1975a, b, 1980, 1981).

4.2.2 The solution of Menzel: We here consider Menzel's (1951) solution of the magnetostatic equilibrium equation (4.5). The Kippenhahn-Schluter solution (Eq. (4.7)) has recently been discussed in detail by Oliver et al. (1992a, b, 1993a). We will discuss their results in a later section. In Menzel's model, we may reduce Eq. (4.4), with the help of Eq. (4.6), to the form

$$4H_B^2 \frac{d^2 f}{dx^2} + f = A_1 f^{\left(1 - \frac{2H_B}{H_0}\right)} . \tag{4.8}$$

Eq. (4.8) integrates to give

$$B_0^2 \exp\left(\frac{z}{H_B}\right) = \left(\frac{df}{dx}\right)^2 + \frac{f^2}{4H_B^2} = K_1 - \frac{A_1}{q f^{2q}} , \tag{4.9}$$

where K_1 is a constant and $B_0 = |\mathbf{B_0}|$. The exponent q in Eq. (4.9) is defined by $q+1 = \frac{H_B}{H_0}$. With the help of Eqs. (4.3) - (4.6), we can also write the corresponding expression for the gas pressure as

$$p_0(x, z) = -\frac{1}{4\pi}\exp\left(-\frac{z}{H_o}\right)\int\Phi(F)dF = \frac{A_1}{8\pi q}\left(\frac{1}{f}\right)^{2q}\exp\left(-\frac{z}{H_B}\right) = P(x)\exp\left(-\frac{z}{H_B}\right). \qquad (4.10)$$

The constant K_1 in Eq. (4.9) can be eliminated by the application of the boundary conditions

$$f=f_0 \text{ and } f' = 0 \text{ at } x= 0, \qquad (4.11)$$

where f' denotes $\frac{df}{dx}$.

It is convenient to introduce $\beta_0 = \frac{8\pi p_0}{B_0^2}$, the plasma-beta at x=0. Then, with the help of Eq. (4.11), Eq. (4.8) can be written as (cf. Menzel, 1951; Dungey, 1953; Cowling, 1957; Brown, 1958; Tandberg-Hanssen, 1974)

$$4H_B^2\frac{d^2f}{dx^2} = -f + q\beta_0 f_0\left(\frac{f_0}{f}\right)^{2q+1}. \qquad (4.12)$$

We may note, from Eqs. (4.9) and (4.10), that the total (gas + magnetic) pressure is independent of the x-coordinate and so varies only in the vertical direction. On the other hand, the Alfven speed $v_A(x) = \frac{B_0}{(4\pi\rho)^{1/2}}$ does not vary with height z.

Equation (4.12) along with the boundary conditions (4.11) describe the magnetic field configuration in the magnetostatic equilibrium model of Menzel. These equations can be solved numerically, with the solutions generally being periodic in nature. The lines of force (F = constant) form a set of parallel curves

$$z - z_0 = 2H_B \log\left(\frac{f}{f_0}\right), \qquad (4.13)$$

where z_0 is a constant. These curves show a very similar behaviour to that of the function f(x); see Fig. 4.1.

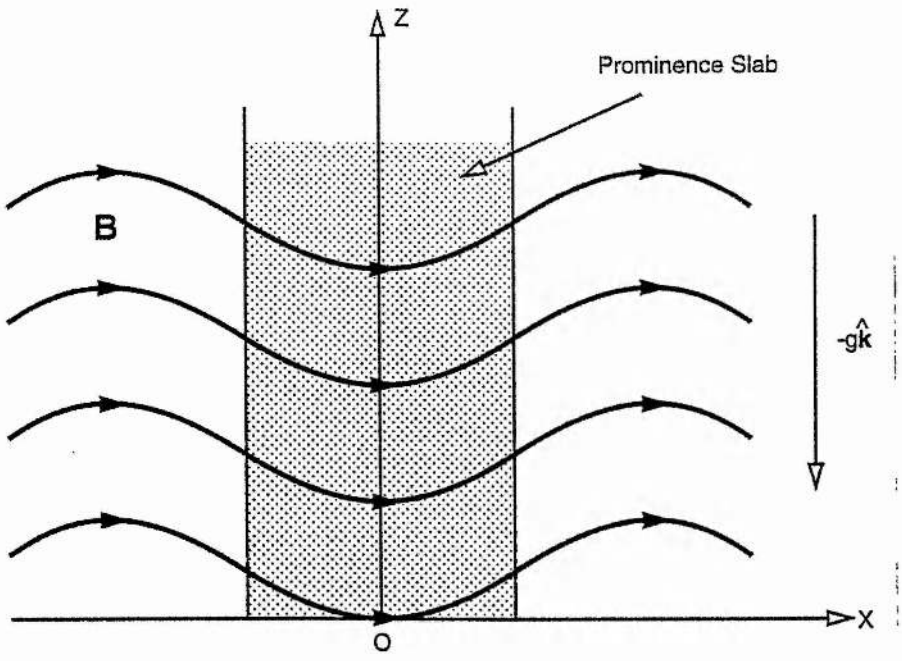

Fig. 4.1. A sketch of the magnetic field lines supporting the prominence in the two dimensional model of Menzel (1951).

For $q > 1$ and $q\beta_0 > 1$, the function f(x) has a minimum at x=0 with a corresponding maximum in the gas pressure P(x). Qualitatively, this then gives a picture of a prominence-like equilibrium. The special case $q\beta_0 = 1$ gives $f = f_0$ as a solution of Eq. (4.12), giving horizontal field lines with a constant Alfven speed v_A, and with the gradient of magnetostatic gas pressure $\nabla\left(p_0 + \frac{B_0^2}{8\pi}\right)$ balancing the weight of the prominence.

For the parameter β_0, we choose a value in the range 0.1-0.5. Considering an average transverse field strength of around 3-5 G, a prominence temperature of around 7000 K and an average particle density of 10^{11} cm^{-3}, this range for β_0 provides reasonable values for the plasma-beta in the transverse field component at the centre of the prominence. For the parameter q, we choose a value of 9.0, which yields a modified scale-height H_B that is ten times the actual scale height H_0 in the prominence. Such a value of H_B may not be entirely realistic (see discussion below), but

was considered by Brown (1958). Such a choice for the parameters β_0 and q gives a width (which is taken as the distance between the points of inflexion of the function f(x), as the density of the plasma generally becomes insignificantly low beyond these points) of around 3000 km for our model prominence, which is somewhat smaller than the values generally quoted in the observations (see Section 1.1.2, Chapter I). A larger value of q tends to widen the prominence, but also implies a rather large dip in the magnetic field lines, which increases as β_0 deviates from its value in the horizontal magnetic field configuration (corresponding to $q\beta_0 = 1$). We here confine ourselves to a small deviation from the horizontal field configuration.

Due to the spatially periodic nature of the field lines (see Fig. 4.1), we confine ourselves to no more than one spatial period and place rigid walls at $x = \pm d$, where the gas pressure P(x) reduces by an order of magnitude (or less) below its central (x = 0) value; see also the discussion in Brown (1958). We may note that this distance $2d$ is different from the anchor point separation distance $2l$ of the magnetic field lines, as was considered in Chapters I and III, and is simply an artefact of the particular equilibrium model considered here. In our calculations d = 4426 km, corresponding to the positions of the first maxima in the function f(x) for β_0 = 0.3 and q = 9.0. For the range of values of the plasma beta considered above, the gas pressure reduces by a factor of 1 (for the particular case of horizontal magnetic field configuration) to 30 below its central value at the positions $x = \pm d$. The average gas pressure of the quiet corona is less than 2 dyne cm^{-2} (see the summary of observational results in Bray et al. 1991; see also Rosner et al. 1978; Hollweg, 1990) and so is about the same as the central pressure in a prominence (cf. Table 1.1, Chapter I). A region of lower pressure surrounding the model prominence (the effective width of which is taken to be the distance between the points of inflexion of the function f(x)), as suggested by the Menzel's model, was considered by Brown (1958) as an indication of the observed decrease in the coronal pressure (density) in the neighbourhood of a prominence (eg. Waldmeir, 1941, 1970; Leroy and Servajan, 1966; Kawaguchi, 1967; Saito and Tandberg-Hanssen, 1973; Bessey and Liebenberg, 1984; Engvold, 1989). We may note, however, that the extreme simplicity of the isothermal Menzel model does not allow us to draw such a direct comparison with the observational results obtained for quiescent prominences.

4.3 Linearized Equations

We consider small perturbations about the equilibrium configuration described in the previous section. The linearized equations of ideal MHD (cf. Eqs. (1.4)-(1.8) in Section 1.3.1, Chapter I) ultimately yield a single second order differential vector equation in the velocity perturbation **v**. In the particular case of a two dimensional ($B_y = 0$) magnetic field, this equation is (Brown, 1958)

$$\frac{\partial^2 \mathbf{v}}{\partial t^2} = \frac{gH_0}{p_0} \mathcal{F}(\mathbf{v}), \tag{4.14a}$$

where

$$\mathcal{F}(\mathbf{v}) = \nabla (\mathbf{v}.\nabla p_0 + \gamma p_0 \mathrm{div}\ \mathbf{v}) + \frac{1}{H_0} \hat{\mathbf{k}}\ \mathrm{div}\ (p_0 \mathbf{v}) + \frac{1}{4\pi} [\nabla^2 F \nabla (\mathbf{v}.\nabla F) + \nabla^2 (\mathbf{v}.\nabla F) \nabla F]. \tag{4.14b}$$

Here we have made use of Eq. (4.2) to express the equilibrium magnetic field $\mathbf{B}_0$ in terms of the flux-function F(x, z).

Write the velocity perturbation **v** as $\mathbf{v} = (v_x(x,z,t),\ 0,\ v_z(x,z,t))$. Then Eq. (4.14) yields a solution of the form (cf. Yu, 1965; Nye and Thomas, 1974; Roberts, 1988; Campbell and Roberts, 1989)

$$\begin{pmatrix} v_x \\ v_z \end{pmatrix} = \begin{pmatrix} u(x) \\ w(x) \end{pmatrix} \exp\left\{ i\omega t + \left(\frac{1}{2H_B} + ik_z\right) z \right\}, \tag{4.15}$$

where ω is the frequency of the normal modes of oscillation and k_z is their wavenumber in the vertical (z) direction. The normal modes consist of waves that propagate vertically with their velocity amplitudes increasing with height. However, the total (kinetic + magnetic) energy density in these waves is independent of height.

With the above assumption regarding the perturbations, the governing differential equations (Eq.(4.14)) take the following forms

$$A\,u'' + B\,w'' + C\,u' + D\,w' + E\,u + F\,w = 0 \tag{4.16a}$$

and

$$I\,u'' + J\,w'' + K\,u' + L\,w' + M\,u + N\,w = 0, \tag{4.16b}$$

where the coefficients A to F and I to N are given in the following. Writing $f_D = f(x)/f_0$, we have

$$A = \frac{\gamma\beta_0}{32\pi H_B^2}\left(\frac{1}{f_D}\right)^{2q} + \frac{\left(f_D'\right)^2}{4\pi}, \tag{4.17}$$

$$B = -\frac{f_D f_D'}{8\pi H_B}, \tag{4.18}$$

$$C = \frac{f_D'}{2\pi}\left[f_D'' - \frac{\gamma q\beta_0}{8H_B^2}\left(\frac{1}{f_D}\right)^{2q+1}\right], \tag{4.19}$$

$$D = \frac{\beta_0}{32\pi H_B^3}(\gamma k H_B - q - 1)\left(\frac{1}{f_D}\right)^{2q} - \frac{(f_D')^2}{4\pi H_B}, \tag{4.20}$$

$$E = \frac{\omega^2\beta_0(q+1)}{32\pi H_B^3 g}\left(\frac{1}{f_D}\right)^{2q} + k(kH_B - 1)\frac{(f_D')^2}{4\pi H_B}, \tag{4.21}$$

$$F = -\frac{qkf_D'}{8\pi H_B^2}\left[\frac{1}{2}\gamma q\beta_0\left(\frac{1}{f_D}\right)^{2q+1} + (kH_B - 1)f_D\right], \tag{4.22}$$

$$I = B = -\frac{f_D f_D'}{8\pi H_B}, \tag{4.23}$$

$$J = \frac{f_D^2}{16\pi H_B^2}, \tag{4.24}$$

$$K = \frac{\beta_0}{32\pi H_B^3}\left[\gamma(\mathfrak{k}H_B - 1) - q + 1\right]\left(\frac{1}{f_D}\right)^{2q} + \frac{f_D^2}{16\pi H_B^3}, \tag{4.25}$$

$$L = \frac{f_D f_D'}{8\pi H_B^2}, \tag{4.26}$$

$$M = -\frac{\mathfrak{k}(\mathfrak{k}H_B - 1)}{8\pi H_B^2} f_D f_D', \tag{4.27}$$

$$N = \frac{\beta_0}{32\pi H_B^3}\left[\frac{\omega^2}{g}(q+1) + \gamma\mathfrak{k}(\mathfrak{k}H_B - 1)\right]\left(\frac{1}{f_D}\right)^{2q} + \mathfrak{k}(\mathfrak{k}H_B - 1)\frac{f_D^2}{16\pi H_B^3}, \tag{4.28}$$

$$\text{where } \mathfrak{k} = \frac{1}{2H_B} + ik_z . \tag{4.29}$$

In the above the superscript ($'$) denotes derivatives with respect to the variable x.

Equations (4.16), together with Eqs. (4.11) and (4.12) defining the flux function f(x), constitute the system of equations governing the perturbations in the system. We supplement these ordinary differential equations with the line-tying boundary conditions

$$u(x) = w(x) = 0 \text{ at } x = \pm \mathfrak{d}. \tag{4.30}$$

The choice of distance $\mathfrak{d}$ is discussed in Section 4.2.2.

4.4 Solution of the system of equations

Equations (4.11), (4.12), (4.16), and (4.30) together constitute a two-point boundary value problem that must be solved numerically to determine the eigenmodes of oscillation of the model prominence. Some guidance as to the nature of the solutions is required from an analytical approach. To find such a guidance, we first observe that the symmetry of the equilibrium

configuration around x = 0 suggests that the eigensolutions may be devided into *even* (u(x) = u(-x)) and *odd* (u(x) = -u(-x)) forms. As in Chapter III, the normal modes of the system represented by these two groups of solutions will here be called *kink* and *sausage* modes, respectively.

Further insight into the problem can be obtained by investigating the special case $q\beta_0 = 1$, corresponding to the solution $f = f_0$ and giving a horizontal field configuration with a constant Alfven speed v_A. For this case, Eqs. (4.16a, b) reduce to a single fourth order differential equation with constant coefficients:

$$c_T^2 \frac{d^4u}{dx^4} + \left\{ \omega^2 + \frac{g^2}{c_f^2}(1-\Gamma) - c_T^2\left[\frac{1}{4H_B^2}+k_z^2\right]\right\}\frac{d^2u}{dx^2} + \omega^2\left\{\frac{\omega^2}{c_f^2} - \left[\frac{1}{4H_B^2} + k_z^2\right]\right\}u = 0, \quad (4.31)$$

where $c_T = \dfrac{c_s v_A}{(c_s^2 + v_A^2)^{1/2}}$ is the 'cusp speed' in the plasma and $c_f = (c_s^2+v_A^2)^{1/2}$ is the fast speed (see, for example, Roberts, 1985). We have also introduced $\Gamma = \dfrac{c_s^2}{gH_B}$, the magnetically-modified adiabatic constant (cf. Campbell and Roberts, 1989; Evans and Roberts, 1991; Roberts, 1989, 1992; Miles and Roberts, 1992) . For a non-magnetic medium, $H_B = H_0$ and hence $\Gamma = \gamma$.

It may be noted that Eq. (4.31) reduces to Eq. (3.11) of Chapter III in the case when g= 0. Moreover, in the case of an uniform unbound medium (for which we may write $\dfrac{d}{dx} = ik_x$) Eq. (4.31) reduces to the well known dispersion relation for the magnetoacoustic modes in a stratified plasma with constant Alfven speed (Yu, 1965; Nye and Thomas, 1974; Thomas, 1982, 1983), namely,

$$\omega^4 - \left[(c_s^2+v_A^2)\left(k_x^2+k_z^2+\frac{1}{4H_B^2}\right)\right]\omega^2 + k_x^2\left[c_s^2v_A^2\left(k_x^2+k_z^2+\frac{1}{4H_B^2}\right) - g^2(1-\Gamma)\right] = 0. \quad (4.32)$$

In the case of purely horizontal field lines ($q\beta_0$=1), Eq. (4.16) gives

$$w(x) = \frac{1}{\left[\omega^2-\left(c_s^2+v_A^2\right)\left(\frac{1}{4H_B^2}+k_z^2\right)\right]\left[\left(\frac{1}{2H_B}+ik_z\right)c_s^2-g\right]}$$

$$\times\left\{v_A^2c_s^2\frac{d^3u}{dx^3}+\left[\omega^2v_A^2+c_s^4\left(\frac{1}{4H_B^2}+k_z^2\right)+g^2(1-\Gamma)\right]\frac{du}{dx}\right\}. \qquad (4.33)$$

Eqs. (4.31) and (4.33), together with the boundary conditions (4.30), lead to a transcendental dispersion relation for the kink and the sausage modes in horizontal magnetic field. For the kink modes the dispersion relation is

$$\left\{v_A^2\left(k^{+2}-\frac{\omega^2}{c_s^2}\right)-c_s^2\left(\frac{1}{4H_B^2}+k_z^2+\frac{1-\Gamma}{\Gamma^2H_B^2}\right)\right\}k^+\tan(k^+d)$$

$$=\left\{v_A^2\left(k^{-2}-\frac{\omega^2}{c_s^2}\right)-c_s^2\left(\frac{1}{4H_B^2}+k_z^2+\frac{1-\Gamma}{\Gamma^2H_B^2}\right)\right\}k^-\tan(k^-d). \qquad (4.34)$$

The sausage modes satisfy a similar dispersion relation obtained by replacing 'tan' by 'cot' in Eq. (4.34).

The quantities $k^{\pm}$ are defined as:

$$(k^{\pm})^2=\frac{1}{2}\left[\frac{\omega^2}{c_T^2}-k_z^2-\frac{1}{4H_B^2}+\frac{g(1-\Gamma)}{\Gamma H_Bv_A^2}\right]\pm\frac{1}{2}\left[\left\{\frac{\omega^2}{c_T^2}+k_z^2+\frac{1}{4H_B^2}-\frac{g(1-\Gamma)}{\Gamma H_Bv_A^2}\right\}^2-4\frac{\omega^2}{c_T^2}\left\{\frac{\omega^2}{c_f^2}-\frac{g(1-\Gamma)}{\Gamma H_Bv_A^2}\right\}\right]^{1/2}, \qquad (4.35)$$

which are the effective wavenumbers of the magnetoacoustic modes in the direction of the magnetic field with '+' representing the slow modes and '-' representing the fast modes. Note that Eq. (4.35) simply represents the positive solutions for k_x of the constant Alfven speed dispersion relation Eq. (4.32).

The dispersion relation (4.34) for the horizontal magnetic field configuration proves too complicated to yield simple solutions for the normal modes except in the special case g=0 obtained by letting $H_B \to \infty$. In this case, the kink modes of extremely long wavelengths ($k_z d << k_z H_B << 1$) yield

$$\frac{\omega d}{c_s} = \left(\nu + \frac{1}{2}\right)\pi \ , \text{ for the } \textit{slow} \quad \textit{kink} \text{ modes} \tag{4.36a}$$

and

$$\frac{\omega d}{v_A} = (\mu+1)\pi \ , \qquad \text{for the } \textit{fast} \text{ kink modes} \tag{4.36b}$$

with μ , ν = 0,1,2..... Solutions for the sausage modes are obtained in a similar way. These are

$$\frac{\omega d}{c_s} = (\nu +1)\pi \ , \text{ for the } \textit{slow} \quad \textit{sausage} \text{ modes} \tag{4.37a}$$

and

$$\frac{\omega d}{v_A} = \left(\mu + \frac{1}{2}\right)\pi \ , \text{ for the } \textit{fast} \quad \textit{sausage} \text{ modes.} \tag{4.37b}$$

Once we identify the normal modes of oscillation in a non-gravitating medium in this way, the solutions of the horizontal field dispersion relation (4.34) can easily be obtained numerically for the stratified case (with g= 274 ms^{-2}). These solutions then provide initial approximations for the more general boundary value problem given by Eqs. (4.16)- (4.30). For the solution of the general problem we simply use an iterative 'shooting and matching' technique.

The solutions for the Menzel equilibrium are shown in Fig. 4.2a,b for kink and sausage modes, respectively, taking three values of the plasma-beta β_0 at the centre of the prominence, namely $\beta_0 = \frac{1}{9}$ (corresponding to the horizontal magnetic field configuration), $\beta_0 = 0.3$ and $\beta_0 = 0.5$.

The normal modes depicted in Fig.4.2 show signatures of 'avoided crossings' (see Chapter III). It is interesting to note that, as the curvature of the field lines increases, corresponding to an increase in the parameter β_0, the avoided crossings between different modes tend to become more 'gentle', indicating that the 'kissing modes' transform themselves into 'embracing modes'; avoided crossings are discussed in Jones (1970).

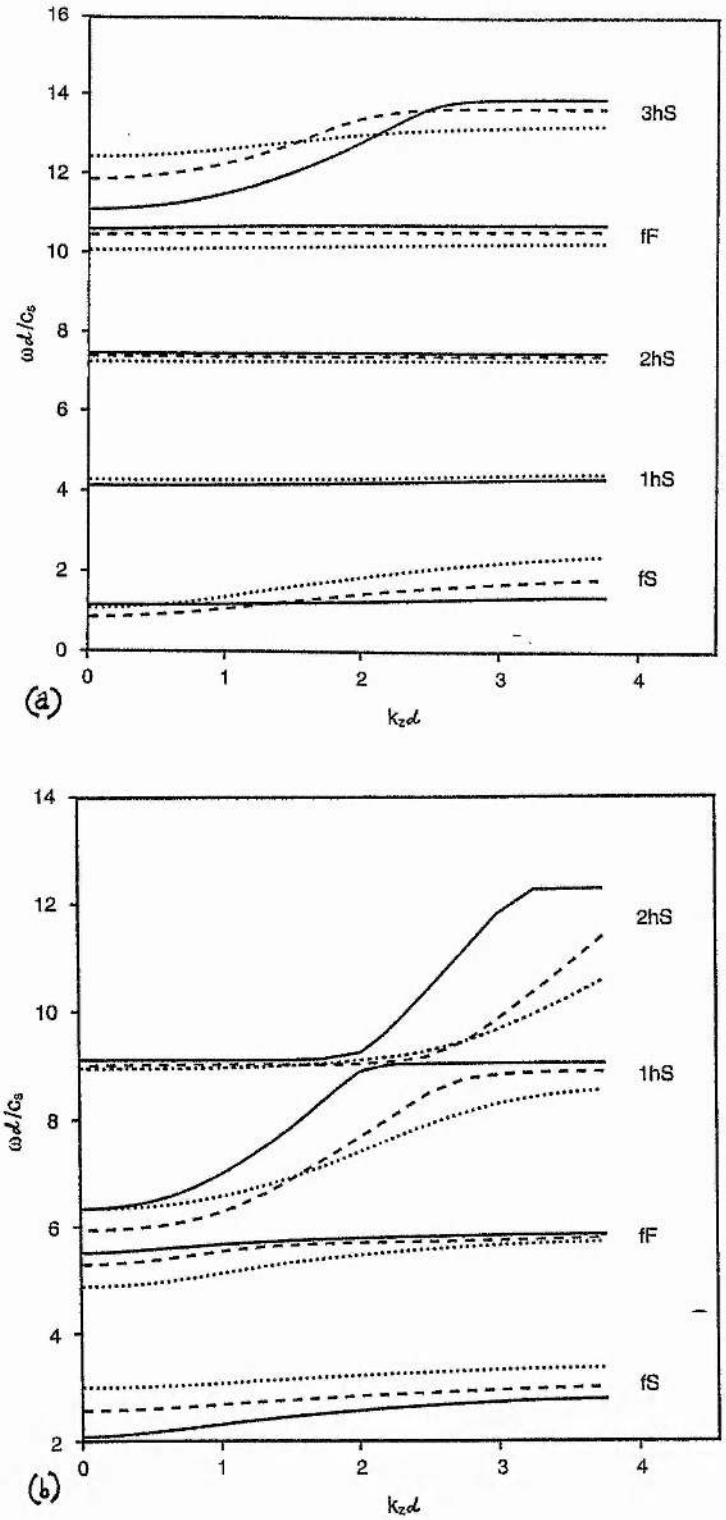

Fig. 4.2a and b. Dimensionless frequency $\omega d/c_s$ vs. dimensionless wavenumber $k_z d$ for (a) the kink modes and (b) the sausage modes of vibration of Menzel's model, with a sound speed 12 kms^{-1} and a scale height ratio H_B/H_0 = 10.0 (giving q = 9.0). The solid (_____) curves are for a plasma beta β_0 = 1/9, corresponding to a horizontal field configuration. The dashed (- - - - -) lines are for modes with β_0 = 0.3 and the dotted (.....) lines are for modes with β_0 = 0.5. The modes are identified as fast (F) or slow (S) magnetoacoustic modes, with f denoting the fundamental and h denoting a higher harmonic (first harmonic 1h; second harmonic 2h, etc.)

4.5 Periods of oscillation of Menzel's prominence

Having determined the frequency-wavenumber curves for Menzel's equilibrium, we turn now to an investigation of the numerical values of the periods of the fundamental modes that might arise in a prominence-type configuration. In a two dimensional geometry, such as the one considered here, the wavenumber of the fundamental modes is taken to be (see Section 3.4, Chapter III)

$$k_z = \frac{n\pi}{H}, \tag{4.38}$$

with the integer n describing the modal structure over the height H of the prominence. With $H = 5\ 10^4$ km and $\mathbf{d} = 4426$ km, this gives a wavenumber $k_z\mathbf{d} \approx 0.3$ for the principal (n=1) eigenmode. For such a value of the wavenumber the periods of the fundamental modes are displayed in Table 4.1, taking cases $\beta_0 = \frac{1}{9}$, $\beta_0 = 0.3$ and $\beta_0 = 0.5$. Table 4.1 also compares the period of each of the fundamental modes with its corresponding period, τ_0, in the limit $g = 0$ with $\beta_0 = \frac{1}{9}$. The formulae given in Table 4.1 provide a simple estimate for the periods in the non-gravitating limit [see Eqs. (4.36) and (4.37)].

Table 4.1. *Periods (in minutes) of the fundamental modes of oscillation of a Menzel prominence (T_0 = 7000 K, q = 9, $\mathbf{d}$ = 4426 km) and their comparison with the periods τ_0 of the magnetoacoustic modes in an uniform, non-gravitating, bound medium with plasma-beta β_0 = 1/9.*

Mode name		Slow sausage mode	Fast sausage mode	Slow kink mode	Fast kink mode
Period (min)	$\beta_0 = 1/9$	18	7	36	4
	$\beta_0 = 0.3$	16	7	48	4
	$\beta_0 = 0.5$	13	8	36	4
	$g = 0$, $\beta_0 = 1/9$	12 ($\tau_0 \approx 2\mathbf{d}/c_s$)	8 ($\tau_0 \approx 4\mathbf{d}/v_A$)	25 ($\tau_0 \approx 4\mathbf{d}/c_s$)	4 ($\tau_0 \approx 2\mathbf{d}/v_A$)

As noted earlier, Menzel's model does not provide a good representation of a real prominence, for it allows neither for the non-isothermality nor a longitudinal field component and furthermore possesses a small effective scale height ($H_B = 10H_0 \approx 3000$ km is much smaller than the observed prominence height $H \approx 5\ 10^4$ km). However, it provides a means of comparison of a model which includes both gravity and field line curvature with simple slab models, such as the ones developed in Chapters II and III. In particular, we may examine how its periods of oscillation compare with those obtained for a slab with a transverse magnetic field. Chapter III considered such a slab configuration in which its transverse magnetic field was anchored at a distance ℓ from the slab's centre. The slab had a prominence temperature of 8000 K and was located in a coronal environment.

Such a comparison shows that in both models the fundamental fast kink mode (fF^k in the notation of Chapter III) has a period in the range 3-5 min, whereas the fundamental slow sausage mode (fS^s) presents a period in the range 10-15 min. The analysis in Chapter III shows that these time-scales are provided by the time it takes an Alfven wave (for the 3-5 min range) or sound wave (for the 10-15 min modes) to cross the prominence width and back again.

In the presence of a temperature discontinuity, the fast kink and the slow sausage modes undergo an additional phase change of $\pi/2$ compared to the situation in an uniform bound medium. Such a phase change is approximately equivalent to the additional distance traversed by the waves outside the prominence [whose edges are considered to be defined by the points of inflexion of the flux function f(x)] in an isothermal Menzel model. The fast kink and the slow sausage modes thus present similar periodicities in both these models.

The fast sausage mode (fF^s) possesses a period of about 7 min in Menzel's model (see Table 4.1). This period is essentially determined by the magnetoacoustic time-scale and so is practically unaffected by the effects of stratification. In fact, as shown in Chapter III, the period of the fast sausage mode is largely influenced by the effects of temperature inhomogeneity and photospheric line-tying. When these effects are included the fast sausage mode is analogous to the fundamental vibration of a mass loaded stretched string (Roberts, 1991; Joarder and Roberts, 1992b,c), presenting a period $\tau \approx 2\pi(\ell a)^{1/2}/v_A$, with v_A being the average Alfven speed within the prominence of width 2a with its anchor points

separated by a distance 2ℓ. The numerical value of the period of this fast sausage mode is thus greatly modified when these two effects are introduced. This mode provides a period of the order of an hour.

The most complicated mode in a prominence-type equilibrium seems to be the fundamental slow kink (fS^k) mode. The numerical results presented in Table 4.1 shows that the period of this mode may change appreciably from its non-gravitating magnetohydrodynamic value to its value in the presence of stratification. This mode is also sensitive to the effect of a temperature discontinuity at the prominence-corona interface and to photospheric line-tying (cf. Joarder and Roberts, 1992b,c). We found in Chapter III that, in the absence of gravity, this mode has a periodicity that is of the order of $\tau \approx 2\pi(\ell a)^{1/2}/c_s$, giving about an hour for prominence values. To provide a more accurate estimate for the period of this mode it is necessary to examine a prominence equilibrium model that includes the effects of gravitational stratification, temperature discontinuity and photospheric line-tying. A first step towards such an investigation has recently been taken by Oliver et al. (1992a,b; 1993a) by examining the modes of oscillation in a generalized, two temperature Kippenhahn-Schlüter (1957)-type prominence model. We will discuss their results in the Section 4.6, below. For the present, however, we can conclude that despite the complex nature of the slow kink mode a rough estimate of its period is provided by the model calculations of Chapter III. Overall, then, the simple model of Chapter III provides a useful guide to the periods of the Menzel model and, presumably, to the periods of more realistic prominence models (as discussed below).

4.6. Oscillations in Kippenhahn-Schluter (1957)-type prominences

The modes of oscillation of an isothermal Kippenhahn-Schlüter (1957) type prominence model was examined by Oliver et al. (1992a, b). Recently, Oliver et al. (1993a) have extended their calculations to the case of a non-isothermal, generalized Kippenhahn-Schlüter prominence model, that is obtained by ignoring the non-adiabatic effects in the calculations of Poland and Anzer (1971).

4.6.1. Kippenhahn-Schlüter prominence model: In their original model, Kippenhahn-Schlüter (1957) provided solutions for the magnetic field topology both inside and outside the prominence slab; see Section

1.1.3, Chapter I. In the following, we however consider only the solution given for the internal field structure of the prominence-sheet. This particular solution for prominence equilibrium, although isothermal, is more realistic than the Menzel model, as it predicts a prominence height that is much larger (in fact, infinite) than the width of the prominence; this is closer to the actual situation observed in solar quiescent prominences (see Section 1.1.2, Chapter I for a summary of the observed characteristics of quiescent prominences). As noted in Section 4.2.1, the Kippenhahn-Schluter (1957) model corresponds to the choice (4.7) for the function $\Phi(F)$ and the flux-function F(x, z) for the magnetic field lines in the basic magnetostatic equilibrium equation (4.5). Integrating Eq. (4.5), we then obtain

$$\left[\frac{d}{dx}\left(\frac{F_1(x)}{A_3H_0}\right)\right]^2 = \frac{2A_2}{A_3H_0}\left\{\exp\left(\frac{F_3(x)}{A_3H_0}\right) - 1\right\}, \tag{4.39}$$

where we have used the boundary conditions

$$F_1(x) = \frac{d}{dx} F_1(x) = 0 \text{ at } x = 0. \tag{4.40}$$

For the choice $A_3 < 0$ (cf. Eq.(4.7a)), Eq.(4.39) can readily be integrated to give

$$F_1(x) = 2A_3H_0 \ln\left\{\operatorname{sech}\left(\frac{A_2}{2|A_3|H_0}\right)^{1/2} x\right\}. \tag{4.41}$$

From Eqs. (4.2) and (4.7b), we obtain

$$A_3 = -B_x = \text{constant, and } \frac{d}{dx} F_1(x) = B_z(x), \tag{4.42}$$

which, along with Eq. (4.41), ultimately gives

$$B_z(x) = \pm B_z(\infty) \tanh\left[\frac{B_z(\infty)x}{2H_0B_x}\right], \tag{4.43}$$

where $B_z(\infty) = (2A_2B_xH_0)^{1/2}$ is the strength of the z-component of the magnetic field at $x \to \infty$.

Eqs. (4.42) and (4.43) together gives the magnetic field configuration in the isothermal Kippenhahn-Schlüter equilibrium model of a prominence; see Fig. 4.3 for a schematic description of the magnetic field lines. We

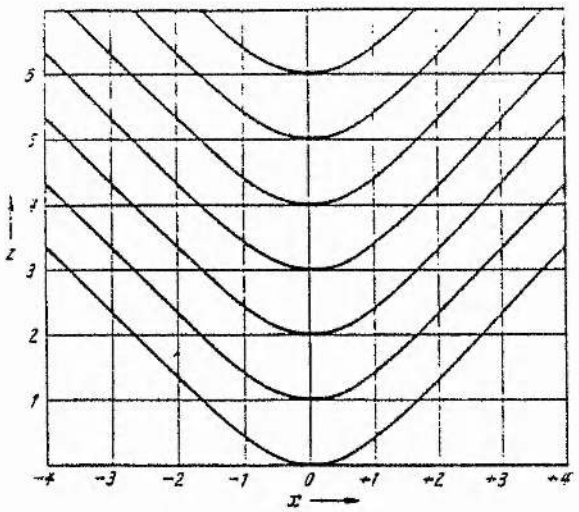

Fig. 4.3. A sketch of the magnetic field lines supporting the prominence in an isothermal Kippenhahn-Schlüter (1957) prominence model.

may note that, the magnetic field is invariant in the vertical (z) direction, as also the equilibrium pressure p_0 (and hence the density ρ_0) given by (cf. Eq. (4.10))

$$p_0(x, z) = p_0(x) = \frac{B_z^2(\infty)}{8\pi} \operatorname{sech}^2\left[\frac{B_z(\infty)x}{2B_xH_0}\right]; \tag{4.44}$$

$p_0(x,z)$ vanishes asymptotically as $x \to \infty$. In this isothermal prominence model, the edges of the prominence-sheet are generally considered to be at a distance $a = \frac{B_xH_0}{B_z(\infty)}$ from the prominence centre, where the gas pressure falls off appreciably from its central value (see, for example, Priest (1982)).

This isothermal model for the internal magnetic field structure of prominences has been modified by Poland and Anzer (1971) to incorporate

the energy balance of the cool and dense prominence embedded in a hotter and rarer coronal medium. Following Oliver et al. (1993a), we only consider the temperature and density inhomogeneity, ignoring the non-adiabatic effects in the calculations of Poland and Anzer. We thus consider a discontinuous temperature profile with temperatures T_o and T_e inside and outside the prominence of an arbitrary width 2a, such that

$$T_0(x) = \begin{cases} T_o , & 0 \leq |x| \leq a , \\ T_e , & |x| > a . \end{cases} \tag{4.45}$$

The equilibrium magnetic field configuration and the gas pressure distribution in this generalized, non-isothermal Kippenhahn-Schlüter prominence model is then given by simply replacing (x/H_0) in Eq. (4.43) and Eq. (4.44) by a function $\Psi(x)$, where

$$\Psi(x) = \frac{g}{R}\int \frac{\mu(x')}{T_0(x')}\, dx' = \begin{cases} \mu_o \dfrac{x}{T_o} , & 0 \leq |x| \leq a , \\ \mu_o \dfrac{x}{T_o} + \mu_e \dfrac{x-a}{T_e} , & |x| > a , \end{cases} \tag{4.46}$$

with μ_o and μ_e being the mean molecular weights inside and outside the prominence-sheet, respectively.

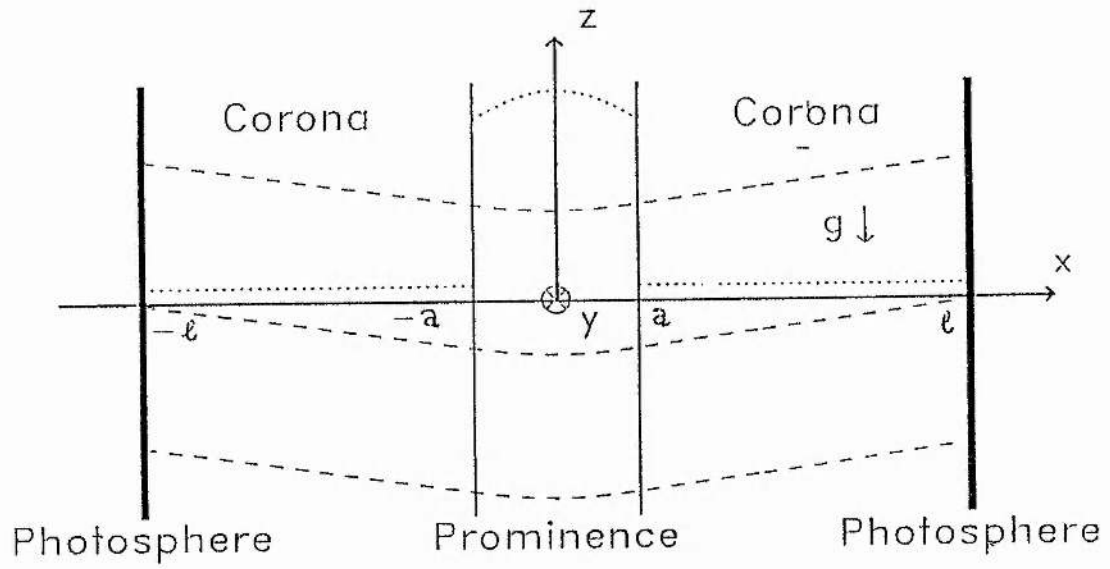

Fig. 4.4. Diagram representing the generalized, non-isothermal Kippenhahn-Schlüter prominence equilibrium, as considerd by Oliver et al. (1993a). The dashed (-------) curve shows the typical shape of the field lines and the dotted (.....) curve represents the corresponding density profile.

In their calculations of prominence oscillations, Oliver et al.(1993a) further assumed that the magnetic field lines are anchored at a distance x = ± ℓ (say) from the centre of the prominence, representing the coronal-photospheric boundary. With this assumption, the equilibrium configuration considered by Oliver et al. (1993a) is similar to that given in Fig. 4.4.

4.6.2. Linearized equations: The equations for the amplitudes of the velocity perturbation $\mathbf{v}(x,z) = (u, 0, w)$ in the Kippenhahn-Schlüter equilibrium can readily be obtained from the generalized perturbation equation (4.14), after using Eq. (4.7) for the flux function F(x, z). The resulting equation is then linearized to give the following two coupled, second order differential equations (cf. Oliver et al. 1992a, b,1993a)

$$\left(c_s^2 + \frac{B_z^2}{4\pi\rho_0}\right)u'' - \frac{B_x B_z}{4\pi\rho_0}w'' + \frac{B_z}{B_x}g(2-\gamma)u' - \left(\mathfrak{k}c_s^2 + g\right)w' + \left(\omega^2+\mathfrak{k}^2\frac{B_z^2}{4\pi\rho_0}\right)u$$
$$+\mathfrak{k}\left(\gamma g\frac{B_z}{B_x} - \mathfrak{k}\frac{B_x B_z}{4\pi\rho_0}\right)w = 0\,, \qquad (4.47a)$$

and

$$-\frac{B_x B_z}{4\pi\rho_0}u'' + \frac{B_x^2}{4\pi\rho_0}w'' - \left(\mathfrak{k}c_s^2 + g\right)u' - \mathfrak{k}^2\frac{B_x B_z}{4\pi\rho_0}u + \left[\omega^2+\mathfrak{k}^2\left(\frac{B_x^2}{4\pi\rho_0}+c_s^2\right)\right]w = 0. \qquad (4.47b)$$

Here $\mathfrak{k} = \alpha + ik_z$ is a complex wavenumber of perturbation (see Eqs. (4.15) and (4.29)) in the case of a Kippenhahn-Schlüter prominence model (Oliver et al. 1992a, b, 1993a). The reason for the appearance of such a complex wavenumber $\mathfrak{k}$ is, however, not completely clear from the works of Oliver et al.. On the other hand, a consideration of the conservation of total (kinetic + magnetic) energy density of the perturbations, that led us to the assumption of the particular form (4.15) in Section 4.3, now suggests that $\mathfrak{k}$ is most likely to be purely imaginary ($\mathfrak{k} = ik_z$) in this particular case of a verically unstratified plasma with $H_B \to \infty$. In any case, we simply describe the results of Oliver et al. (1993a) in the following.

Eq. (4.47a, b) represents the equations governing the velocity perturbations in an isothermal Kippenhahn-Schlüter (1957) prominence model. In the case of the generalized, non-isothermal, Kippenhahn-Schlüter model (Oliver et al. 1993a), Eq. (4.47) still pertains, but with $\rho_0 = \rho_o(x)$, $c_s = c_{so}$ inside the prominence-sheet, and $\rho_0 = \rho_e(x)$, $c_s = c_{se}$ outside the prominence. The prominence satisfies the pressure balance condition $p_o(a) = p_e(a)$ at its edges $x = \pm a$; see Eqs. (4.44)-(4.46).

For the boundary conditions across the edges of the prominence-sheet, Oliver et al. (1993a) impose the conditions that both the components u(x) and w(x) of the velocity perturbation and their first derivatives must be continuous across the prominence-coronal interface. At the corona-photosphere boundary $x = \pm \ell$ these authors assume the line-tying boundary conditions (3.25) of Chapter III.

4.6.3. Modes of oscillation: The modes of oscillation obtained by Oliver et al. (1993a) for the case of a generalized, non-isothermal, Kippenhahn-Schluter prominence model are similar to the oscillatory modes obtained in Chapter III (see Fig. 3.2a, b) for a low-beta ($c_{so} < v_{Ao}$, $c_{se} < v_{Ae}$), non-gravitating plasma slab threaded by a transverse magnetic field. Two different types of modes, namely, the internal and the external modes (cf. Section 3.3, Chapter III; see also Joarder and Roberts, 1992b, c), that were present in the simple slab model of a prominence, are still present in the prominence model considered by Oliver et al.. We may here note that, due to the isothermal nature of the Menzel model, we obtained only the internal magnetoacoustic modes in our calculations for this model; see Sections 4.5 and 4.6. Similar solutions of Eq. (4.47), that contain only the internal modes, have also been obtained by Oliver et al. (1992a, b) in their analysis of the modes of oscillation of an isothermal Kippenhahn-Schlüter-prominence equilibrium.

To identify the various eigenmodes of oscillation in a generalized Kippenhahn-Schlüter prominence, Oliver et al. (1993a) adopt the analytical mode classification scheme given in Section 3.3, Chapter III, for the case of a non-gravitating slab in a transverse magnetic field. Moreover, the analogy of the oscillatory modes with the modes of vibration of a mass-loaded stretched string (Roberts, 1991c; Joarder and Roberts, 1992b, c) provides a valuable guidance to the physical nature of the modes even in the case of a more realistic magnetostatic equilibrium model of a prominence. Particularly interesting is the presence of the fundamental

slow kink (slow string) mode and the fundamental fast sausage (fast string) mode. It was found in Chapter III (see Section 3.3) that these modes are analogous to the fundamental modes of a mass-loaded elastic string. In the absence of either the coronal medium or the prominence slab, these modes coincide with the fundamentals of the slow kink and the fast sausage modes of a uniform (either prominence or coronal) plasma (cf. Section 3.3, Chapter III). In a way, the (slow or fast) magnetoacoustic string modes then pertain to both the media internal and external to the prominence-sheet. Due to the special nature of these modes, Oliver et al. (1993a) refer to the magnetoacoustic string modes as the *hybrid (slow or fast)* modes. We may also note, that for all the modes considered by Oliver et al. (1993a), the values of the dimensionless exponent $a|\alpha|$ of the modal amplitudes are extremely small ($\leq 10^{-4}$), so that the presence of gravity does not greatly influence the amplitudes of these modes, that remain almost the same at different positions along the height of the model prominence.

With such a classification for the normal modes of oscillation, the periods obtained numerically by Oliver et al. (1993a) for the fundamental modes in a non-isothermal, Kippenhahn-Schlüter prominence is then displayed in Table 4.2.

A comparison of Table 4.2 with Table 4.1 for the periods in a Menzel (1951) prominence model, or with Table 3.2 (Chapter III) for a non-gravitating slab model, shows that the internal slow sausage (fIS^s) mode presents a period of around 10-15 min, and the internal fast kink (fIF^k) mode presents a period of around 3-5 min in all three models of quiescent prominences.

Table 4.2. *Periods of the four fundamental modes in a Poland and Anzer (1971) prominence with* $T_o = 10^4 K$, $\rho_o\ (x=0) = 5\ 10^{-14}\ gcm^{-3}$, $2a = 6000$ *km*, $H = 5\ 10^4$ *km*, $B_x = 5G$, *and* $2\ell = 2\ 10^5$ *km. (After Oliver et al. 1993)*

Name of the mode	Period (min)
Slow string mode or Hybrid slow mode	130
Fast string mode or Hybrid fast mode	27
Internal slow mode	14
Internal fast mode	3

In an isothermal Menzel equilibrium (see Table 4.1), the slow kink mode and the fast sausage mode present periodicities that are much shorter than the corresponding periodicities of the (slow and fast) string (or hybrid) modes in a non-gravitating slab prominence (cf. Table 3.2, Chapter III), or a non-isothermal Kippenhahn-Schlüter prominence (Table 4.2). In Chapter III (see Eq. (3.48b) and Table 3.2), we found that in a non-gravitating slab model of prominence, the periods of the string modes scaled approximately as $\sqrt{\ell a}$, with 2ℓ being the anchor point separation distance of the magnetic field lines threading the prominence of width 2a. The periods of these modes are also inversely proportional to the average sound speed c_{so} (for the slow string mode) or the average Alfven-speed v_{Ao} (for the fast string mode) in the prominence; cf. Table 3.2, Chapter III. With $2\ell = 5\ 10^4$ km, 2a = 5000 km, $c_{so} = 15$ kms^{-1}, and $v_{Ao} = 28$ kms^{-1}, the string modes presented periodicities of 53 min and 20 min, respectively, in the simple slab model of Chapter III. For the parameter values chosen by Oliver et al. (1993), namely $2\ell = 2\ 10^5$ km, 2a = 6000 km, a sound speed $c_{so} = 12$ kms^{-1}, and an Alfven speed $v_{Ao} = 60$ kms^{-1}, these modes present periodicities of around 145 min and 20.5 min., values that are not too far from the actual numerically determined periods obtained in Table 4.2. Thus the simple non-gravitating slab model of a prominence, such as the one presented in Chapter III, gives a reasonable estimate of the periods of the modes of oscillation that pertain even in a more realistic prominence model, of course, the exact numerical values of these periods depend upon the precise details of the equilibrium model of a prominence that is under consideration.

4.7. Conclusions

To obtain detailed and accurate predictions regarding the observable characteristics of the modes of oscillation of a prominence, it is of course necessary to perform detailed numerical investigations of complicated equilibrium models of prominences. However, such numerical studies gain greatly from complementary studies of simple magnetohydrodynamic slab-type models, such as the ones discussed in Chapters II and III. By drawing examples from two different investigations of relatively simpler magnetostatic models of prominence equilibria, we have here tried to establish the fact that the study of simple slab-type models of quiescent prominences can indeed provide useful guidance to the oscillatory

behaviour of more complicated prominence models. Moreover, such simple models allow us to draw on analogies with various classical vibratory systems, such as an elastic membrane (Chapter II) or a mass-loaded stretched elastic string (Chapter III), thus shedding some light on the physical nature of the oscillatory modes in solar quiescent prominences.

From our discussions so far, it would seem that the modes of oscillation of a prominence are basically magnetohydrodynamic in nature, with the magnetic field and the compressibility of the plasma playing a dominant role in determining the periods. Gravity and field-line curvature seem to play a subsidiary role. To investigate the physical nature of these modes, it is therefore important to take a proper consideration of the orientation of the magnetic field lines with respect to the prominence axis, since this may influence appreciably the nature of the modes as well as their periods.

It was emphasized in Chapter I, Section 1.1.2, that a prominence is in fact embedded in a skewed magnetic field, with the skew-angle being approximately 20^{o} with respect to the long axis of the prominence. In the next chapter, we therefore investigate the basic magnetohydrodynamic modes of oscillation of a simple, non-gravitating prominence slab embedded in such a skewed magnetic field. It is intended that such an analysis will ultimately enable us to obtain the basic magnetohydrodynamic time-scales of the oscillatory motions in solar quiescent prominences, time-scales that can be compared with the observations of prominence oscillations.

Chapter V

The slab in a skewed magnetic field

5.1 Introduction

In Chapters II and III we examined the modes of oscillation of a dense slab embedded in a uniform magnetic field. The purpose of these investigations was to set out the general structure of such modes of vibration, making clear the principal ingredients that determine the periods of oscillation of the slab. Our study was motivated by the observations of oscillations in quiescent prominences which indicate periods ranging from about a minute to an hour (cf. Section 1.2.3, Chapter I). A detailed understanding of these modes may ultimately provide seismic information about the prominence and its coronal environment.

The complex equilibrium structure of a quiescent prominence makes likely a complicated discussion of its modes of oscillation, with an essentially numerical treatment being required. In such a situation it is important to obtain some insight into the nature of its vibration by exploring simple models of prominence-like equilibria. Of course, such simple models cannot capture all of the actual structure of a prominence with its inherent complexity. But the study of simple models offers the hope that they may delineate the various ingredients that go together to determine the modes of vibration of real prominences. This was the motivation behind Chapters II and III, which set out the modes of oscillation of a dense plasma slab in the presence of either a longitudinal field (Chapter II) or a transverse field (Chapter III). Here we complete that description, examining the role of a skewed field, ie. a field with both longitudinal and transverse components (see also Joarder and Roberts, 1993b). Observations show that the magnetic field in a quiescent prominence is generally inclined at an angle of about 20° to the long axis of the prominence sheet (Section 1.1.2, Chapter I). With an average field strength of about 12 G (cf. Table 1.1 in Chapter I), this produces a longitudinal component of about 10-11 G and a weaker transverse component of 3-5 G.

Complementary theoretical investigations of prominence oscillations have recently been carried out, an objective of which was to examine the influence of gravitational stratification on the oscillatory modes. This was

done by considering various simple, two-dimensional, magnetostatic equilibrium models, such as the Kippenhahn-Schlüter (1957)-type prominence models (Oliver et al. 1992a, b, 1993a) or Menzel's (1951) equilibrium model (Joarder and Roberts ,1993a). We pointed out in Chapter IV that studies of these models have revealed modal structures that are similar to those found in Chapter III, thus indicating that the basic ingredients that principally determine the modes of oscillation in a prominence are: the strength of temperature and density inhomogeneity at the prominence-coronal interface, the magnetic field strength, and the photospheric line-tying effect (cf. Section 1.4.3, Chapter I). Gravity and field line curvature play only subsidiary roles, at least in the elementary magnetostatic models of prominences that have so far been explored.

To examine the effect on oscillations of a skewed magnetic field, we here consider the simple slab model of Chapter I (see Fig. 1.5 in Section 1.5). In this model the prominence slab is embedded in a uniform magnetic field that makes an angle ϕ to the long axis of the slab. The prominence is of length L in the y-direction, of dimension H in the z-direction and of width 2a ($\ll H < L$) in the x-direction. The effect of gravity is ignored. The magnetic field permeating the medium is $\mathbf{B} = (B_x, B_y, 0)$ with $B_x = B_y \tan\phi$. The special case $\phi = \pi/2$, corresponding to a transverse field, was discussed in Chapter III. Pressure balance between the slab and its environment implies that $\rho_o T_o = \rho_e T_e$, assuming, for simplicity, that the mean molecular weight μ (=1/2) is the same in both the media internal and external to the slab. The magnetic field lines are tied to rigid walls at $x = \pm \ell$ on either side of the prominence slab, representing the photospheric line-tying effect.

The characteristic speeds that enter our description of the modes of oscillation of a prominence slab are the Alfven speed $v_A = (v_{Ax}^2 + v_{Ay}^2)^{1/2}$, the sound speed c_s, the magnetoacoustic slow (cusp) speed $c_T = \dfrac{c_s v_A}{(c_s^2 + v_A^2)^{1/2}}$, and the fast speed $c_f = (c_s^2 + v_A^2)^{1/2}$ (cf. Roberts, 1985). These speeds take different values in the interior of the slab, where they carry a suffix 'o' (for object), and the exterior carrying a suffix 'e'. Thus v_{Ao} denotes the Alfven speed within the slab, v_{Ae} its value in the environment, etc. It is necessary also to introduce Alfven speeds based upon the separate field components B_x, B_y of the prominence-coronal field. We set $v_{Ax} = B_x/(4\pi\rho)^{1/2}$ and $v_{Ay} =$

$B_y/(4\pi\rho)^{1/2}$, with ρ ($=\rho_o$ or ρ_e) denoting the gas density; then $v_A^2 = B^2/4\pi\rho = v_{Ax}^2 + v_{Ay}^2$, with $B^2=B_x^2+B_y^2$.

5.2. Derivation of the dispersion relation

5.2.1 Basic equations: We first eliminate the magnetic field and gas pressure perturbations from the linearized MHD equations (1.10)-(1.14) in Section 1.3.1, Chapter I, to obtain three coupled second-order ordinary differential equations in the components $v_x(x)$, $v_y(x)$ and $v_z(x)$ of the velocity perturbation. These equations are:

$$v_{Ax}^2 D^2 v_z + ik_z(c_s^2+v_{Ay}^2)Dv_x - v_{Ax}v_{Ay}\left(ik_z Dv_y - 2ik_y Dv_z - k_y k_z v_x\right) - k_y k_z (c_s^2+v_{Ax}^2)v_y + \left\{\omega^2 - k_z^2 c_f^2 - k_y^2 v_{Ay}^2\right\}v_z = 0, \quad (5.1a)$$

$$(c_s^2 + v_{Ay}^2)\left(D^2 v_x + ik_z Dv_z\right) - v_{Ax}v_{Ay}\left\{ D^2 v_y - k_y\left(k_y v_y + k_z v_z\right)\right\} + ik_y c_s^2 Dv_y + (\omega^2 - k_y^2 v_{Ay}^2)v_x = 0, \quad (5.1b)$$

$$v_{Ax}v_{Ay}\left(D^2 v_x + ik_z Dv_z - k_y^2 v_x\right) - v_{Ax}^2 D^2 v_y - ik_y c_s^2 Dv_x - \left\{\omega^2 - k_y^2(c_s^2+v_{Ax}^2)\right\}v_y + k_y k_z (c_s^2+v_{Ax}^2)v_z = 0, \quad (5.1c)$$

where $D \equiv \frac{d}{dx}$.

Elimination of v_y and v_z from Eqs. (5.1) in favour of v_x yields the following sixth-order ordinary differential equation

$$\left[v_{Ax}^2 D^2 + 2ik_y v_{Ax}v_{Ay}D + (\omega^2 - k_y^2 v_{Ay}^2)\right]\left[c_s^2 v_{Ax}^2 D^4 + 2ik_y c_s^2 v_{Ax}v_{Ay} D^3 + (\omega^2 c_f^2 - \kappa^2 c_s^2 v_{Ax}^2 - k_y^2 c_s^2 v_{Ay}^2)D^2 - 2ik_y \kappa^2 c_s^2 v_{Ax} v_{Ay} D + (\omega^4 - \kappa^2 \omega^2 c_f^2 + \kappa^2 k_y^2 c_s^2 v_{Ay}^2)\right]v_x = 0. \quad (5.2)$$

The first bracketed expression represents an Alfven operator and the second expression represents a magnetoacoustic operator.

The special case of a purely longitudinal magnetic field ($B_x=0$, $v_{Ax}=0$)

was discussed in Chapter II. From Eq. (2.3) in Chapter II, we found that, in the case of a purely longitudinal field, the Alfven operator in Eq. (5.2) presents simple Alfven waves propagating along the y-direction with frequencies $\omega = k_y v_{Ay}$. The order of the magnetoacoustic operator in Eq. (5.2), however, reduces, with the resulting second order differential equation allowing only for a restricted class of solutions that consist of magnetoacoustic surface and body waves; see Section 2.3 in Chapter II.

By contrast, in Chapter III, where we considered the case of purely transverse field ($B_y = 0$, $v_{Ay} = 0$), we also assumed $k_y = 0$. The Alfven operator in Eq. (5.2) can then be ignored by seeking solutions with $v_y = 0$, and so satisfy Eq. (5.1c) trivially. Eq. (5.2) then reduces to Eq. (3.11) of Chapter III, giving coupled magnetoacoustic waves. In this chapter we consider the general solution of Eq. (5.2).

Equations (5.1) and (5.2) apply both inside ($|x| \leq a$) the slab (where the unperturbed density is ρ_o and $c_s = c_{so}$, $v_{Ax} = v_{Axo}$, $v_{Ay} = v_{Ayo}$, $v_A = v_{Ao}$ and $c_f = c_{fo}$) and outside ($a < |x| \leq L$) the slab (where the density is ρ_e and $c_s = c_{se}$, $v_{Ax} = v_{Axe}$, $v_{Ay} = v_{Aye}$, $v_A = v_{Ae}$ and $c_f = c_{fe}$).

For a uniform unbounded medium, we can substitute $Dv_x = ik_x v_x$ in Eq. (5.2) to give

$$\left[\omega^2 - \frac{(\mathbf{k}.\mathbf{B})^2}{4\pi\rho_o}\right]\left[\omega^4 - \omega^2 c_f^2 k^2 + k^2 c_s^2 \frac{(\mathbf{k}.\mathbf{B})^2}{4\pi\rho_o}\right] = 0 , \tag{5.3}$$

with $k^2 = k_x^2 + k_y^2 + k_z^2 = k_x^2 + \kappa^2$ (where $\kappa^2 = k_y^2 + k_z^2$). Eq. (5.3) is the standard dispersion relation for MHD waves in a uniform medium; cf. Eqs. (1.19) and (1.23) in Chapter I.

From the linearized equations of MHD, we may also obtain the relationships between various perturbations. These relationships may be given as follows.

Write

$$X = \omega^4 - \omega^2\kappa^2 c_f^2 + k_y^2\kappa^2 c_s^2 v_{Ay}^2 , \tag{5.4}$$

$$Y = \omega^2 v_{Ax}\left[\left(\omega^2 - \kappa^2 c_s^2\right)\left\{v_{Ay}^2\left(k_y^2 c_s^2 - \omega^2\right) - \kappa^2 c_s^2 v_{Ax}^2\right\} - k_y^2 c_s^2 v_{Ay}^2\left(\omega^2 - 2\kappa^2 c_s^2\right)\right] , \tag{5.5}$$

$$Z=ik_y v_{Ay}\omega^2\left[v_{Ax}^2\left(\omega^2-\kappa^2c_s^2\right)^2+c_s^2X\right], \tag{5.6}$$

$$A_4=\frac{c_s^2v_{Ax}^3\left(\omega^2-\kappa^2c_s^2\right)^2}{Y}, \tag{5.7}$$

$$A_3=-c_s^2v_{Ax}^2\left(\omega^2-\kappa^2c_s^2\right)\left[\frac{Zv_{Ax}\left(\omega^2-\kappa^2c_s^2\right)}{Y^2}-\frac{2ik_yv_{Ay}\left(\omega^2-k^2c_s^2\right)}{Y}\right], \tag{5.8}$$

$$A_2=v_{Ax}^2\left(\omega^2-\kappa^2c_s^2\right)\left[\frac{v_{Ax}\left(\omega^2-\kappa^2c_s^2\right)^2}{Y}-\frac{ik_yZ\omega^2c_s^2v_{Ay}}{Y^2}\right] - \frac{k_y^2\omega^2c_s^2v_{Ax}v_{Ay}^2\left(\omega^2-2\kappa^2c_s^2\right)}{Y}-1, \tag{5.9}$$

$$A_1=v_{Ax}^2\left(\omega^2-\kappa^2c_s^2\right)^2\left[\frac{ik_yv_{Ay}\left(\omega^2-2\kappa^2c_s^2\right)}{Y}-\frac{Zv_{Ax}\left(\omega^2-\kappa^2c_s^2\right)}{Y^2}\right], \tag{5.10}$$

$$A_0=\frac{Z^2v_{Ax}^2\left(\omega^2-\kappa^2c_s^2\right)}{Y^2}-\frac{iZk_yv_{Ax}v_{Ay}\left(\omega^2-2\kappa^2c_s^2\right)}{Y}+X, \tag{5.11}$$

$$B_5=-v_{Ax}^2\left(\frac{A_4}{A_0}\right),\ B_4=-\frac{\left(v_{Ax}^2A_3+2ik_yv_{Ax}v_{Ay}A_4\right)}{A_0}, \tag{5.12}$$

$$B_3=-\frac{\left[v_{Ax}^2A_2+2ik_yv_{Ax}v_{Ay}A_3+A_4\left(\omega^2-k_y^2v_{Ay}^2\right)\right]}{A_0}, \tag{5.13}$$

$$B_2=-\frac{\left[v_{Ax}^2A_1+2ik_yv_{Ax}v_{Ay}A_2+A_3\left(\omega^2-k_y^2v_{Ay}^2\right)\right]}{A_0}, \tag{5.14}$$

$$B_1=-\frac{\left[2ik_yv_{Ax}v_{Ay}A_1+A_2\left(\omega^2-k_y^2v_{Ay}^2\right)\right]}{A_0}, \tag{5.15}$$

$$B_0=-\frac{A_1\left(\omega^2-k_y^2v_{Ay}^2\right)}{A_0}, \tag{5.16}$$

$$C_6=-c_s^2B_5\tan\phi, \tag{5.17}$$

$$C_5 = -c_s^2\left(B_4\tan\phi + ik_yB_5\right), \tag{5.18}$$

$$C_4 = -c_s^2\left(B_3\tan\phi + ik_yB_4\right), \tag{5.19}$$

$$C_3 = -c_s^2\left(B_2\tan\phi + ik_yB_3\right), \tag{5.20}$$

$$C_2 = -c_s^2\left(B_1\tan\phi + ik_yB_2\right), \tag{5.21}$$

$$C_1 = -c_s^2\left(B_0\tan\phi + ik_yB_1\right), \tag{5.22}$$

$$C_0 = -\left(\tan\phi + ik_yc_s^2B_0\right), \tag{5.23}$$

$$E_6 = -C_6\frac{k_y}{k_z}, \tag{5.24}$$

$$E_5 = -\left(i\frac{\omega^2}{k_z}B_5 + C_5\frac{k_y}{k_z}\right), \tag{5.25}$$

$$E_4 = -\left(i\frac{\omega^2}{k_z}B_4 + C_4\frac{k_y}{k_z}\right), \tag{5.26}$$

$$E_3 = -\left(i\frac{\omega^2}{k_z}B_3 + C_3\frac{k_y}{k_z}\right), \tag{5.27}$$

$$E_2 = -\left(i\frac{\omega^2}{k_z}B_2 + C_2\frac{k_y}{k_z}\right), \tag{5.28}$$

$$E_1 = -\left\{\frac{i}{k_z}\left(\omega^2B_1 - 1\right) + C_1\frac{k_y}{k_z}\right\}, \tag{5.29}$$

$$E_0 = -\left(i\frac{\omega^2}{k_z}B_0 + C_0\frac{k_y}{k_z}\right), \tag{5.30}$$

$$F_7 = c_s^2B_5B_x\tan\phi, \tag{5.31}$$

$$F_6 = \left(B_4\tan\phi + 2ik_yB_5\right)c_s^2B_x, \tag{5.32}$$

$$F_5 = \left(B_3\tan\phi + 2ik_yB_4\right)c_s^2B_x + \left(\omega^2 - k_y^2c_s^2\right)B_5B_y, \tag{5.33}$$

$$F_4 = \left(B_2\tan\phi + 2ik_yB_3\right)c_s^2B_x + \left(\omega^2 - k_y^2c_s^2\right)B_4B_y, \tag{5.34}$$

$$F_3 = \left(B_1\tan\phi + 2ik_yB_2\right)c_s^2B_x + \left(\omega^2 - k_y^2c_s^2\right)B_3B_y, \tag{5.35}$$

$$F_2 = \left(B_0\tan\phi + 2ik_yB_1\right)c_s^2B_x + \left(\omega^2 - k_y^2c_s^2\right)B_2B_y, \tag{5.36}$$

$$F_1 = \left(\tan\phi + 2ik_yc_s^2B_0\right)B_x + \left(\omega^2 - k_y^2c_s^2\right)B_1B_y, \tag{5.37}$$

$$F_0 = ik_y B_x + \left(\omega^2 - k_y^2 c_s^2\right) B_0 B_y \,, \tag{5.38}$$

$$G_7 = -B_x E_6 \,, \tag{5.39}$$

$$G_6 = -\left(B_x E_5 + ik_y B_y E_6\right) \,, \tag{5.40}$$

$$G_5 = -\left(B_x E_4 + ik_y B_y E_5\right) \,, \tag{5.41}$$

$$G_4 = -\left(B_x E_3 + ik_y B_y E_4\right) \,, \tag{5.42}$$

$$G_3 = -\left(B_x E_2 + ik_y B_y E_3\right) \,, \tag{5.43}$$

$$G_2 = -\left(B_x E_1 + ik_y B_y E_2\right) \,, \tag{5.44}$$

$$G_1 = -\left(B_x E_0 + ik_y B_y E_1\right), \tag{5.45}$$

$$G_0 = -ik_y B_y E_0 . \tag{5.46}$$

In Eqs. (5.4)-(5.46), the quantities have their appropriate values X_o , Y_o , Z_o ,..... and X_e , Y_e , Z_e .... etc in the regions 'o' and 'e', respectively.

In terms of the above definitions (Eqs. (5.4)-(5.46)) we may write the perturbations in velocity (v_x, v_y, v_z), pressure $p(x)$, and magnetic field (b_x, b_y, b_z) thus:

$$v_y = \left(C_6 D^6 + C_5 D^5 + C_4 D^4 + C_3 D^3 + C_2 D^2 + C_1 D + C_0 \right) v_x \,, \tag{5.47}$$

$$v_z = \left(E_6 D^6 + E_5 D^5 + E_4 D^4 + E_3 D^3 + E_2 D^2 + E_1 D + E_0 \right) v_x \,. \tag{5.48}$$

$$p = i\omega \rho_o c_s^2 \left(B_5 D^5 + B_4 D^4 + B_3 D^3 + B_2 D^2 + B_1 D + B_0\right) v_x \,, \tag{5.49}$$

$$b_x = i\omega B_x \{B_5 D^5 v_x + B_4 D^4 v_x + B_3 D^3 v_x + B_2 D^2 v_x + \left(B_1 - \frac{1}{\omega^2}\right) D +$$

$$\left(B_0 - \frac{ik_y}{\omega^2}\cot\phi\right)\} v_x \,, \tag{5.50}$$

$$b_y = \frac{i}{\omega} \left(F_7 D^7 + F_6 D^6 + F_5 D^5 + F_4 D^4 + F_3 D^3 + F_2 D^2 + F_1 D + F_0\right) v_x \,, \tag{5.51}$$

and

$$b_z = \frac{i}{\omega} \left(G_7 D^7 + G_6 D^6 + G_5 D^5 + G_4 D^4 + G_3 D^3 + G_2 D^2 + G_1 D + G_0\right) v_x \,, \tag{5.52}$$

where (as earlier) $D \equiv \frac{d}{dx}$.

Unlike the situations considered in Chapters II-IV, the magnetic field is no longer aligned to an axis of symmetry of the equilibrium configuration displayed in Fig. 1.5. Consequently, the solutions of Eq. (5.2) do not possess a very high degree of symmetry (cf. Schwartz and Bel, 1984a). We write them in the general form

$$
\begin{cases}
\alpha_1 e^{ik^{a}_{1e}(x+a)} + \alpha_2 e^{ik^{a}_{2e}(x+a)} + \alpha_3 e^{ik^{+}_{1e}(x+a)} + \alpha_4 e^{ik^{+}_{2e}(x+a)} \\
\qquad + \alpha_5 e^{ik^{-}_{1e}(x+a)} + \alpha_6 e^{ik^{-}_{2e}(x+a)} \quad -\ell \le x < -a \\
\beta_1 e^{ik^{a}_{1o}x} + \beta_2 e^{ik^{a}_{2o}x} + \beta_3 e^{ik^{+}_{1o}x} + \beta_4 e^{ik^{+}_{2o}x} \\
\qquad + \beta_5 e^{ik^{-}_{1o}x} + \beta_6 e^{ik^{-}_{2o}x} \quad -a \le x \le a \\
\gamma_1 e^{ik^{a}_{1e}(x-a)} + \gamma_2 e^{ik^{a}_{2e}(x-a)} + \gamma_3 e^{ik^{+}_{1e}(x-a)} + \gamma_4 e^{ik^{+}_{2e}(x-a)} \\
\qquad + \gamma_5 e^{ik^{-}_{1e}(x-a)} + \gamma_6 e^{ik^{-}_{2e}(x-a)} \quad a < x \le \ell
\end{cases}
\tag{5.53}
$$

where α_1-α_6, β_1-β_6 and γ_1-γ_6 are arbitrary constants. In each of the regions 'o' and 'e', the wavenumbers k_1^a and k_2^a are simply the effective x-aligned wavenumbers of the two oppositely propagating Alfven waves and are given by the solutions of the first bracketed term in Eq. (5.3):

$$
k_1^a = \frac{(\omega - k_y v_{Ay})}{v_{Ax}}, \quad k_2^a = -\frac{(\omega + k_y v_{Ay})}{v_{Ax}}. \tag{5.54}
$$

Similarly, the quantities $k_1^{\pm}$ and $k_2^{\pm}$ are the x-aligned wavenumbers of the two (slow or fast) magnetoacoustic waves, with '+' representing the slow waves and '-' representing the fast waves. They are simply the solutions of the quartic (in k_x) equation given by the second bracketed expression in Eq. (5.3). This quartic equation is

$$c_s^2 v_{Ax}^2 k_x^4 + 2k_y c_s^2 v_{Ax} v_{Ay} k_x^3 - \left(\omega^2 c_f^2 - c_s^2 \kappa^2 v_{Ax}^2 + k_y^2 c_s^2 v_{Ay}^2\right) k_x^2 + 2c_s^2 \kappa^2 v_{Ax} v_{Ay} k_y k_x$$

$$+ \left\{\omega^4 - \omega^2 \kappa^2 c_f^2 + k_y^2 \kappa^2 c_s^2 v_{Ay}^2\right\} = 0. \qquad (5.55)$$

Exact analytical solutions of this quartic equation can be obtained; see the formulae in Ambramowitz and Stegun (1964). We also note that the wavenumbers $k^a_{(1,2)}$ and $k^+_{(1,2)}$ are always real, whereas the wavenumbers $k^-_{(1,2)}$ are in general complex conjugate pairs (cf. Schwartz and Bel, 1984a).

In the limit of extremely long wavelengths ($\kappa\ell \ll 1$), all six wavenumbers are real with $k_1^a = -k_2^a$, $k_1^+ = -k_2^+$ and $k_1^- = -k_2^-$. We may then classify the solutions of Eq. (5.2) in terms of *even (kink)* or *odd (sausage)* eigenmodes (cf. Chapters II, III and IV; see also Joarder and Roberts, 1993b) pertaining to their behaviour in the long wavelength extreme. Following Chapter III, the normal modes of the equilibrium configuration (Fig.1.5) can further be classified as *internal modes* or *external modes*. The dispersion relations for the former is principally determined by the wavenumbers (k^a_{1o}, k^a_{2o}, $k^\pm_{1o}$, $k^\pm_{2o}$) internal to the slab, whereas the dispersion relation for the latter modes are principally determined by the wavenumbers (k^a_{1e}, k^a_{2e}, $k^\pm_{1e}$, $k^\pm_{2e}$) external to the slab.

The eighteen arbitrary constants in Eq. (5.53) are determined by the choice of appropriate boundary conditions. As in Chapter III, we impose line-tying boundary conditions at $x=\pm\ell$:

$$v_x(\pm\ell) = v_y(\pm\ell) = v_z(\pm\ell) = 0. \qquad (5.56)$$

For the remaining twelve boundary conditions, we impose the MHD continuity conditions (3.17)-(3.23) in Section 3.2.2, Chapter III. For the situation considered here, these conditions imply that

$$v_x,\ v_y,\ v_z,\ p,\ b_y \text{ and } b_z \text{ are continuous across } x=\pm a. \qquad (5.57)$$

Note that the continuity of the normal component b_x of the magnetic field perturbation is implied by conditions (5.57).

5.2.2 The dispersion relation: Application of the above boundary conditions to solutions (5.53) leads to the governing dispersion relation. This dispersion relation is given in the following. For brevity, we write

$$k_1 = k_1^a,\ k_2 = k_2^a,\ k_3 = k_1^+,\ k_4 = k_2^+,\ k_5 = k_1^-,\ k_6 = k_2^- . \tag{5.58}$$

It is convenient to define the following quantities:

$$L_j = -C_6 k_j^6 + iC_5 k_j^5 + C_4 k_j^4 - iC_3 k_j^3 - C_2 k_j^2 + iC_1 k_j + C_0 , \tag{5.59}$$

$$M_j = -E_6 k_j^6 + iE_5 k_j^5 + E_4 k_j^4 - iE_3 k_j^3 - E_2 k_j^2 + iE_1 k_j + E_0 , \tag{5.60}$$

$$N_j = iB_5 k_j^5 + B_4 k_j^4 - iB_3 k_j^3 - B_2 k_j^2 + iB_1 k_j + B_0 , \tag{5.61}$$

$$O_j = iF_7 k_j^7 + F_6 k_j^6 - iF_5 k_j^5 - F_4 k_j^4 + iF_3 k_j^3 + F_2 k_j^2 - iF_1 k_j - F_0 , \tag{5.62}$$

$$P_j = iG_7 k_j^7 + G_6 k_j^6 - iG_5 k_j^5 - G_4 k_j^4 + iG_3 k_j^3 + G_2 k_j^2 - iG_1 k_j - G_0 , \tag{5.63}$$

where $j=1,2,.....,6$, and the constants C_j, E_j, F_j and G_j are defined in Eqs. (5.4)-(5.46). The quantities in Eqs. (5.58) - (5.63) take on their appropriate values k_{jo}, L_{jo}, M_{jo}, N_{jo}, O_{jo}, P_{jo} and k_{je}, L_{je}, M_{je}, N_{je}, O_{je}, P_{je} in the regions 'o' and 'e', respectively.

The dispersion relation describing the various modes of the slab can now be written in the form of a determinant of order 18, which must be singular for the normal modes to exist. The elements $\Pi_{m,n}$ $(m, n = 1,...18)$ of this determinant are given in terms of the quantities defined in Eqs. (5.58) - (5.63). These elements are

$$\Pi_{1,n} = \begin{cases} \exp\left[-ik_{ne}(\ell-a)\right] & n \le 6 \\ 0 & 18 \ge n > 6 \end{cases} ; \tag{5.64}$$

$$\Pi_{2,n} = \begin{cases} 0 & n \le 12 \\ \exp\left[ik_{(n-12)e}(\ell-a)\right] & 18 \ge n > 12 \end{cases} ; \tag{5.65}$$

$$\Pi_{3,n} = \begin{cases} L_{ne}\exp\left[-i\mathbf{k}_{ne}(\mathbf{l}-a) \right] & n \le 6 \\ 0 & 18 \ge n > 6 \end{cases}; \qquad (5.66)$$

$$\Pi_{4,n} = \begin{cases} 0 & n \le 12 \\ L_{(n-12)e}\exp\left[i\mathbf{k}_{(n-12)e}(\mathbf{l}-a) \right] & 18 \ge n > 12 \end{cases}; \qquad (5.67)$$

$$\Pi_{5,n} = \begin{cases} M_{ne}\exp\left[-i\mathbf{k}_{ne}(\mathbf{l}-a) \right] & n \le 6 \\ 0 & 18 \ge n > 6 \end{cases}; \qquad (5.68)$$

$$\Pi_{6,n} = \begin{cases} 0 & n \le 12 \\ M_{(n-12)e}\exp\left[i\mathbf{k}_{(n-12)e}(\mathbf{l}-a) \right] & 18 \ge n > 12 \end{cases}; \qquad (5.69)$$

$$\Pi_{7,n} = \begin{cases} 1.0 & n \le 6 \\ -\exp\left[-i\mathbf{k}_{(n-6)o}a \right] & 12 \ge n > 6 \\ 0 & 18 \ge n > 12 \end{cases}; \qquad (5.70)$$

$$\Pi_{8,n} = \begin{cases} 0 & n \le 6 \\ \exp\left[i\mathbf{k}_{(n-6)o}a \right] & 12 \ge n > 6 \\ -1.0 & 18 \ge n > 12 \end{cases}; \qquad (5.71)$$

$$\Pi_{9,n} = \begin{cases} L_{ne} & n \le 6 \\ -L_{(n-6)o}\exp\left[-i\mathbf{k}_{(n-6)o}a \right] & 12 \ge n > 6 \\ 0 & 18 \ge n > 12 \end{cases}; \qquad (5.72)$$

$$\Pi_{10,n} = \begin{cases} 0 & n \le 6 \\ L_{(n-6)o}\exp\left[i\mathbf{k}_{(n-6)o}a \right] & 12 \ge n > 6 \\ -L_{(n-12)e} & 18 \ge n > 12 \end{cases}; \qquad (5.73)$$

$$\Pi_{11,n} = \begin{cases} M_{ne} & n \le 6 \\ -M_{(n-6)o}\exp\left[-i\mathbf{k}_{(n-6)o}a \right] & 12 \ge n > 6 \\ 0 & 18 \ge n > 12 \end{cases}; \qquad (5.74)$$

$$\Pi_{12,n} = \begin{cases} 0 & n \le 6 \\ M_{(n-6)o}\exp\left[i\mathbf{k}_{(n-6)o}a \right] & 12 \ge n > 6 \\ -M_{(n-12)e} & 18 \ge n > 12 \end{cases}; \qquad (5.75)$$

$$\Pi_{13,n} = \begin{cases} N_{ne} & n \leq 6 \\ -N_{(n-6)o}\exp\left[-ik_{(n-6)o}a\right] & 12 \geq n > 6; \\ 0 & 18 \geq n > 12 \end{cases} \tag{5.76}$$

$$\Pi_{14,n} = \begin{cases} 0 & n \leq 6 \\ N_{(n-6)o}\exp\left[ik_{(n-6)o}a\right] & 12 \geq n > 6; \\ -N_{(n-12)e} & 18 \geq n > 12 \end{cases} \tag{5.77}$$

$$\Pi_{15,n} = \begin{cases} O_{ne} & n \leq 6 \\ -O_{(n-6)o}\exp\left[-ik_{(n-6)o}a\right] & 12 \geq n > 6; \\ 0 & 18 \geq n > 12 \end{cases} \tag{5.78}$$

$$\Pi_{16,n} = \begin{cases} 0 & n \leq 6 \\ O_{(n-6)o}\exp\left[ik_{(n-6)o}a\right] & 12 \geq n > 6; \\ -O_{(n-12)e} & 18 \geq n > 12 \end{cases} \tag{5.79}$$

$$\Pi_{17,n} = \begin{cases} P_{ne} & n \leq 6 \\ -P_{(n-6)o}\exp\left[-ik_{(n-6)o}a\right] & 12 \geq n > 6; \\ 0 & 18 \geq n > 12 \end{cases} \tag{5.80}$$

$$\Pi_{18,n} = \begin{cases} 0 & n \leq 6 \\ P_{(n-6)o}\exp\left[ik_{(n-6)o}a\right] & 12 \geq n > 6. \\ -P_{(n-12)e} & 18 \geq n > 12 \end{cases} \tag{5.81}$$

The vanishing of the determinant of these elements provides the dispersion relation for the normal modes of vibration of the slab. In view of its obvious complexity, this dispersion relation will not be written out explicitly.

5.3. The nature of the modes

The matrix dispersion relation whose elements are described by Eqs. (5.64)-(5.81) is too complicated to permit us to draw immediately any conclusions as to the nature of the magnetohydrodynamic normal modes of oscillation of the plasma slab and its environment. However, in the extreme of long wavelengths ($\kappa l \ll 1$; equivalently, $k_y = k_z = 0$) we can make significant simplifications and these permit us to describe the various

modes in some detail. The general case of arbitrary $\kappa\ell$ is determined entirely numerically. For conditions in prominences it turns out that $\kappa\ell$ is of the order of unity or larger and so the limit of small $\kappa\ell$ is not directly applicable to prominences (see Section 5.4). However, it turns out that there are generally small changes in the frequencies of the modes as $\kappa\ell$ increases from small values to values of order unity. Thus an examination of the extreme of small $\kappa\ell$ serves as a useful guide to the nature of the modes even when $\kappa\ell$ is of order unity or larger.

In the limit of long wavelengths the various wavenumbers describing the Alfven modes (Eq. (5.54)) and the (slow or fast) magnetoacoustic modes (Eq. (5.55)) take the following simplified forms:

$$k^a_{1o} = -k^a_{2o} = \frac{\omega}{v_{Axo}}, \quad k^a_{1e} = -k^a_{2e} = \frac{\omega}{v_{Axe}}, \tag{5.82a}$$

$$k^{\pm}_{1o} = -k^{\pm}_{2o} = \frac{\omega}{c^{\pm}_o}, \quad k^{\pm}_{1e} = -k^{\pm}_{2e} = \frac{\omega}{c^{\pm}_e}, \tag{5.82b}$$

with the speeds $c^{\pm}_{(o,e)}$ given by

$$c^{\pm}_o = \sqrt{2} v_{Axo} c_{so} \left\{ c^2_{fo} \pm \left(c^4_{fo} - 4 v^2_{Axo} c^2_{so} \right)^{1/2} \right\}^{-1/2}, \tag{5.83a}$$

$$c^{\pm}_e = \sqrt{2} v_{Axe} c_{se} \left\{ c^2_{fe} \pm \left(c^4_{fe} - 4 v^2_{Axe} c^2_{se} \right)^{1/2} \right\}^{-1/2}. \tag{5.83b}$$

The speeds $c^{\pm}_{(o,e)}$ are simply the x-aligned phase speeds of the slow and fast magnetoacoustic modes, with '+' referring to the slow modes and '-' referring to the fast modes.

For a purely transverse field ($v_{Ayo}=v_{Aye}=0$ giving $v_{Axo}= v_{Ao}$ and $v_{Axe}= v_{Ae}$), Eq. (5.83) gives $c^+_o = c_{so}$, $c^+_e = c_{se}$, $c^-_o = v_{Ao}$ and $c^-_e = v_{Ae}$, consistent with Chapter III. We note, however, that the asymptotic speeds that were obtained for the magnetoacoustic modes in Chapter II, in the long wavelength extreme, cannot be recovered in this way by simply substituting $v_{Axo}=v_{Axe}=0$ in Eq. (5.83). This is because of the fact that Eq.

(5.83) is derived from a differential equation that is of higher order than that obtained in Chapter II and owes its existence solely to a non-vanishing transverse field component ($v_{Ax} \neq 0$), thus yielding a characteristically different spectrum for the modes than that was found in Chapter II; see also Schwartz and Bel, 1984b. We may, of course, obtain the limiting values for the x-aligned phase speeds in Eq. (5.83) in the case of an extremely small angle ϕ of inclination of the applied magnetic field with the axis of the slab (ie, for $|\tan\phi| \ll 1$). the limiting values are

$$c_o^+ \approx c_{To}\sin\phi,\ c_e^+ \approx c_{Te}\sin\phi\ ,\ c_o^- \approx c_{fo},\ c_e^- \approx c_{fe}\ . \tag{5.84}$$

We now describe the behaviour of the various MHD modes, namely (a) the Alfven modes and (b) the magnetoacoustic modes of the plasma slab in the limit of long wavelengths ($\kappa\ell \ll 1$).

(a) *The Alfven modes.* In the extreme of long wavelengths ($\kappa\ell \ll 1$), Eq. 5.1(a) takes the form

$$\left(D^2 + \frac{\omega^2}{v_{Ax}^2}\right) v_z = 0. \tag{5.85}$$

In both the regions 'o' and 'e', the Alfven waves thus satisfy a simple harmonic wave equation and are decoupled from the magnetoacoustic waves. The Alfven waves have velocity perturbations that are predominantly in the z-direction. Accordingly, the dispersion relation for the Alfven modes of the slab, in the limit $\kappa\ell \ll 1$, can now be obtained for the even (cosine) or odd (sine) solutions of Eq. (5.85) by imposing the boundary conditions (5.56) and (5.57) on v_z and b_z ($\equiv \frac{dv_z}{dx}$); see Eqs. (5.48) and (5.52). For the *even Alfven modes*, the resulting dispersion relation is

$$\left(\frac{\rho_e}{\rho_o}\right)^{1/2} \cot\frac{\omega(\ell-a)}{v_{Axe}} - \tan\frac{\omega a}{v_{Axo}} = 0. \tag{5.86}$$

This equation is similar to the dispersion relation (3.41) obtained in Section 3.3, Chapter III for the slow kink modes or the fast sausage modes of a low-β two dimensional plasma slab.

When, as in the case of a prominence, the plasma slab is much denser than its surroundings (see Table 1.1, Section 1.1.2 in Chapter I) so that $\left(\frac{\rho_e}{\rho_o}\right)$ $<<1$, the frequencies of the even Alfven modes are given by

$$\frac{\omega a}{v_{Axo}} = \lambda\pi, \tag{5.87}$$

for the harmonics (λ = 1,2,3.....) of the internal even Alfven (IA^e) modes, and

$$\frac{\omega(\ell-a)}{v_{Axe}} = \lambda'\pi\,, \tag{5.88}$$

for the harmonics (λ' =1,2,3....) of the external even Alfven (EA^e) modes.

The frequency of the *fundamental* even Alfven (fA^e) mode is, however, given by the *lowest* frequency solution of Eq. (5.86). For small ρ_e/ρ_o and small a/ℓ, this solution gives (see Eq. (3.47) and (3.48) in Chapter III for a detailed derivation)

$$\omega \approx \frac{v_{Axo}}{(\ell a)^{1/2}}\,. \tag{5.89}$$

The result (5.89) for the frequency of the fundamental even Alfven mode is similar to Eq. (3.48b) in Chapter III for the case of the fundamental slow kink mode in a low-beta ($v_{Axo} > c_{so}$, $v_{Axe} > c_{se}$) plasma slab threaded by a purely transverse ($B_y = v_{Ayo} = v_{Aye} = 0$) magnetic field (see also Table 3.1), Eq. (5.89) here provides a good approximation for the actual frequency of the even Alfven mode, provided a/ℓ is in the range (ρ_e/ρ_o) to $(\rho_e/\rho_o)^{1/2}$. For example, in a slab of width 2a= 5000 km and a density contrast of $\rho_o=10^2\rho_e$, Eq. (5.89) provides a good estimate to the frequency of the even mode solution for 2ℓ in the range $5\ 10^4$-$5\ 10^5$ km. These values are in accordance with prominence parameters (see Section 5.4 for details), and so the estimate (5.89) is generally applicable under prominence conditions.

Thus, the frequency of the fundamental even Alfven mode is essentially the same as the fundamental frequency of a mass-loaded stretched string;

cf. Eq. (1.39), Section 1.4.3 in Chapter I. Accordingly, we refer to this mode as the *string Alfven* (A_{string}) *mode*. The existence of such an oscillatory mode in prominences has also been pointed out by Roberts (1991c) and Joarder and Roberts (1992b, c, 1993a,b).

The dispersion relation for the *odd* Alfven modes follows from Eq. (5.86) on replacing $\tan\frac{\omega a}{v_{Axo}}$ by $-\cot\frac{\omega a}{v_{Axo}}$. In the limit of long wavelengths and for an extremely dense plasma slab, the frequencies of these odd modes are given by

$$\frac{\omega a}{v_{Axo}} = (2\lambda + 1)\frac{\pi}{2}, \quad \lambda = 0,1,2,..... \tag{5.90a}$$

for the internal odd Alfven (IA^o) modes, and

$$\frac{\omega(\ell - a)}{v_{Axe}} = \lambda'\pi, \quad \lambda' = 1,2,.... \tag{5.90b}$$

for the external odd Alfven (EA^o) modes.

(b)*The Magnetoacoustic Modes.* In the limit of long wavelengths, Eq. (5.1b, c) reduce to,

$$\left(c_s^2 + v_{Ay}^2\right)D^2 v_x - v_{Ax}v_{Ay}D^2 v_y + \omega^2 v_x = 0 \tag{5.91a}$$

and

$$v_{Ax}v_{Ay}D^2 v_x - v_{Ax}^2 D^2 v_y + \omega^2 v_y = 0. \tag{5.91b}$$

Elimination of either v_x or v_y from Eq. (5.91a, b) results in

$$\left(D^2 + \frac{\omega^2}{c^{+2}}\right)\left(D^2 + \frac{\omega^2}{c^{-2}}\right)v_x = 0\,, \tag{5.92a}$$

or

$$\left(D^2+\frac{\omega^2}{c^{+2}}\right)\left(D^2+\frac{\omega^2}{c^{-2}}\right)v_y = 0. \tag{5.92b}$$

Each of the magnetoacoustic (slow and fast) waves thus satisfy a simple harmonic wave equation with its direction of vibration being confined in the x-y plane in this limit of long wavelength of propagation of the waves; note that the terms containing v_z and its derivatives in Eq. (5.1b, c) become arbitrarily small as k_y and k_z approach to zero.

When the applied magnetic field is in a nearly longitudinal direction, $\phi \approx 0$ and $B_x \approx v_{Ax} \approx 0$, Eq. (5.92a, b) gives,

$$\left(D^2 + \frac{\omega^2}{c_f^2}\right) v_x \approx 0, v_y \approx 0 \tag{5.93}$$

for the magnetoacoustic fast waves. So for nearly longitudinal magnetic field, the long wavelength fast waves have their polarization predominantly in the x-direction.

For perturbations of long wavelengths ($\kappa\ell \ll 1$) and for a nearly longitudinal ($\phi \approx 0$) magnetic field direction, the limiting value of the x-aligned wavenumber of the slow waves is given by (see Eq. 5.84)

$$k^{\pm} \approx \frac{\omega\left(v_A^2 + c_s^2\right)^{1/2}}{v_{Ax}c_s} \approx \frac{\omega}{c_T \sin\phi}. \tag{5.94}$$

It then follows, from Eq. (5.91), that

$$\left|\frac{v_x}{v_y}\right| \approx 0\left(\frac{B_x}{B_y}\right) \tag{5.95}$$

for the magnetoacoustic slow waves. The direction of vibration for these slow waves is predominantly in the y-direction in this extreme of long wavelengths and for an almost longitudinal applied magnetic field.

For a purely transverse magnetic field ($\phi = \pi/2$, $B_y = v_{Ay} = 0$), we obtain from Eq. (5.91),

$$\left(D^2 + \frac{\omega^2}{c_s^2}\right) v_x = 0 \qquad (5.96a)$$

for the slow waves, and

$$\left(D^2 + \frac{\omega^2}{v_{Ax}^2}\right) v_y = 0 \qquad (5.96b)$$

for the fast waves. Note that Eq. (5.96a, b) is, in fact, the same as Eqs. (3.43) and (3.44) of Chapter III with v_z replaced by v_y.

In the general case of a skewed ($0 < \phi < \frac{\pi}{2}$) magnetic field, both the long wavelength slow and fast magnetoacoustic modes of the slab will, however, have an appreciable velocity perturbation in the x-direction, thus displacing the slab interfaces laterally. Therefore, as in Chapters II-IV, we apply the terms *kink* and *sausage* modes for a description of these magnetoacoustic modes of the slab, in the limit $kl \ll 1$.

To obtain the dispersion relations for the kink and sausage magnetoacoustic modes of the slab, we simply consider the even (cosine) or odd (sine) solutions of Eq. (5.92) in both the regions inside and outside the slab. Application of the boundary conditions (5.56) and (5.57) on v_x, v_y, $p\left(\equiv \frac{dv_x}{dx}\right)$ and $b_y\left(\equiv \frac{dv_y}{dx}\right)$ then yields the required dispersion realtions for the magnetoacoustic modes in their long wavelength extreme. For the kink modes this dispersion relation reads

$$\left(\frac{\rho_e}{\rho_o}\right)^{1/2} \cot\frac{\omega(l-a)}{c_e^{\pm}} - \tan\frac{\omega a}{c_o^{\pm}} = 0, \qquad (5.97)$$

with '+' representing the slow modes and '-' representing the fast modes. The dispersion relation for the magnetoacoustic sausage modes can be obtained by replacing '$\tan\frac{\omega a}{c_o^{\pm}}$' by '$-\cot\frac{\omega a}{c_o^{\pm}}$' in Eq. (5.97).

It may be noted that in Chapter III (cf. Section 3.3), a dispersion

relation of the form (5.97) was associated with the fast sausage modes (and not the fast kink modes, as is the case here). This was because the velocity perturbation of the long wavelength fast modes was predominantly in the z-direction in the two dimensional case of Chapter III. As noted in Section 3.3 (see also Eq. (5.48) in Section 5.2.1), an even functional behaviour of $v_z(x)$ implied an odd functional behaviour of $v_x(x)$, and so fast modes associated with an even $v_z(x)$ were there classified as fast sausage modes. This complication in referring to the modes is here removed as the velocity perturbations pertaining to the long wavelength fast modes are now confined to the x-y plane, with the perturbation amplitudes $v_x(x)$ and $v_y(x)$ being either both even or both odd, simultaneously; see Eq. (5.46) with $k_y = k_z = \kappa = 0$.

Since the dispersion relations for the kink and sausage magnetoacoustic modes in Eq. (5.97) are essentially similar to the corresponding dispersion relations for the even or odd Alfven modes (see Eq. (5.86)), the frequencies of these magnetoacoustic modes follow immediately from Eqs. (5.87) - (5.90). We only write here the frequencies of those fundamental magnetoacoustic modes which may be important in the context of prominence oscillations (see Sect. 5.4). For the magnetoacoustic kink modes, frequencies are given by

$$\omega \approx \frac{c_o^+}{(\ell a)^{1/2}} \tag{5.98a}$$

for the fundamental slow kink (fS^k) mode, and

$$\omega \approx \frac{c_o^-}{(\ell a)^{1/2}} \tag{5.98b}$$

for the fundamental fast kink (fF^k) mode. In writing (5.98a, b) we have assumed the same ordering in ρ_e/ρ_o and a/ℓ as for the Alfven mode case discussed earlier; see discussions following Eq. (5.89). Both the fundamental magnetoacoustic kink modes are then analogous to the fundamental mode of vibration of a mass-loaded stretched string (see Chapter I, Section 1.4.3). Following Section 3.3 in Chapter III, we refer to these modes as the *slow* (S_{string}) *string mode* and the *fast* (F_{string}) *string*

mode.

Finally, turning to the sausage modes, the frequencies of the fundamental (slow and fast) magnetoacoustic internal sausage modes are given by

$$\frac{\omega a}{c_o^{\pm}} = \frac{\pi}{2}, \qquad (5.99)$$

with '+' referring to the slow (fIS^s) mode and '-' referring to the fast (fIF^s) mode.

5.4. Periods

The formulation in Section 5.2 provides us with a means for determining the frequencies of the modes of oscillation of a dense slab in a skewed magnetic field, but its algebraic complexity (see Eqs. (5.64)-(5.81)) serves to obscure the nature of those modes. Only in the limit of very long wavelengths ($\kappa a \ll 1$) is that obscurity lifted sufficiently for us to shed light on the basic simplicity of the slab's modal structure and particularly, its analogy with the vibrations of a mass-loaded stretched string (Section 5.3). To further our investigation, it is necessary to consider a numerical approach, adopting parameter values appropriate to a prominence.

We consider a slab of gas density $\rho_o = 2\,10^{-13}$ gcm^{-3} (number density of about 10^{11} per cm^3) and temperature $T_o = 8000$ K, embedded in a magnetic field of strength B= 12G which is inclined at an angle $\phi = 20^o$ to the long axis of the slab. The sound speed within the slab is accordingly $c_{so} = 15$ kms^{-1} and the slab's Alfven speed is $v_{Ao} = 74$ kms^{-1}; these speeds imply a cusp speed of $c_{To} = 14.6$ kms^{-1} and a fast speed of $c_{fo} = 75.5$ kms^{-1}. The slab's environment is assumed to have a temperature $T_e = 10^6$ K, implying a density (since $\rho_o T_o = \rho_e T_e$) of $\rho_e = 1.67\ 10^{-15}$ gcm^{-3} (corresponds to a number density of about 10^9 particles per cm^3). The number density in the slab's environment is rather larger than the 10^8 particles per cm^3 that observations of the prominence environment suggest; see Table 1.1 in Section 1.1.2, Chapter I. Such an over-estimation of the value of ρ_e may be an artefact of our model's simplicity; in any case, it does not greatly influence the periods of the oscillatory modes of a prominence, those periods being principally determined by the conditions internal to the prominence slab (see Section 3.4, Chapter III).

With the above values of the plasma parameters in the prominence environment, the associated coronal speeds are then given by c_{se} = 166 kms^{-1}, v_{Ae} = 828 kms^{-1}, c_{Te}=163 kms^{-1} and c_{fe}=844 kms^{-1}. The prominence slab is taken to be of width 2a = 5000 km, length L=2 10^5km and height H=5 10^4 km.

In Chapter III we considered, somewhat arbitrarily, an anchor point separation distance of 2ℓ = 20a for the magnetic field lines threading the prominence. In view of the uncertainty in determining an effective anchor point separation distance for the magnetic field lines in the complicated structure of a quiescent prominence, we now consider two values for this distance 2ℓ, namely, a distance 2ℓ = 7.3 10^4 km (=Ltanϕ), and a distance 2ℓ = 1.6 10^5 km (=πH). The first case provides a minimum value for the separation distance 2ℓ, while the second case provides a (presumably) more realistic estimate (which in fact corresponds to the circumference of an almost semi-circular coronal arcade supporting the prominence). A consideration of these two different values allows us to demonstrate the nature of the dependence of the periods of the modes on the distance 2ℓ.

The vertical and horizontal modal structure of the vibrating slab is defined by setting $k_y=m\pi/L$ and $k_z=n\pi/H$, for integers m and n describing that structure along the length L and height H (see Chapters II and III). This corresponds to our choosing modes that have either nodal lines (even modes) or antinodal lines (odd modes) on the edges of the slab; see Section 2.4, Chapter II. With the above choice of values for the length and height of the slab, the principal (fundamental, ie. m=1, n=1) mode has dimensionless wavenumbers $\kappa\ell \approx 2.4$ and 5.0 for 2ℓ = 7.3 10^4 km and 2ℓ=1.6 10^5 km, respectively.

From the discussion in Section 5.3, we may suppose that the modes of most interest in a prominence slab are the three string modes, together with the fundamentals of the internal Alfven mode (fIA^o) and the slow (fIS^s) and fast (fIF^s) internal magnetoacoustic modes. These modes typically have appreciable kinetic energy densities.

Figure 5.1 displays the results of a numerical solution of the full dispersion relation, indicating the fundamentals and their first harmonics for both internal and external modes. The figure is drawn for 2ℓ = 7.3 10^4 km, enabling us to demonstrate the general behaviour of the modes. The periods of the string modes and the internal modes are, however, displayed in Table 5.1, for both values of the anchor point separation

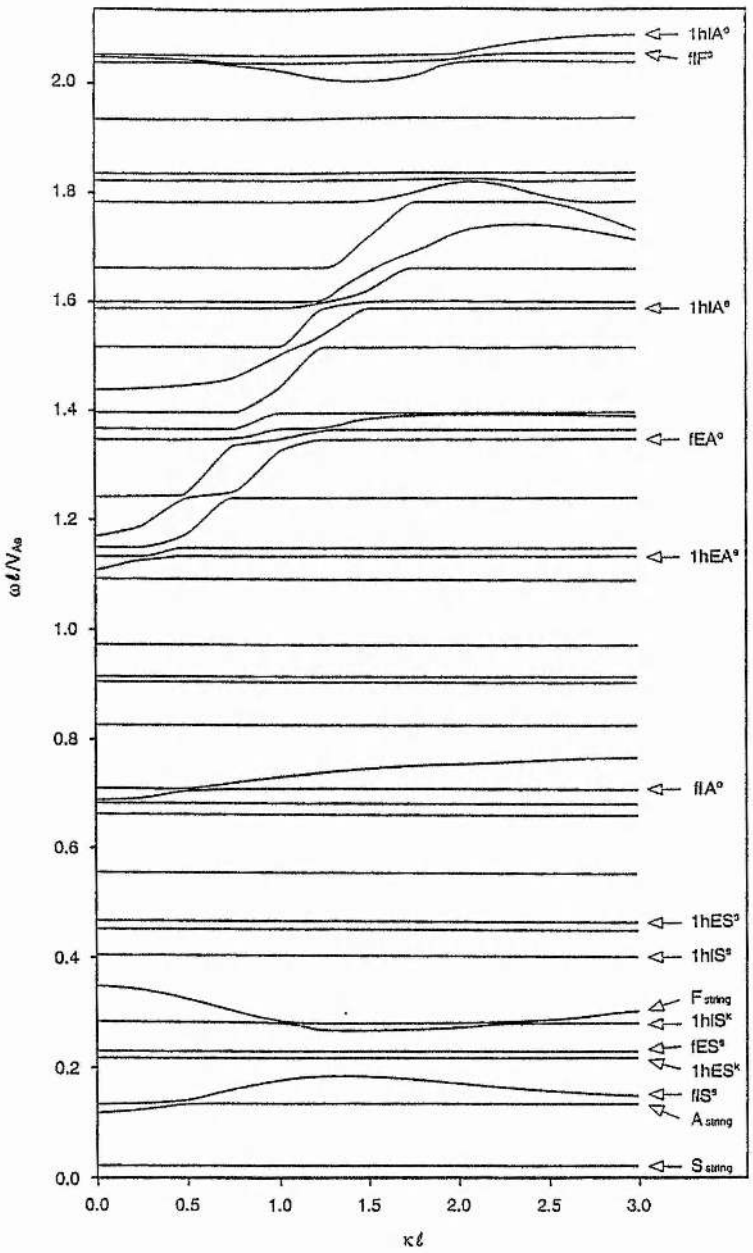

Fig. 5.1. Frequency (in units of v_{Ae}/ℓ) vs. wavenumber (in units of ℓ^{-1}) for the various wave modes of the plasma slab and its environment in a case when c_{so}=15 kms^{-1}, v_{Ao}=74 kms^{-1}, c_{se}=166 kms^{-1}, and v_{Ae}=828 kms^{-1}. The plasma slab is of width 2a=5000 km and is threaded by a magnetic field of strength 12G that is inclined at an angle ϕ = 20^{o} with the long axis of the slab. The separation 2ℓ between the anchor points of the magnetic field lines on either side of the slab is taken to be 7.3 10^4 km. The modes are identified as the Alfven(A) mode, and the slow(S) or fast(F) magnetoacoustic modes, with 'I' denoting an internal mode and 'E' an external mode. The string modes are denoted by a subscript 'string'. The superscript 'e' or 'k' denotes an even (for Alfven mode) mode or a kink mode, and the superscript 'o' or 's' denotes an odd mode or a sausage mode, according to the mode's nature in the limit $\kappa\ell \ll 1$. The first letter in the name of a mode indicates whether it is a fundamental (f) or a first harmonic(1h). The higher harmonics are not shown in the diagram.

Table 5.1. *Periods of the fundamental modes of vibration of the prominence slab with $\rho_o = 2\ 10^{-13}\ gcm^{-3}$, $T_o = 8000\ K$, $\phi = 20^o$, $L = 2\ 10^5$ km, $H = 5\ 10^4$ km and $2a = 5000$ km. Two different values of the anchor point separation distance 2ℓ and the magnetic field strength B ($= |B|$) are considered.*

Names of The Modes	Periods			
	$2\ell = L \tan\phi =$ $7.3\ 10^4$ km		$2\ell = \pi H =$ $1.6\ 10^5$ km	
	B= 5.0 G	B = 12.0 G	B= 5.0 G	B = 12.0 G
Slow String (S_{string}) Mode $\left(\tau \approx \frac{2\pi(\ell a)^{1/2}}{c_o^+} \approx \frac{2\pi(\ell a)^{1/2}}{c_{To}\sin\phi} \right)$	4 hr	3 hr	5.5 hr	5 hr
String Alfven (A_{string}) Mode $\left(\tau \approx \frac{2\pi(\ell a)^{1/2}}{v_{Axo}} \right)$	68 min	34 min	2 hr	53 min
Internal Slow (fIS^s) Mode $\left(\tau \approx \frac{4a}{c_o^+} \approx \frac{4a}{c_{To}\sin\phi} \right)$	38 min	28 min	35 min	32 min
Fast String (F_{string}) Mode $\left(\tau \approx \frac{2\pi(\ell a)^{1/2}}{c_o^-} \approx \frac{2\pi(\ell a)^{1/2}}{c_{fo}} \right)$	29 min	16 min	46 min	20 min
Internal Alfven (fIA^o) Mode $\left(\tau \approx \frac{4a}{v_{Axo}} \right)$	14 min	7 min	14 min	7 min
Internal Fast (fIF^s) Mode $\left(\tau \approx \frac{4a}{c_o^-} \approx \frac{4a}{c_{fo}} \right)$	5 min	2 min	5 min	2 min

distance 2ℓ (and hence of the dimensionless wavenumber $k\ell$) chosen above. Table 5.1 also displays the approximate formulae for these periods (as determined in Sect. 5.3 for the case $k\ell \ll 1$). These formulae provide convenient order of magnitude estimates for the actual periods, shed light on the physical nature of the modes, and allow reasonable estimates for these periods for slab parameters different from those chosen here. For convenience, we have also displayed in Table 5.1 the numerically determined periods for the case of a weak magnetic field of 5 G, again for the two different choices for the anchor point separation distance 2ℓ.

The results displayed in Table 5.1 for a skewed ($\phi \approx 20^\circ$) magnetic field may be compared with those found in Chapter III for a purely transverse field ($\phi=90^\circ$). In Chapter III periods of the order of 1/2-1 hour were given by the magnetoacoustic string modes. Here the consideration of a larger anchor point separation distance 2ℓ of the prominence slab, along with a factor $\sin\phi$ evident in the estimates for the slow modes in Table 5.1, leads to a substantial increase in the period of such (slow) modes when $\phi = 20^\circ$, the slow string mode has a period of 3-5 hour that is somewhat similar to the very long periods obtained for the slow body modes in the purely longitudinal ($\phi = 0$) field model of Chapter II (see Table 2.1). Similarly, the internal slow mode here has a period of about 1/2 hour, compared with some 10 minutes in the transverse case of Chapter III. The Alfven modes, ignored in Chapter III because of the two-dimensional situation discussed there, here provide both long and intermediate periods. Periods of the order of 1/2-2 hour are associated with the string Alfven (A_{string}) mode (as well as the fast (F_{string}) string mode in a weak magnetic field), whereas the internal Alfven (fIA$^\circ$) mode produces periods of about 7-14 min.

We end this discussion with a brief comparison of the results of Table 5.1 with the observations of prominence oscillations summarized earlier in Tables 1.2a, b, c in Section 1.2.3 of Chapter I. The simplicity of our basic slab model precludes a very detailed comparison with the observations. For that we must await the development of oscillation calculations for more realistic equilibria, as well as more detailed observational studies of prominence oscillations. Nonetheless, the simple model investigated here is expected to provide a guide to the classes of modes to be expected and a reasonable estimate of their periods. As was noted earlier in Chapter IV, a comparison of the results of Chapter III for a prominence slab in a purely

transverse field with the results obtained by Oliver et al. (1992a, b, 1993a) and Joarder and Roberts (1993a) for simple gravitational models of prominences supports such a view.

Periods in the range 40-90 min detected in prominences (see Table 1.2(a)) may be a reflection of the string Alfven mode, with a period of about 50 min in a 12G field anchored at some $L \approx 78{,}500$ km and scaling directly with $\sqrt{L}$ and inversely with field strength (Table 5.1). The string Alfven mode has velocity perturbations that are appreciable in the vertical (z) direction, so such modes should in principle also be detected in disk observations of filaments. Intermediate periodicities in the range 8-20 minutes have been detected in prominences (cf. Table 1.2(b)) and may here be associated with the internal Alfven mode or the fast string mode. The periods of both these modes scales (roughly) inversely with field-strength, the fast string mode also scaling directly with $\sqrt{L}$. We may of course note that in the case of a weak magnetic field (of strength 5 G, say), the fast string mode presents a rather long periodicity of about 50 min, which is similar to the observed long period oscillations in prominences. Finally, we note that the short periods of 2-5 minutes reported in prominences (cf. Table 1.2(c), Chapter I) may here be associated with an internal fast mode, which produces a period of 2 min in a 12G field increasing to 5 min in a 5 G field (Table 5.1).

These simple comparisons of observed periods and those calculated from our slab model offer considerable encouragement for the further development of prominence oscillation studies, both theoretical (perhaps by considering more sophisticated equilibria) and observational (perhaps by making detailed studies of many prominences, so as to learn how periods vary with prominence parameters). The elementary model and its modes of oscillations that we have explored will hopefully provide some guidance in such future developments.

Chapter VI

Concluding remarks

Recent observations of velocity oscillations in quiescent solar prominences are increasingly revealing a complex array of oscillatory motions. These oscillations can broadly be classified into three major groups according to their periods. These groups are: long period oscillations with periodicities in the range 1/2-2 hours, intermediate periodicities in the range 8-20 minutes, and short periodicities of about 2-5 minutes; see Section 1.2.3, Chapter I for a summary of observational results on prominence oscillations. Apart from this classification of oscillatory periods, observations of prominence oscillations are yet to arrive at any definite conclusions regarding the other important physical properties of these oscillatory motions, such as their polarizations, their wavelengths or the phase coherence lengths and phase coherence times of these velocity oscillations in prominences.

As an aid to observational attempts to understand the nature of prominence oscillations, we here carried out a systematic theoretical investigation of the basic physical nature of the oscillatory modes that might be present in solar quiescent prominences. We view this thesis as a first step towards the development of theoretical models of the various oscillatory motions observed in solar prominences, a development that is grounded in terms of the fundamentals of the global magnetohydrodynamic modes of oscillation open to a prominence. To develop such models, it has been necessary to ignore several important factors, such as the role of prominence fine structure, the effect of non-adiabaticity on the modes, their non-dissipative damping or the non-linear development of the modes, etc. It is possible that the highly intermittent, time-dependent nature of some of these oscillations or their localized behaviour, as have been suggested by several observations (see Section 1.2.3, Chapter I), may be attributed to some of these factors ignored in this thesis.

To find out the basic physical ingredients that must go together to determine the periods of oscillation in prominences, it is however necessary that we begin with some simple equilibrium models to represent the quiesecnt prominences. The approach we considered in this thesis is in fact the same as was considered by Kleczek and Kuperus (1969) in their

development of a theoretical model of flare induced oscillations in prominences in terms of the leaky hydromagnetic wavemodes excited in a prominence-coronal system; see Section 1.4.2 in Chapter I and Section 2.5 in Chapter II. Kleczek and Kuperus approximated a quiescent prominence as a thin plasma slab embedded in a purely longitudinal coronal magnetic field. This model was also the starting point of our theoretical discussions on prominence oscillations in this thesis. In Chapter II, we examined the Kleczek and Kuperus model in somewhat greater detail, taking explicitly into consideration the effect of the coronal environment of the prominence plasma on the modes of oscillation of the prominence slab. Unlike Kleczek and Kuperus (1969), who emphasized the role of the leaky magnetoacoustic modes of the prominence slab, we placed emphasis on the internal normal modes of the model prominence, as such normal modes seem to be of much greater relevance in the context of the oscillatory motions observed recently in quiescent prominences.

A serious drawback of the model calculations in Kleczek and Kuperus (1969) and in Chapter II of this thesis was the assumption of a purely longitudinal magnetic field in prominences. Almost all the equilibrium models of prominences (Section 1.1.3 in Chapter I) assume the prominence to reside in a coronal magnetic arcade that threads the prominence plasma transversely, thus producing a weak transverse magnetic field component in prominences. The foot-points of this magnetic arcade are supposed to be anchored tightly in the dense photosphere, thus producing a photospheric line-tying effect (Section 1.4.3, Chapter I). Indirect evidence for the existence of such a magnetic arcade can perhaps be obtained from the fact that the prominences are always seen to reside over a neutral line separating opposite, line-of-sight, magnetic polarities in the photosphere (Section 1.1.1, Chapter I). The introduction of such arcades is necessary in theoretical prominence models, in order to explain the necessary support of the prominence plasma against gravity (see Fig. 1.4). The arcades themselves are of course not seen, probably because of the fact that they are filled with very low density plasma that has little emissivity, and therefore, tend not to be visible in observations (eg. Priest, 1990).

In Chapter III, we have attempted to examine the effect of such an arcade magnetic field on the modes of oscillation of a prominence. We there confined ourselves to a two dimensional geometry, ignoring the dominant longitudinal component of the magnetic field threading the prominence. This simplification allowed us to compare our results obtained

in Chapter III to the oscillatory modes in some of the simple magnetostatic equilibrium models of quiescent prominences. Such comparisons were drawn in Chapter IV.

The non-gravitational, two dimensional slab model of Chapter III suffers from a major shortcoming, in that it ignores the curvature of the magnetic field lines in a coronal arcade threading the prominence, approximating the arcade field as a planer, uniform magnetic field anchored at rigid walls on either side of the prominence slab (thus simulating the photospheric line-tying effect on the field-lines). This assumption simplifies the problem considerably. Moreover, it is expected to give the approximate periods of the global oscillations of the prominence residing in a two-dimensional coronal arcade. We may, however, note that in a more realistic arcade geometry with curvature, we should in principle obtain slow continuum (cf. Goossens et al. 1984, 1985; see also Oliver et al. 1993b), instead of the discrete slow magnetoacoustic normal modes obtained in Chapter III. (The existence of the Alfven continuum can be ignored in the two dimensional geometry considered in Chapter III.) Such continuous spectra arise as the magnetic field-lines of differing lengths oscillate with different acoustic frequencies. The presence of such a slow continuum would generally suggest a resonant damping of the global (collective) slow oscillations of the two dimensional structure (cf. 1.3.1, Chapter I), that are expected to be excited by any impulsive disturbances imposed on the system. The behaviour of these collective oscillations are, however, very likely to mimic the behaviour of the normal modes of oscillation that are obtained in calculations with a plane parallel geometry; see Lee and Roberts, (1986), Davila (1987), Hollweg (1987), Grossmann and Smith (1988), Hollweg and Yang (1988), and Cally (1991) for illuminating discussions of such resonant processes that excite continuum modes through the damping of the global oscillations in large scale solar coronal structures.

The most important feature of the model calculations presented in Chapter III is perhaps the discovery of the magnetoacoustic (slow and fast) string modes that are similar to the fundamental vibrations of a mass-loaded stretched string that is clamped at its edges (cf. Rayleigh, 1877; Lamb, 1910). The importance of such modes in the context of the observed long period oscillations in prominences was pointed out earlier by Roberts (1991c; see Section 1.4.3 in Chapter I) and Joarder and Roberts (1992b, c). Such string modes owe their existence to the photospheric line-tying of

the field lines and consist of waves that are reflected off the photospheric boundaries. In Chapter III, we showed that in a prominence-like situation, the periods of such magnetoacoustic string modes are (to a reasonable approximation) given by the formula

$$\tau \approx 2\pi \frac{(\ell a)^{1/2}}{c}, \qquad (6.1)$$

with 2ℓ being the photospheric anchor point separation distance, and 2a being the width of the prominence. In Eq. (6.1), the physical speed c is a magnetoacoustic (slow or fast) speed in prominences.

Apart from such string modes, we also obtained magnetoacoustic internal modes in our simple slab model (Chapter III). Such internal modes consist of waves that are trapped within the prominence slab with their periods being approximately equal to the back and forth acoustic (generally for the slow-type modes) or Alfvenic (generally for the fast-type modes) travel-time across the width of the prominence. Such modes presented intermediate to short periodicities in our model calculations of Chapter III.

Given this simple picture of the magnetoacoustic modes in a two dimensional prominence slab embedded in a purely transverse magnetic field (Chapter III), it would be of some interest to see how these modes are modified in the presence of gravity. Towards this aim, we examined in Chapter IV the modes of oscillation of a simple, isothermal magnetostatic equilibrium model, namely the Menzel (1951) prominence model. We found that the numerically determined periods of the magnetoacoustic-gravity modes in the simple equilibrium model of Menzel are close to the periods of the magnetoacoustic modes that are present in an uniform, non-gravitational, magnetic plasma, thus showing that an order of magnitude estimate of the periods of the fundamental vibrations of a prominence-like equilibrium may be given by the simple slab model of Chapter III. This suggestion has also been supported by a recent investigation by Oliver et al. (1993a), who considered the modes of oscillation of a generalized Kippenhahn-Schlüter-type equlibrium model that is obtained by ignoring the non-adiabatic effects in the Poland and Anzer (1971) prominence model. This model introduces a temperature and density discontinuity in the classical Kippenhahn-Schlüter (1957) solution for the internal structure of a prominence (cf. Section 4.6.1 in Chapter IV), thus allowing for a hotter,

rarer coronal plasma surrounding the prominence slab. In Chapter IV (Section 4.6), we described the work of Oliver et al. (1993a) in some detail, showing that the periods obtained in their numerical investigation of the two-temperature Kippenhahn-Schlüter prominence model can readily be interpreted in terms of the periods of oscillation of a two-dimensional simple slab model of a prominence threaded by a purely transverse magnetic field, as determined in Chapter III.

The discussion presented in Chapter IV suggested that the periods of vibration of a prominence slab is principally determined by the strength of the temperature and density discontinuities at the prominence-corona interfaces; the magnetic field strength in the prominence; and by the photospheric line-tying effect. Gravitational stratification and field-line curvature play only subsidiary roles.

A word of caution should, however, be added, as the prominence models we examined in Chapter IV to arrive at this conclusion are, in fact, too simple to represent the extremely complicated situation that may actually be present in solar quiescent prominences. Both the Menzel (1951) equilibrium model and the non-isothermal Kippenhahn-Schlüter (1957) prominence model ignore a realistic curvature of the magnetic arcade that may exist in the external, coronal part of the field-lines. Such models thus neglect or fail to fully represent the possibility of the existence of the slow continuum. Moreover, the artificial boundary conditions introduced in Menzel's (1951) equilibrium, and the simplifying assumption of an infinitely large prominence height (see Section 4.6 in Chapter IV) in the Kippenhahn-Schlüter (1957)-type models, both rule out the possibility of the occurrence of a magnetic Rayleigh-Taylor type instability (cf. Newcomb, 1961; Parker, 1966; Hughes and Proctor (1988); see also Gilman, 1970; Zweibel, 1981; Hood, 1986a, b; De Bruyne and Hood, 1989 for various forms of this instability) that may arise due to an unstable stratification of the plasma that is partially supported against gravity by a magnetic field. In fact, recent investigations of De Bruyne (1991) show that even the most realistic prominence equilibria may turn out to be unstable when a linear stability analysis is carried out, thus indicating that in future oscillation calculations with more realistic prominence models, we may have to take into account both the possibilities of the existence of continuous spectra and also the problem of stabilization of the prominence models against the magnetic Rayleigh-Taylor instability. Such considerations may complicate the simple pictures drawn in Chapter IV to a considerable extent.

It should also be noted that in our investigation of the gravitational prominence models in Chapter IV we do not obtain a mode that possesses the distinctive features of a purely gravitational oscillation, such as the ones predicted by Hyder (1966) and also Roberts (1991c) in simpler models of prominences; see Section 1.4.2, Chapter I. Such oscillations are expected to be present in a stable magnetostatic prominence model, but are perhaps not easily identifiable in a purely numerical study of the behaviour of the modes, as was done in Chapter IV. This indicates that along with the numerical study of sophisticated prominence equilibria it is also necessary to obtain some analytical guidance regarding the detailed behaviour of the magnetoacoustic-gravity modes in simple, magnetohydrostatic configurations, if we are to clearly understand the complicated nature of the oscillatory modes in prominences.

The simplified assumption we considered in our calculations to take the finite dimensions of a prominence slab into account may also be open to some criticism. The prominence width is observed to be much shorter than the length or the height of a prominence (see Section 1.1.2 in Chapter I). This led us to assume plane wave-like behaviour of the perturbations in these two directions, thus retaining a true inhomogeneity only across the width of the model prominence. This may not be a major drawback of the theory, as both the length and the height of a large quiescent prominence are comparable to the coronal scale-height (typically of the order of 10^5 km). It is therefore not too unrealistic to impose periodic boundary conditions on the perturbations in these two directions, as is generally done in the normal mode analysis of certain classical vibrating systems, such as in the case of the modes of vibration of a rectangular elastic membrane; see, for example, Rayleigh (1877). In any case, such an application of the periodic boundary conditions, to take the finite length and the height of the prominence slab into account, allowed us to formulate the problem of prominence oscillations in a simple way, and thus enabling us to shed some light on the simple physical nature of the modes. Such modelling is hopefully of use also in a numerical study of complicated, coupled partial differential equations representing the perturbations, and in studies with more realistic boundary conditions at the edges of a prominence.

A more fundamental question may be raised regarding our representing the prominence as a plasma slab in a line-tied magnetic field. Such a representation seems to be appropriate for the direct-polarity,

Kippenhahn-Schlüter (1957)-type prominences (see Fig. 1.1(a) in Chapter I). Our model is, therefore, expected to provide useful information about the periods of oscillation of such prominences. In the case of the direct-polarity prominences, the magnetic field within the prominence is directly connected to the photosphere and hence the effect of line-tying boundary conditions on the modes of oscillation of such a prominence must be important. The magnetic topology in an inverse-polarity, Kuperus-Raadu (1974)-type prominence (Fig. 1.1(b) in Chapter I) is, however, more subtle. There, the magnetic field within the prominence-slab does not seem to be connected directly to the photosphere in any obvious way, and therefore it is difficult to assess the importance of the line-tying boundary conditions in such prominences. On the other hand, the slab modes in a purely longitudinal magnetic field configuration (Chapter II) also seem to be too simplistic a model to represent, even approximately, the oscillations in inverse-polarity prominences. Further developments of the giant flux-tube model (Fig. 1.1(c)) may perhaps resolve this conceptual difficulty, provided they can successfully incorporate the internal field structure of the prominence slab residing in the flux-tube. Even then, to find some simple analytical guidance to the modes would be difficult, if not impossible, in such a case and therefore one may have to resort to a complete numerical approach for the inverse-polarity prominences.

Turning back now to our basic goal in this thesis, which is to determine the fundamental MHD modes of oscillation of a prominence slab in a line-tied, coronal magnetic arcade, it is evidently necessary that we improve the model calculations of Chapter III by incorporating a more realistic magnetic field configuration, even within the framework of our idealized non-gravitating, plane-parallel geometry for a prominence and its magnetic field. In Chapter V, we presented the results of such an investigation of the MHD modes of a prominence slab embedded in a skewed magnetic field, that makes a small angle (of approximately 20^{o}) with the long axis of the prominence (Fig. 1.5, Chapter I). This representation of prominences is, in fact, consistent with the magnetic field geometry observed in solar quiescent prominences; cf. Section 1.1.2 in Chapter I.

In Chapter V we found that the introduction of a dominant longitudinal component of the magnetic field somewhat alters the nature and the periods of the (slow and fast) magnetoacoustic (both internal and string) modes that were found in the calculations in Chapter III for a

purely transverse magnetic field. Due to their highly anisotropic propagation characteristics (cf. Table 1.3 in Chapter I), the slow magnetoacoustic modes are particularly sensitive to the direction of the magnetic field. Accordingly, we obtained considerably longer periodicities for the slow magnetoacoustic modes in Chapter V than that were obtained for these modes in the purely transverse field case of Chapter III, with the slow string mode presenting a periodicity of about 3-5 hours in a skewed field. Such long periodicities have not so far been detected in the observations of prominence oscillations; see Section 1.2.3 in Chapter I.

In addition to the (slow and fast) magnetoacoustic modes, we also obtained two fundamental Alfven modes, namely the String Alfven (A_{string}) mode and the internal Alfven (fIA^{o}) mode in the situation of a slab with a skewed magnetic field (Chapter V). These Alfven modes were absent in Chapter III because of the two-dimensional geometry considered there. Similar to the magnetoacoustic string modes, the string Alfven mode is also analogous to the fundamental vibration of a mass loaded stretched string, with a periodicity given approximately by Eq. (6.1) with c now replaced by an Alfven speed determined solely by the transverse component of the magnetic field (B_{xo}); see Table 5.1 in Chapter V. This mode perhaps corresponds to the long period oscillations (Table 1.2a, Chapter I) observed in quiescent prominences. The periods of the other modes (except the slow string mode discussioned above) are also consistent with the observed periodicities in prominence oscillations; see Table 5.1.

It may be noted that the classification of the slab modes that we have described in this thesis are all derived from the asymptotic behaviour of the modes in their long wavelength extreme-see discussions in Section 5.3, Chapter V. There, we found that in the limit of long wavelength and also for extremely small angle of inclination ϕ of the magnetic field vector with the axis of the slab, the Alfven modes have a predominant polarization in the vertical (z) direction, whereas the velocity perturbations pertaining to the fast and the slow magnetoacoustic modes are predominantly in directions along (y-direction) and across (x-direction) the axis of the slab, respectively. We may note, however, that such a simple picture regarding the velocity eigenfunctions pertaining to different fundamental modes of the prominence slab may be modified appreciably due to the strong coupling between the modes for parameter values relevant to the situation observed in quiescent prominences (see

discussions in Section 5.4). The degree and the nature of such modal coupling is, of course, dependent on the detailed nature of the equilibrium considered, and therefore any conclusion regarding the detailed nature of these eigenfunctions that may be drawn from simple slab models, may not be of much use in the context of the actual observations of prominence oscillations. For the most part of our thesis, then, we have therefore confined ourselves mainly to a discussion of the periods of the modes together with the scaling laws that they approximately follow. These features are expected to be relatively insensitive to the detailed nature of the mode coupling and on the details of the various equilibrium models used to represent the prominences.

Our calculations in Chapter V, with the slab model of a prominence, have presented periodicities in the range 2 minutes to a few hours. It may, however, be of interest to note that, apart from such periodicities noted in Table 1.2, observations of prominence oscillations have recently confirmed the existence of very short periodicities of about 30 seconds in some prominences (Balthasar et al. 1993). Such periodicities, of the order of a few tens of seconds or even shorter, may perhaps be associated with the observed field-aligned fibril structures (cf. Section 1.1.2, Chapter I) in quiescent prominences, that may possibly arise due to a plasma inhomogeneity, rather than an inhomogeneity in the magnetic field in prominences (Tandberg-Hanssen, 1970; Leroy, 1985; Nikolsky et al., 1985; Leroy, 1989). To examine the oscillations that may be sustained in such fibril structures of the quiescent filaments, we may draw on the investigations by Edwin and Roberts (1983) and Roberts et al. (1984) of the nature of magnetosonic oscillations in a filamentary corona. These investigations revealed that regions of high density (and correspondingly low Alfven speed) are able to support ducted fast magnetosonic waves referred to as magnetic Love and magnetic Pekeris modes (see Chapter I for a description of such magnetosonic modes in a slab-type geometry); these modes are confined to the wave guide defined by the high-density, low Alfven speed structures. In cylindrical fibrils, the fundamental of the magnetic Pekeris modes present a period of the order (Roberts et al., 1984)

$$\tau^{P}_{fibril} \approx \frac{2.6R}{v_{A\,fibril}}, \qquad (6.2)$$

where R is the radial structure within the prominence and $v_{A\,fibril}$ is the Alfven-speed within the fibril. With R≈100-1000 km (cf. Section 1.1.2 in

Table 6.1. *The nature of the fundamental MHD modes that may be responsible for the observed oscillations in quiescent prominences.*

Observed oscillatory periods	Names of the MHD modes	Theoretically estimated periods	Possible predominant velocity directions
$\frac{1}{2}$ -2 hr	String Alfven mode	$\tau \approx \frac{2\pi(\ell a)^{1/2}}{v_{Axo}}$	Vertical
	Fast string mode in a weak magnetic field?	$\tau \approx \frac{2\pi(\ell a)^{1/2}}{c_{fo}}$	Transverse (Horizontal)
	Internal slow mode	$\tau \approx \frac{4a}{c_{To}\sin\phi}$	Longitudinal (Horizontal)
8-20 min	Internal Alfven mode	$\tau \approx \frac{4a}{v_{Axo}}$	Vertical
	Fast string mode in a moderate to strong magnetic field?	$\tau \approx \frac{2\pi(\ell a)^{1/2}}{c_{fo}}$	Transverse (Horizontal)
2-5 min	Internal fast mode	$\tau \approx \frac{4a}{c_{fo}}$	Transverse (Horizontal)
< 1 min	magnetic Pekeris mode in quiescent fibrils	$\tau^{P}_{fibril} \approx \frac{2.6R}{v_{A\,fibril}}$	Radial in cylindrical fibrils

Chapter I) and an assumed Alfven speed of 30 kms^{-1} (say) within the prominence fibril, we obtain $\tau^{P}_{fibril} \approx$ 8-80 s. Much shorter periodicities can be obtained in this way, by either increasing the Alfven speed or decreasing the radius of the quiescent fibrils. These considerations suggest to us that modes in a fibrous prominence medium are worthy of further theoretical study to complement the increasing observational interest in short period oscillations.

Finally, we end our discussion with a tabular summary (see Table 6.1) of the results of our theoretical investigations into the physical

characteristics of the oscillations observed in quiescent prominences. The theoretical explanation of the oscillatory periods that we have provided with our simple prominence models will hopefully serve as a useful guide to future investigations into the nature of prominence oscillations.

References

Abdelatif T. E., 1988, Astrophys. J. 333, 395

Abramowitz M. and Stegun I. A., 1964, 'Handbook of Mathematical Functions', NBS Applied math. Series No. 55, NBS, Washington D. C.

Adam J. A., 1977, Solar Phys. 52, 293

Adam J. A., 1982, Phys. Rep. 86, 217

Adam J. A., 1986, Phys. Rep. 142, 263

Alfven H. 1950, 'Cosmical Electrodynamics', 1st ed., Clarendon Press, Oxford

Aly J. J. and Amari T., 1988, Astron. Astrophys. 207, 154

Amari T. and Aly J. J., 1989, Astron. Astrophys. 208, 261

Amari T. and Aly J. J., 1990, Astron. Astrophys. 231, 213

An C. H., 1984, Astrophys. J. 281, 419

Anderson G. F., 1966, Ph. D. Thesis, Univ. of Colorado

Antia H. M. and Chitre S. M., 1979, Solar Phys. 63, 67

Anzer U., 1969, Solar Phys. 8, 37

Anzer U., 1972, Solar Phys. 24, 324

Anzer U., 1979, in: E. Jensen, P. Maltby and F. Q. Orrall (eds.), 'Physics of Solar Prominences', IAU Colloq. 44, p. 322

Anzer U., 1984, in: M. J. Hagyard (ed.) 'Measurements of Solar Magnetic Fields', NASA Conference Publ. 2374, p. 101

Anzer U., 1989, in: E. R. Priest (ed.) 'Dynamics and Structure of Quiescent Solar Prominences', D. Riedel, Dordrecht, p. 143

Anzer U. and Tandberg-Hanssen E., 1970, Solar Phys. 11, 61

Appert K., Gruber R. and Vaclavik J., 1974, Phys. Fluids, 17, 1471

Athay R. G. and Moreton G. E., 1961, Astrophys. J. 133, 935

Athay R. G., Gurman J. B., Henze N. and Shine R. A., 1983a, Astrophys. J. 265, 219

Athay R. G., Querfeld C. W., Smartt R. N., Landi degl' Innocenti E. and Bommier V. 1983b, Solar Phys. 89, 3

Ballester J. L. and Priest E. R. (eds.) 1988, 'Dynamics and Structure of Solar Prominences', Univ. les Illes Balears Press, Mallorca, Spain

Balthasar H., Wiehr, E. and Stellmacher G., 1988a, in: J. L. Ballester and E. R. Priest (eds.) 'Dynamics and Structure of Solar Prominences', Univ. les Illes Balears Press, Mallorca, Spain, p. 63

Balthasar H., Stellmacher G. and Wiehr E., 1988b, Astron. Astrophys. 204, 286
Balthasar H., Knolker M., Stellmacher G. and Wiehr E. 1986, Astron. Astrophys. 163, 343
Balthasar H., Wiehr E., Schleicher H. and Wohl H., 1993, Astron. Astrophys. (in press)
Bashkirtsev V. S. and Mashnich G. P., 1984, Solar Phys. 91, 93
Bashkirtsev V. S., Kobanov N.I., and Mashnich G. P., 1983, Solar Phys. 82, 443
Bessey R. J. and Liebenberg D. H., 1984, Solar Phys. 94, 239
Bommier V., Landi degl'Innocenti E., Leroy J. L. and Sahal-Brechot S., 1985a, in: M. J. Hagyard (ed.) 'Measurements of Solar Magnetic Fields', NASA Conf. Publ. 2374, p. 335
Bommier V., Leroy J. L. and Sahal-Brechot S., 1985b, in M. J. Hagyard (ed.) 'Measurements of Solar Magnetic Fields', NASA Conf. Publ. 2374, p. 375
Bray R. J., Cram L. E., Durrant C. J. and Loughhead R. E., 1991, 'Plasma Loops in the Solar Corona', Cambridge Univ. Press, Cambridge.
Brown A., 1958, Astrophys. J. 128, 646
Bruzek A., 1951, Z. Astrophys. 13, 277
Bruzek A., 1958, Z. Astrophys. 44, 183
Cally P. S., 1985, Aust. J. Phys. 38, 825
Cally P. S., 1986, Solar Phys. 103, 277
Cally P. S., 1991, J. Plasma Phys. 45, 453
Campbell W. R. and Roberts B., 1989, Astrophys. J. 338, 538
Chen L. and Hasegawa A., 1974, Phys. Fluids, 17, 1399
Cheuderi-Drago F., Engvold O. and Jensen E., 1992, Solar Phys. 139, 47
Christensen-Dalsgaard J., 1980, Mon. Notices of Roy. Astron. Soc. 190, 765
Christensen-Dalsgaard, J., 1989, 'Lecture Notes on Stellar Oscillations', Astronomisk Institut, Aarhus Universitet
Coulson C. A., 1955, 'Waves', Oliver and Boyd, Edinburgh.
Cowling T. G., 1957, 'Magnetohydrodynamics', Wiley-Interscience, New York.
Davila J. M., 1985, Astrophys. J. 291, 328
Davila J. M., 1987, Astrophys. J. 317, 514
De Brunye P., and Hood A. W., 1989, Solar Phys. 123, 241.

De Bruyne P., 1990, Ph. D. Thesis, Univ. of St Andrews.
De Jager C., 1959, 'Hanbuch der Physik', 52, 80
Defouw R. J., 1976, Astrophys. J. 209, 266
Demoulin P., 1991, in: E. R. Priest and A. W. Hood (eds.) 'Advances in Solar System MHD', Cambridge Univ. Press, Cambridge, p. 281
Demoulin P. and Vial J. C., 1992, Solar Phys. 141, 289
Demoulin P., Malherbe J. M. and Priest E. R., 1989, Astrophys. J. 211, 428
Demoulin P., Raadu M. A., Malherbe J. M. and Schmieder B., 1987, Astron. Astrophys. 183, 142
Deubner F. L. and Gough D. O., 1984, Ann. Rev. Astron. Astrophys. 22, 593
Dodson H. W., 1949, Astrophys. J. 110, 382
Dodson H. W., and Hedeman E. R., 1964, AAS-NASA Symp. on the Phys. of Solar Flares, 1963, p. 15
Dungey J. W., 1953, Mon. Notices Roy. Astron. Soc. 113, 180
Dunn R. B., 1959, Astrophys. J. 130, 972
Dunn R. B., 1960, Ph.D Thesis, Harvard Univ.
Edwin P. M. and Roberts B., 1982, Solar Phys. 76, 239
Edwin P. M. and Roberts B., 1983, Solar Phys. 88, 179
Edwin P. M. and Roberts B., 1988, Astron. Astrophys. 192, 343
Edwin P. M., Roberts B. and Hughes W. J., 1986, Geophys. Res. Letter, 13, 373
Engvold O., 1976, Solar Phys. 49, 283
Engvold O., 1978, Solar Phys. 56, 87
Engvold O., 1981, Solar Phys. 70, 315
Engvold O., 1988, in: R. C. Altrock (ed.) 'Proc. 9th Sacramento Peak Summer Meeting', p. 155
Engvold O., 1989, in: E. R. Priest (ed.) 'Dynamics and Structure of Quiescent Solar Prominences', D. Reidel, Dordrecht, p. 47
Engvold O., Jensen E., Zhang Yi. and Brynildson N., 1989, Hvar Obs. Bull. 13, No 1, 205
Engvold O., Hirayama T., Leroy J. L., Priest E. R. and Tandberg-Hanssen E., 1990, in: V. Ruzdjak and E. Tandberg-Hanssen (eds.) 'Dynamics of Quiescent prominences', Springer-Verlag, Berlin, p. 294
Evans D. J. and Roberts B., 1990a, Astrophys. J. 348, 346
Evans D. J. and Roberts B., 1990b, Astrophys. J. 356, 704

Evans D. J. and Roberts B., 1991, Astrophys. J. 371, 387
Field G. B., 1965, Astrophys. J. 142, 531
Galindo-Trejo J., 1987, Solar Phys. 108, 265
Galindo-Trejo J., 1989a, Geophys. Astrophys. Fluid. Dyn. 47, 69
Galindo-Trejo J., 1989b, Rev. Mexicana Astron. Astrof. 17, 47
Galindo-Trejo J. and Schindler K., 1984, Astrophys. J. 277, 422
Gheonjian L. A., Klepikov V. Yu. and Stepanov A. I., 1990, Academy of Sciences of the USSR, Reprint No. 4
Gilman P. A., 1970, Astrophys. J. 162, 1019
Goedbloed J. P., 1983, 'Lecture Notes On Ideal Magnetohydrodynamics', Rijnhuizen Rep. 83-145, Nieuwegein.
Goossens M., 1991, in: E. R. Priest and A. W. Hood (ed.) 'Advances in Solar System Magnetohydrodynamics', Cambridge Univ. Press, Cambridge, p. 137
Goossens M. and Hollweg J. V., 1993, Solar Phys. 145, 19
Goossens M., Hermans D., Poedts S., 1984, in: 'Proc. 25th Liege Int. Astrophys. Collq.', p. 382
Goossens M., Poedts S. and Hermans D., 1985, Solar Phys. 102, 51
Grossmann W. and Smith R., Astrophys. J., 1988, 332, 476
Harvey J. W., 1969, Ph. D. Thesis, Univ. of Colorado
Hasan S. S., 1979, in: E. Jensen, P. Maltby and F. Q. Orrall (eds.) 'Physics of Solar Prominences', IAU Coll No. 44, p. 97
Hasan S. S., 1991, Astrophys. J. 366, 328
Hasan S. S. and Sobouti Y., 1987, Mon. Not. Roy. Astron. Soc. 228, 427
Hasan S. S. and Abdelatif T., 1990, in: C. T. Russel, E. R. Priest and L. C. Lee (eds.) 'Physics of Magnetic Flux Ropes', AGU Monograph, p. 23
Hasan S. S. and Christensen-Dalsgaard J., 1992 (preprint)
Heasley J. N. and Mihalas D., 1976, Astrophys. J. 205, 273
Heinzel P., and Vial J. C., 1992, in Proc. ESA Workshop on Solar Phys. and Astrophys. at Interferometric Resolution, Paris, p. 57
Heyvaerts J. and Priest E. R., 1983, Astron. Astrophys. 117, 220
Hirayama T., 1985, Solar Phys. 100, 415
Hirayama T., 1986, in: A. Poland (ed.) 'Coronal and Prominence Plasmas', NASA Conf. Publ. 2442, p. 149
Hirayama T., 1990, in: V. Ruzdjak and E. Tandberg-Hanssen (eds.), 'Dynamics of Quiescent Prominences', Springer-Verlag, Berlin, p. 187
Hollweg J. V., 1987a, Astrophys. J. 312, 880

Hollweg J. V., 1987b, Astrophys. J. 320, 875
Hollweg J. V., 1990, Comp. Phys. Reports, 12, 205
Hollweg J. V. and Yang G., 1988, J. Geophys. Res. 93, 5423
Hood A. W., 1985, in: E. R. Priest (ed.) 'Solar System magnetic Fields', D. Reidel, Dordrecht, p. 80
Hood A. W., 1986a, Solar Phys. 103, 329
Hood A. W., 1986b, Solar Phys. 105, 307
Hood A. W., 1989, in: E. R. Priest (ed.), 'Dynamics and Structures of Quiescent Solar Prominences', D. Reidel, Dordrecht, p. 167
Hood A. W., 1990, Computer Phys. Reports, 12, 177
Hood A. W. and E. R. Priest, 1979, Astron. Astrophys. 77, 233
Hood A. W. and Anzer U., 1990, Solar Phys. 126, 117
Hughes D. W. and Proctor M. R. E., 1988, Ann. Rev. of Fluid Mech. 20, 187
Hyder C. L., 1966, Z. Astrophys. 63, 78
Ireland R. C., Van der Linden R. A. M., Hood A. W. and Goossens M. 1992, Solar Phys. 142, 265
Jensen E. and Wiik J. E., 1990, in: V. Ruzdjak and E. Tandberg-Hanssen (eds.), 'Dynamics of Quiescent Prominences', Springer-Verlag, Berlin, p. 82
Joarder P. S. and Roberts B., 1992a, Astron. Astrophys. 221, 326
Joarder P. S. and Roberts B., 1992b, Astron. Astrophys. 261, 625
Joarder P. S. and Roberts B., 1992c, in: M. Heyn and W. Kernbichler (eds.) Proc. International Winter School and Workshop on Plasma Physics, Pichl, Austria, p. 285
Joarder P. S. and Roberts B., 1993a, Astron. Astrophys. (in press)
Joarder P. S. and Roberts B., 1993b, Astron. Astrophys. (in press)
Joarder P. S., Gokhale M. H. and Venkatakrishnan P., 1987, Solar Phys. 110, 255
Jones W. L., 1970, J. Atmos. Terr. Phys. 32, 1555
Kawaguchi I., 1967, Solar Phys. 1, 420
Kim I. S., 1990, in: E. R. Priest (ed.) 'Dynamics of Quiescent Prominences', Springer-Verlag, Berlin, p.49
Kim, I. S., Koutchmy S. and Stellmacher G. and Stepanov A. I. 1988, in: E. Schroter, M. Vazquez, and A. Wyller (eds.) 'Role of Fine Scale Magnetic Field on the Structure of the Solar Atmosphere', Cambridge Univ. Press, Cambridge, p. 289

Kippenhahn R. and Schluter A., 1957, Z. Astrophys. 43, 36
Kleczek J. and Kuperus M., 1969, Solar Phys. 6, 72
Kruskal M. D. and Tuck J. L., 1958, Proc. Roy. Soc. (London), A245, 222
Kuijpers J., 1989, in: M. A. Dubois (ed.) Proc. 9th Cargese Workshop on Plasma Turbulence, Les Edition de Physique, France
Kuperus M. and Raadu M. A., 1974, Astron. Astrophys. 31, 189
Kurokawa H., Hanaoka Y., Shibata K. and Uchida Y., 1987, Solar Phys. 108, 251.
Lamb H., 1910, 'Dynamic Theory of Sound', Edward Arnold, London
Landman D. A., Edberg S. J. and Laney C. D., 1977, Astrophys. J. 218, 888
Lee M. A. and Roberts B., 1986, Astrophys. J. 301, 430
Leibacher J. W. and Stein R. F., 1981, in: S. Jordan (ed.) 'The Sun as a Star', NASA SP-450, p. 263
Leibacher J. W., Noyes R. W., Toomre J. and Ulrich R. K., 1985, Scientific American, 253, 48
Lerche I. and Low B. C., 1977, Solar Phys. 53, 385
Lerche I. and Low B. C., 1980, Solar Phys. 67, 229
Leroy B. and Schwartz S. J., 1982, Astrophys. J. 112, 84
Leroy J. L., 1979, in: E. Jensen, P. Maltby and F. Q. Orral (eds.), 'Physics of Solar Prominences', IAU colloq 44, p.56
Leroy J. L., 1985, in: M. Hagyard (ed.) 'Measurements of Solar Magnetic Fields', NASA Conf. Publ. 2374, p. 121
Leroy J. L., 1989, in: E. R. Priest (ed.) 'Dynamics and Structure of Quiescent Prominences', Kluwer, Dordrecht, p. 77
Leroy J. L. and Servajean R., 1966, Ann. Astrophys. 29, 263
Leroy J. L., Bommier V., and Sahal-Brechot S., 1983, Solar Phys., 83, 135
Leroy J. L., Bommier V. and Sahal-Brechot S., 1984, Astron. Astrophys, 131, 33
Lindsay R. B., 1960, 'Mechanical Radiation', Mc-Grow-Hill, New York
Linhart J. G., 1960, 'Plasma Physics', North-Holland Publ., Amsterdam
Low B. C., 1975a, Astrophys. J. 197, 251
Low B. C., 1975b, Astrophys. J. 198, 211
Low B. C., 1980, Solar Phys. 65, 147
Low B. C., 1981, Astrophys. J. 246, 538
Malherbe J. M. and Priest E. R., 1983, Astron. Astrophys. 123, 80

Malherbe J. M., Schmieder B. and Mein P., 1981, Astron. Astrophys. 55, 103
Malherbe J. M., Schmieder B., and Mein P. and Tandberg-Hanssen E., 1987, Astron. Astrophys. 172, 316.
Malville J. M., 1961, Ph. D. Thesis, Univ. of Colorado.
Malville J. M., 1969, in: Tandberg-Hanssen (1974), 'Solar Prominences', D. Reidel, Dordrecht.
Malville J. M. and Schindler M., 1981, Solar Phys. 70, 115
Martres M., Mein P., Schmieder B. and Soru-Escaut I., 1981, Solar Phys. 69, 301
Mashnich G. P. and Bashkirtsev V. S., 1990, Astron. Astrophys. 235, 428
Mein P., 1977, Solar Phys. 54, 45
Menzel D., 1951, in: P. L. Bhatnagar, M. Krook and D. Menzel (eds.), Proc. Con. on Dynamics of Ionized Media, London
Menzel D. and Evans J. W., 1953, Accad. Naz. Lincei. Convegno Volta, 11, 119
Meyer F., 1968, in: K. O. Kipenheuer (ed.), 'Structure and Development of Solar Active Regions', IAU Symp. 35, 485
Migliuolo S., 1982, J. Geophysical Res. 87, 8057
Miles A. J. and Roberts B., 1989, Solar Phys. 119, 257
Miles A. J. and Roberts B., 1992, Solar Phys. 141, 205
Miles A. J., Allen H. R. and Roberts B., 1992, Solar Phys. 235
Milne A. M., Priest E. R. and Roberts B., 1979, Astrophys. J. 232, 304
Moreton G. E., 1960, Astron. J. 65, 494
Moreton G. E., 1965, in: R. Lust (ed.) 'Stellar and Solar Magnetic Fields', IAU Symp. 22, 371
Newcomb W. A., 1960, Phys. Fluids, 4, 391
Newton H. W., 1934, Mon. Not. Roy. Astron. Soc. 94, 472
Newton H. W., 1935, Mon. Not. Roy. Astron. Soc. 95, 650
Nikolsky G. M., Kim I. S., Koutchmy S., Stepanov A. I. and Stellmacher G., 1985, Soviet Astron. 29, 669
Noccera L., Leroy B. and Priest E. R., 1984, Astron. Astrophys. 133, 387
Nye A. H. and Thomas J. H., 1974, Solar Phys. 38, 399
Nye A. H. and Thomas J. H., 1976a, Astrophys. J. 204, 573
Nye A. H. and Thomas J. H., 1976b, Astrophys. J 204, 582

Oliver R., Ballester J. L., Hood A. W. and Priest E. R., 1992a, Astrophys. J. (in press)
Oliver R., Ballester J. L., Hood A. W. and Priest E. R., 1992b, in: M. Heyn and W. Kernbichler (eds.) Proc. Int. Workshop on Plasma Phys., Pichl, Austria, p. 93
Oliver R., Ballester J. L., Hood A. W. and Priest E. R., 1993a, Astrophys. J. (in press)
Oliver R., Ballester J. L., Hood A. W. and Priest E. R., 1993b, Astrophys. J. (in press)
Parker E. N., 1966, Astrophys. J. 145, 811
Parker E. N., 1968, Astrophys. J. 154, 57
Parker E. N., 1979, 'Cosmical Magnetic Fields', Clarendon Press, Oxford.
Pippard A. B., 1978, 'The Physics of Vibration', Cambridge Univ. press. Cambridge, Vol. 1
Poland A. I. and Anzer U., 1971, Solar Phys. 19, 401
Poland A. I. and Mariska J. T., 1986, Solar Phys. 104, 303
Pikel'ner S. B., 1971, Solar Phys. 17, 44
Pettit E., 1925, Publ. Yerkes Obs. 3, 205
Pettit E., 1932, Astrophys. J. 76, 9
Pettit E., 1936, Astrophys. J. 84, 319
Pettit E., 1943, Astrophys. J. 98, 6
Pettit E., 1950, Publ. Astron. Soc. Pacific, 62, 144
Priest E. R., 1982, Solar Magnetohydrodynamics, D. Riedel, Dordrecht
Priest E. R. (ed.) 1989, 'Dynamics and Structure of Quiescent Solar prominences', D. Reidel, Dordrecht
Priest E. R., 1990, in: V. Ruzdjak and E. Tandberg-Hanssen (eds.) 'Dynamics of Quiescent Prominences', Springer-Verlag, Berlin, p. 150
Priest E. R., Hood A. W. and Anzer U., 1989, Astrophys. J, 344, 1010
Priest E. R., Hood A. W. and Anzer U., 1991, Solar Phys. 132, 199
Querfeld C. W., Smatt R. N., Bommier V., Landi degl'Innocenti E. and House L. L., 1985, Solar Phys. 96, 277
Raadu M. A., 1972, Solar Phys. 22, 425
Rae I. C. and Roberts B., 1982, Astrophys. J. 256, 761
Rae I. C. and Roberts B., 1983, Solar Phys. 84, 99
Ramsey H. and Smith S. F., 1966, Astron. J 71, 197
Rayleigh Lord, 1877, 'The Theory of Sound', Vol I (1945 edition), Dover, New York

Roberts B., 1981a, Solar Phys. 69, 27
Roberts B., 1981b, Solar Phys. 69, 39
Roberts B., 1984, in: 'The Hydromagnetics of the Sun', Noordwijk, ESA SP-220, p. 137
Roberts B., 1985, in: E. R. Priest (ed.), 'Solar System Magnetic Fields', D. Reidel, Dordrecht, p. 37
Roberts B., 1989, in: L. Tanovic, N. Konjevic and N. Tanovic (eds.), 'The Physics of Ionized Gases', SPIG'88, Nova Science, New York, p. 687
Roberts B., 1990a, in: E. R. Priest and V. Krishan (eds.) 'Basic Plasma Processes in the Sun', IAU Symp. Kluwer, Dordrecht, p. 159
Roberts B., 1990b, in: B. Buti (ed.), 'Solar and Planetary Plasma Physics', World Scientific, Singapore, p. 1.
Roberts B., 1991a, in: P. Ulmshneider, E. R. Priest and R. Rosner (eds.) 'Mechanism of Chromospheric and Coronal Heating', Springer-Verlag, Heidelberg, p. 494
Roberts B., 1991b, in: E. R. Priest and A. W. Hood (eds.) 'Advances in Solar System Magnetohydrodynamics', Cambridge Univ. Press, Cambridge, p. 105
Roberts B., 1991c, Geophys. Astrophys. Fluid Dyn. 62, 83
Roberts B., 1992, in: N. O. Weiss and J. H. Thomas (eds.) 'Sunspots, Theory and Observations', Kluwer (in press).
Roberts B. and Campbell W. R., 1986, Nature, 323, 603
Roberts B. and Webb A. R., 1978, Solar Phys. 56, 5
Roberts B. and Webb A. R., 1979, Solar Phys. 64, 77
Roberts B. and Joarder P. S., 1993, in: Proc. Seventh European Meeting on Solar Physics, Catania, Italy (in press).
Roberts B., Edwin P. M. and Benz A. O., 1984, Astrophys. J. 279, 857
Roberts P. H., 1967, 'An Introduction to Magnetohydrodynamics', American Elsevier, New York.
Rompolt B., 1990, Hvar Obs. Bull. 14, 37
Rosner R., Tucker W. H. and Vaiana G. S., 1978, Astrophys. J. 220, 643
Rosner R., Low B. C. and Holzer T., 1984, in: P. Sturrock, T. Holzer, D. Mihalas and R. Ulrich (eds.) 'Physics of the Sun', D. Reidel, Dordrecht, Vol. 2. p. 135
Ruzdjak V. and Tandberg-Hanssen E. (eds.) 1990, 'Dynamics of Solar Prominences', Springer-Verlag, Berlin.
Saito K. and Tandberg-Hanssen E., 1973, Solar Physics, 31, 105

Scheuer M. A. and Thomas J. H., 1981, Solar Phys. 71, 21
Schmieder B., 1989, in: E. R. Priest (ed.) 'Dynamics and Structure of Quiescent Solar Prominences', Kluwer, Dordrecht, p. 15
Schmieder B., 1990, in: V. Ruzdjak and E. Tandberg-Hanssen (eds.) 'Dynamics of Solar Prominences', Springer-Verlag, Berlin, p. 85
Schmieder B., Malherbe J. M., Poland A. I. and Simon G., 1985, Astron. Astrophys. 136, 81
Schwartz S. J. and Bel N., 1984a, Solar Phys. 92, 133
Schwartz S. J. and Bel N., 1984b, Astron. Astrophys. 137, 128
Secchi A., 1875-77, Le Soleil, Gauthier-Villars, Paris, Vols. 1 and 2
Sedlacek Z., 1971, J. Plasma Phys. 5, 239
Severny A. B., 1954, Astron. Zh. 31, 131
Severny A. B., 1959, 'Solar Physics', Foreign Language Publ. Moscow
Severny A. B. and Kholklova V. L., 1953, Izv. Krymsk. Astrofiz. Observ. 10, 9
Solovjev A. A., 1985, Soln. Dann. 9, 65
Somasundaram K. and Uberoi C., 1982, Solar Phys. 81, 3
Spicer D. S., 1979, Solar Phys. 64, 121
Spruit H. C., 1981, in: S. Jordan (ed.) 'The Sun as a Star', NASA SP-450, p. 385
Spruit H. C., 1982, Solar Phys. 75, 3
Spruit H. C. and Roberts B., 1983, Nature 304, 401
Tandberg-Hanssen E., 1970, Solar Phys. 15, 359
Tandberg-Hanssen E., 1974, 'Solar Prominences', D. Reidel, Dordrecht
Tandberg-Hanssen E. and Anzer U., 1970, Solar Phys. 15, 158
Thomas J. H., 1982, Astrophys. J. 262, 760
Thomas J. H., 1983, Ann. Rev. Fluid Mech. 15, 321
Thompson W. T. and Schmieder B., 1991, Astron. Astrophys. 243, 501
Tsubaki T., 1988, in: R. C. Altrock (ed.) 'Proc. 9th Sacramento Peak Summer Meeting', p 140
Tsubaki T. and Takeuchi A., 1986, Solar Phys. 104, 313
Tsubaki T., Ohnishi Y. and Suematsu B., 1987, Publ. Astron. Soc. Japan, 39, 179
Tsubaki T., Toyoda M., Suematsu Y. and Gamboda G. A. R., 1988, Publ. Astron. Soc. Japan, 40, 121
Uberoi C., 1972, Phys. Fluids, 15, 1673
Uberoi C., 1982, Solar Phys. 78, 351

Uberoi C. and Somasundaram K., 1980, Plasma Phys. 22, 747
Uberoi C. and Somasundaram K., 1982, Plasma Phys. 24, 465
Uchida Y., 1968, Solar Phys. 4, 30
Uchida Y., 1970, Publ. Astron. Soc. Japan, 22, 341
Van der Linden R. A. M., 1993, Geophys. Astrophys. Fluid Dynamics (in press)
Van Hoven G., Ma S. S. and Einaudi G., 1981, Astron. Astrophys. 97, 232
Vrsnak B., 1984, Solar Phys. 94, 289
Vrsnak B., 1990a, Solar Phys. 127, 129
Vrsnak B., 1990b, Solar Phys. 129, 295
Vrsnak B., Ruzdjak V. and Rompolt B., 1991, Solar Phys. 136, 151
Vrsnak B., Ruzdjak V., Brajsa R. and Dzubur A., 1988, Solar Phys. 116, 45
Vrsnak B., Ruzdjak V., Brajsa R. and Zloch F., 1990, Solar Phys. 127, 119
Waldmeir M., 1941, Ergebn. u. Probleme der Sonnen-Forsch. Leipzig, p. 234
Waldmeir M., 1970, Solar Phys. 15, 167
Wang J. L., 1985, Scientia Sinica, 28, 1308
Webb A. R. and Roberts B., 1978, Solar Phys. 59, 249
Wentzel D. G., 1979, Astron. Astrophys. 76, 20
Wiehr E., Stellmacher G. and Balthasar H., 1984, Solar Phys. 94, 285
Wilson P. R., 1980, Astron. Astrophys. 87, 121
Yi Zhang and Engvold O., 1991, Solar Phys. 134, 275
Yi Zhang, Engvold O. and Keil S. L., 1991, Solar Phys. 132, 63
Young C. A., 1896, 'The Sun', D. Appleton, New York.
Yu C. P., 1965, Phys. Fluids, 8, 650
Zhugzhda Yu. D., 1979, Soviet Astron. 23, 42
Zhugzhda Yu. D., 1984, Mon. Not. Royal Astron. Soc. 207, 731
Zhugzhda Yu. D. and Dzhalilov N. S., 1982, Astron. Astrophys. 112, 16
Zhugzhda Yu. D. and Dzhalilov N. S., 1984a, Astron. astrophys. 132, 45
Zhugzhda Yu. D. and Dzhalilov, N. S. 1984b, Astron. Astrophys. 132, 52
Zirin H., 1966, 'The Solar Atmosphere', Blaisdell-Ginn, Waltham, Mass.
Zirin H., 1988, 'Astrophysics of Sun', Cambridge Univ. Press. Cambridge
Zirker J. B., 1989, Solar Phys. 119, 341
Zirker J. B. and Koutchmy S., 1990, Solar Phys. 127, 109

Zweibel E., 1981, Astrophys. J. 249, 731
Zweibel E., 1982, Astrophys. J. 258, L53